Competence of Inhibitory Neuron Progenitors in the Telencephalon

Yana Kotlyarenko

München 2025

Competence of Inhibitory Neuron Progenitors in the Telencephalon

Yana Kotlyarenko

Dissertation

an der Fakultät für Biologie

der Ludwig–Maximilians–Universität

München

vorgelegt von

Yana Kotlyarenko

aus Smila, Ukraine

München, den 14.04.2025

Erstgutachter: Prof. Dr. Wolfgang Enard

Zweitgutachter: Prof. Dr. Rüdiger Klein

Tag der Abgabe: 14.04.2025

Tag der mündlichen Prüfung: 09.10.2025

Contents

List of Figures

List of Tables

Publication statement

The findings presented in this PhD thesis have been submitted for publication to *Nature Neuroscience*, under the title "Temporal control of progenitor competence shapes maturation in GABAergic neuron development in mice." The submission has been accepted.

Most of the figures, along with much of the methods section and portions of the results, were taken from the manuscript.

Abstract

Inhibitory neurons of the telencephalon are generated from ventral proliferative zones, called ganglionic eminences. Here, progenitor cells mature and differentiate into specialized GABAergic interneurons and projection neurons. This study explored the competence of inhibitory neuron progenitors, how it is influenced by intrinsic and extrinsic factors during neurogenesis, and how this reflects on the downstream neurons they generate. Multiple important aspects were addressed to gain a comprehensive understanding of progenitor behavior at different embryonic developmental stages. First, the developmental patterns from progenitor cells to neuronal precursors were analyzed, comparing inhibitory and excitatory lineages at different stages utilizing single-cell RNA sequencing (scRNA-seq). This comparison highlighted the temporal dynamics and regional differences in neuronal development, particularly between ventral and dorsal telencephalon lineages. Second, a genetic barcoding method was employed to track the clonal relationships and fate commitment of inhibitory progenitors at the single-cell level. Clonal analysis revealed no transcriptomic signatures in the progenitor pool that could lead the differentiation towards a specific cell state. Third, an in-depth analysis of isochronic cohorts of cells labeled with a fluorescent dye and analyzed with scRNA-seq, revealed a link between the changes in gene expression of the progenitors and a shift in the maturation level of newly born neurons at different time points, indicating a possible birthmark in the progenitor-to-neuron transition. Finally, this study explored the intrinsic and extrinsic factors that could affect the competence of

progenitors, employing chromatin and gene interaction analyses to uncover the intrinsic mechanisms governing inhibitory lineage progression, and transplantation, to shed light on the role of the environmental factors. Overall, this research provides a framework for understanding the patterning of inhibitory progenitor cells, the factors involved in their competence, and the effect on the differentiation and maturation of their daughter cells.

Zusammenfassung

Hemmende Neuronen des Telencephalons entstehen aus ventralen proliferativen Zonen, den sogenannten ganglionischen Eminenzen. Dort reifen Vorläuferzellen heran und differenzieren zu spezialisierten GABAergen Interneuronen und Projektionsneuronen. Diese Arbeit untersucht die Kompetenz inhibitorischer Vorläuferzellen, ihre Regulation durch intrinsische und extrinsische Faktoren während der Neurogenese sowie deren Einfluss auf die nachfolgenden Neuronen. Um das Verhalten der Vorläuferzellen in verschiedenen embryonalen Entwicklungsphasen umfassend zu charakterisieren, wurden mehrere Ansätze kombiniert. Zunächst wurden Entwicklungsverläufe von Vorläuferzellen zu neuronalen Präcursoren mittels Single-Cell RNA Sequencing (scRNA-seq) analysiert und inhibitorische mit exzitatorischen Zelllinien verglichen. Dadurch konnten zeitliche Dynamiken und regionale Unterschiede der neuronalen Entwicklung, insbesondere zwischen ventralem und dorsalem Telencephalon, aufgezeigt werden. Mithilfe genetischer Barcodierung wurde anschließend die klonale Verwandtschaft und Schicksalsfestlegung inhibitorischer Vorläuferzellen auf Einzelzellniveau verfolgt. Die Analysen zeigten, dass innerhalb des Vorläuferpools keine eindeutigen transkriptomischen Signaturen existieren, die eine Differenzierung in einen bestimmten Zelltyp vorhersagen. Eine detaillierte Untersuchung isochroner, mit Fluoreszenzfarbstoff markierter Zellkohorten enthüllte zudem eine Verbindung zwischen Veränderungen in der Genexpression der Vorläufer und dem Reifegrad der neu gebildeten Neuronen zu verschiedenen Zeitpunkten. Dies weist auf eine mögliche „Geburtsmarke“ im Übergang

von der Vorläuferzelle zur reifen Nervenzelle hin. Abschließend wurden intrinsische und extrinsische Faktoren identifiziert, die die Kompetenz der Vorläuferzellen beeinflussen. Chromatin- und Geninteraktionsanalysen verdeutlichten die intrinsischen Mechanismen der inhibitorischen Linienentwicklung, während Transplantationsexperimente die Bedeutung umweltbedingter Einflüsse hervorhoben. Insgesamt bietet diese Arbeit ein umfassendes Rahmenkonzept zum Verständnis der Musterbildung inhibitorischer Vorläuferzellen, der zugrunde liegenden Regulationsmechanismen und deren Auswirkungen auf Differenzierung und Reifung der entstehenden Neuronen.

1 Introduction

1.1 Neural progenitor cells in the telencephalon

Understanding brain development is essential for advancing our knowledge of evolution, investigating the origins of various pathologies, and gaining insight into the factors that define human cognition and behavior. At the heart of this exploration lies the central nervous system (CNS), the dynamic network that orchestrates everything from our most basic reflexes to the highest forms of cognition.

The CNS comprises the brain and the spinal cord and is highly conserved across vertebrate species and throughout evolution. During embryonic development, three germinal layers are formed: endoderm, mesoderm, and ectoderm (Ghimire et al., 2021). The ectoderm gives rise to the neural plate, where the CNS originates from. The neural plate folds to form the neural tube, the internal cavity of which will develop into the ventricular system of the brain and the spinal cord. At the "three-vesicle stage", the brain differentiates into the prosencephalon, mesencephalon, and rhombencephalon. At the "five-vesicle stage", the prosencephalon subdivides further into the telencephalon and diencephalon (Fig.1.1A). Finally, the telencephalon gives rise to the neocortex dorsally and the basal ganglia ventrally, with the cavity becoming the lateral ventricles (Singh (2017); Fig.1.1B).

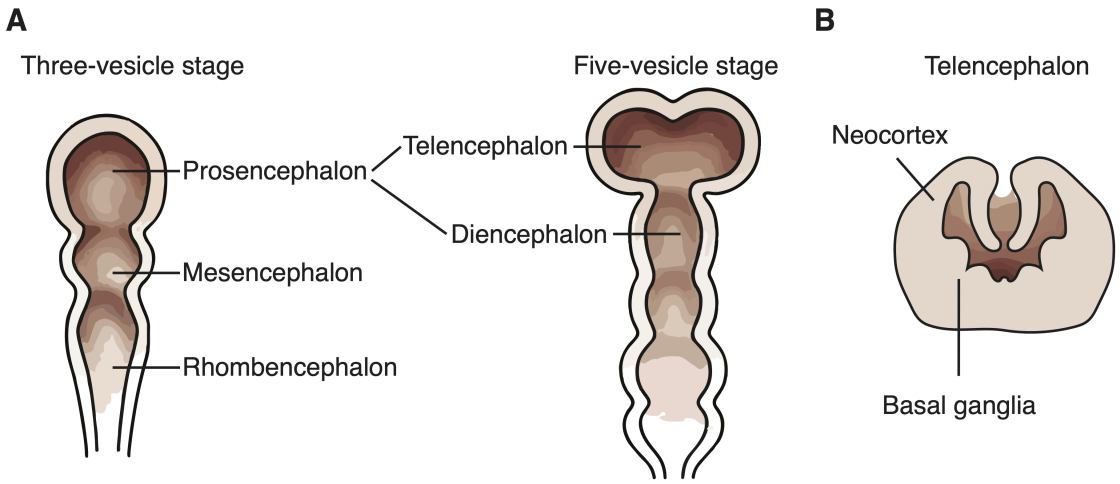

Figure 1.1: **Schematic of the central nervous system development. A.** Representation of the three- and the five-vesicle stage of brain development. **B.** Telencephalon subdivision into neocortex dorsally and basal ganglia ventrally. Adapted from Singh, 2017.

Neural progenitors in the telencephalon are cells that can divide a limited number of times and generate both neuronal and glial cell types (Malatesta et al., 2000; Haubensak et al., 2004; Noctor et al., 2004). They were described for the first time in 1885 by Camillo Golgi and characterized by others between the late 19th and the 20th century (Golgi (1885); Ramón y Cajal (1911); Rakic (2003); Fig.1.2). Neural progenitor cells are most commonly known as radial glial cells (RGCs) because of their elongated radial morphology. They differentiate from neuroepithelial cells (NECs) after the neural tube closure when unique markers for RGCs are expressed (Aaku-Saraste et al., 1996; Morest and Silver, 2003; Hatakeyama et al., 2004; Kageyama et al., 2008).

Radial glial progenitors are located in two transient proliferative zones in the developing brain: the ventricular zone (VZ) and the subventricular zone (SVZ). The VZ is the primary proliferative zone layering the ventricles while the SVZ is the secondary proliferative zone immediately basal to the VZ that appears during later stages of development in both dorsal and ventral telencephalon (Jay Angevine, 1970; Anderson et al., 1997). This zone can vary considerably between gyrencephalic and lissencephalic mammals and is further subdivided

into an outer SVZ (oSVZ) and an inner SVZ (iSVZ) (Smart et al., 2002). The oSVZ appears to be present in the developing cortex of most gyrencephalic mammals (Fietz et al., 2010; Borrell and Reillo, 2012), and only at later stages of neurogenesis in lissencephalic rat cortex (Martínez-Cerdeño et al., 2012). In the proliferative zones, RGCs undergo a phenomenon called interkinetic nuclear migration, meaning that the cell nucleus translocates apically or basally according to the cell cycle phase (Spear and Erickson, 2012). Based on their placement and mitosis location, RGCs can be categorized into apical progenitors (APs) and subapical progenitors (SAPs) in the VZ, and basal progenitors (BPs) in the SVZ (Taverna et al., 2014). In the dorsal VZ, APs initially divide symmetrically, producing additional RGCs and expanding the proliferative population (Takahashi et al., 1995; Cai et al., 2002; Noctor et al., 2008). At the onset of neurogenesis, APs begin undergoing asymmetric divisions (Caviness et al., 2003), which produce self-renewed RGCs, subtypes of BPs, and/or neuronal daughter cells. All of these progenitors appear to have the ability to self-renew and/or directly produce neurons (Malatesta et al., 2000; Hartfuss et al., 2001; Miyata et al., 2001, 2004; Noctor et al., 2001; Taverna et al., 2014). In the ventral telencephalon, there are fewer APs compared to BPs and SAPs (Pilz et al., 2013). While the divisions of BPs and SAPs can generate neurons, they also contribute to proliferative divisions, helping to expand the pool of progenitor cells (Götz and Huttner, 2005; Pilz et al., 2013). In general, the relative abundance of APs, BPs, and SAPs can vary between different telencephalic areas, neurogenesis stages, and species (Borrell and Reillo, 2012; Lui et al., 2011).

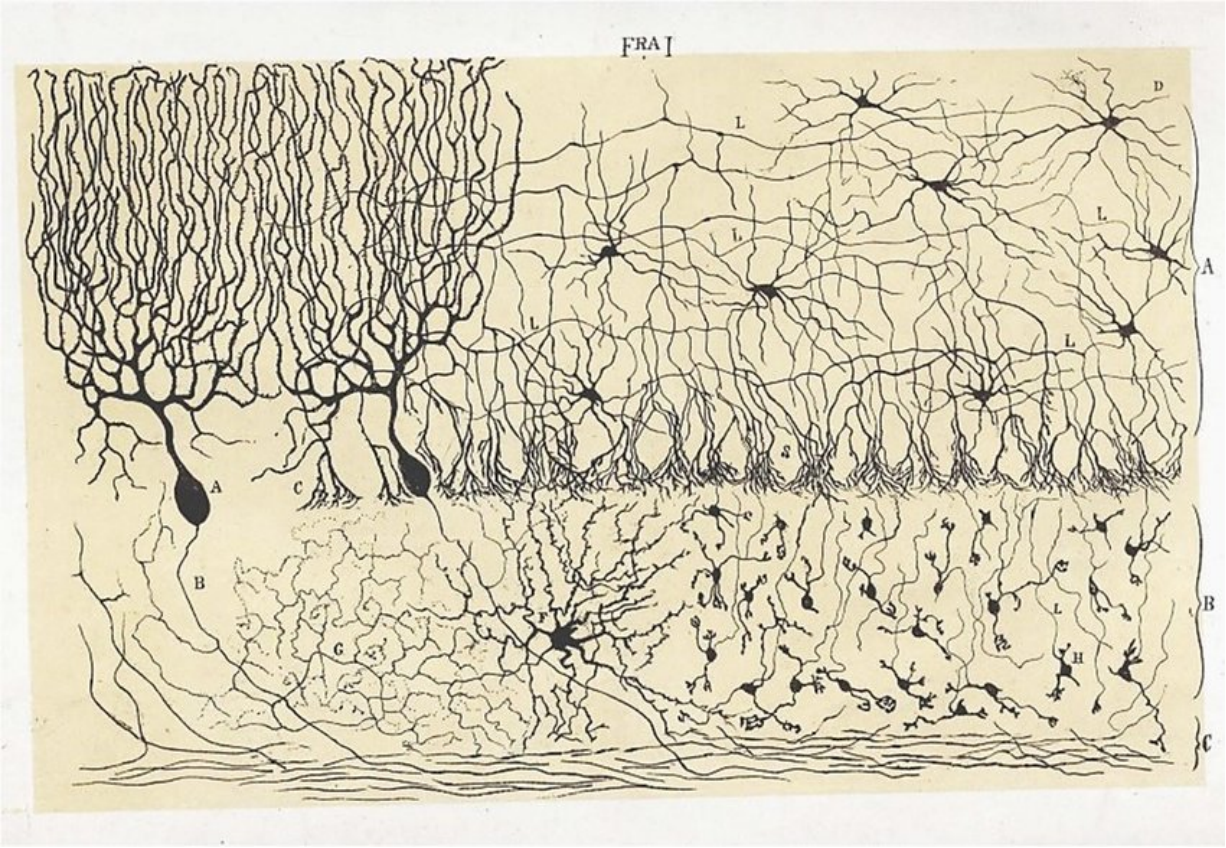

Figure 1.2: **Santiago Ramón y Cajal (1888), *Estructura de los centros nerviosos de las aves.*** Lithograph of the structure of the nervous centers of birds.

1.2 Developmental patterns of telencephalic neurons

External patterning signals organize the telencephalon in distinct domains along the dorso-ventral and anterior-posterior axes (Rubenstein et al., 1998; Wilson and Houart, 2004). In the dorsal telencephalon, RGCs give rise to the glutamatergic neurons of the mammalian cerebral cortex (Puelles et al., 2000) and can be distinguished by the expression of the nuclear transcription factor Pax6 (Götz et al., 1998) and Nes (Hockfield and McKay, 1985; Sunabori et al., 2008) in the VZ and Tbr2 in the SVZ (Englund et al., 2005). The proliferative zone in the ventral telencephalon gives rise to GABAergic neurons and is comprised of three transient structures, the medial, lateral, and caudal ganglionic eminences (MGE,

LGE, and CGE). Here, the RGCs also express Nes in the VZ and ventral-specific genes such as Gad2 and Ascl1 in the SVZ (Erlander et al., 1991; Castro et al., 2011; Le et al., 2017). Furthermore, each of the GEs is characterized by a distinct set of transcription factors. For example, Nkx2-1 is restricted to the MGE (Shimamura et al., 1995), Ebf1 to the LGE (Lobo et al., 2008), and Nr2f1 and Nr2f2 to the CGE (Hu et al., 2017; Mayer et al., 2018). The GABAergic cells originating from the GEs constitute a wide variety of regions in the telencephalon. The MGE produces cortical and striatal interneurons (Anderson et al., 2001; Wonders and Anderson, 2006; Xu et al., 2004; Flames et al., 2007), the LGE gives rise to medium spiny neurons that migrate to the striatum and interneurons that travel to the olfactory bulb (Olsson et al., 1998; Wichterle et al., 2001; Waclaw et al., 2009; Torigoe et al., 2016; Bandler et al., 2017). Finally, the CGE produces interneurons that will innervate the striatum, cortex, and amygdala (Nery et al., 2002; Miyoshi et al., 2010).

The developmental time window of neurogenesis varies widely across species. In mice, neurons are generated between embryonic days 11 and 17 (Caviness et al., 1995), in humans from gestation week 10 to 25 (Clancy et al., 2001). Numerous studies have attempted to model the patterning of different neuron types during development, considering factors like temporal and spatial coordinates or modes of division of mitotic cells. These efforts have led to the development of various theories, many of which continue to be widely debated today (Bandler et al., 2017; Telley and Jabaudon, 2018).

1.2.1 Development of glutamatergic neurons

Neurogenesis in the mammalian cerebral cortex follows a highly ordered developmental program, in which the six cortical layers (L1-L6) are generated sequentially. Early-born neurons form the deep layers (DLs), while late-born neurons give rise to the superficial layers (SLs) in an inside-out pattern (Fig.1.3, Rakic, 1974; Molyneaux et al., 2007; Gaspard

et al., 2008; Di Bella et al., 2021). DL neurons, located in L6 and L5, can be transcriptionally categorized into at least 20 distinct subtypes and primarily project to the subcortex. In contrast, SL neurons, found in L4 and L2/3, are transcriptionally classified into about 5 subtypes and mainly project within the cortex (Florio and Huttner, 2014; Govindan and Jabaudon, 2017; Tasic et al., 2018). Transplantation studies in ferrets in 1985 demonstrated that cortical progenitor cells are intrinsically committed to producing only one specific cortical layer (McConnell, 1985). Subsequent single-cell transcriptomic studies in mice revealed that the transcriptional states of APs are temporally regulated, resulting in progressively distinct neural fates (Yuzwa et al., 2017; Vitali et al., 2018; Telley et al., 2019).

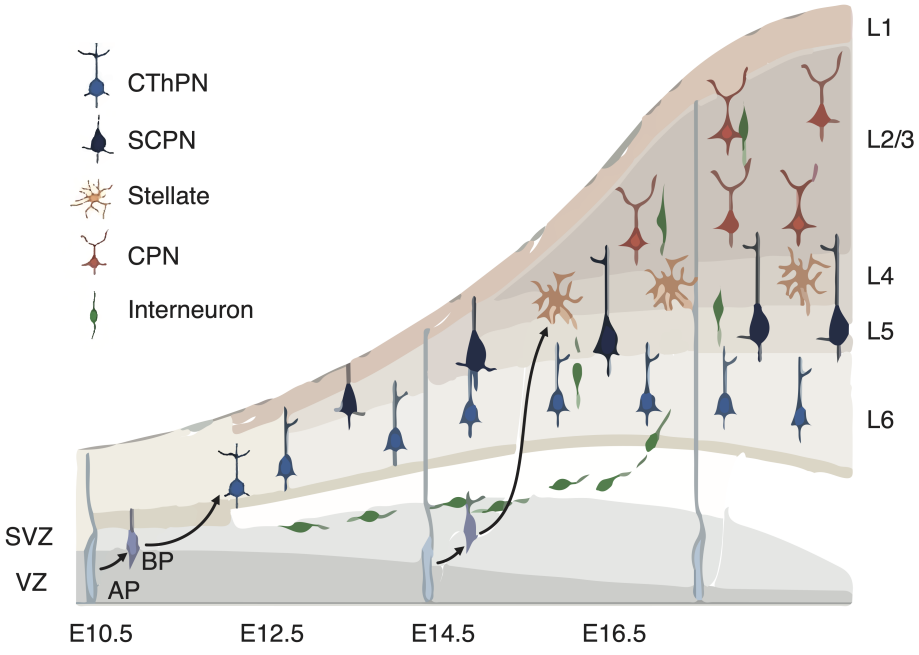

Figure 1.3: **Schematic of glutamatergic neurons development.** Representation of the inside-out pattern of cortical development. CThPN: corticothalamic projection neuron; SCPN: subcerebral projection neuron; CPN: callosal projection neuron; VZ: ventricular zone; SVZ: subventricular zone; AP: apical progenitor; BP: basal progenitor. Adapted from Di Bella *et al.*, 2021.

Early transplantation experiments also showed that progenitors are competent to respond to extrinsic cues, altering the fate of their daughter cells. However, this plasticity becomes increasingly limited as neurogenesis progresses (McConnell and Kaznowski, 1991). More detailed studies, combined with single-cell sequencing, revealed that in the dorsal telencephalon, APs remain temporally plastic while BPs undergo progressive fate restriction, losing the capacity to generate earlier cell types (Shen et al., 2006; Oberst et al., 2019).

1.2.2 Development of GABAergic neurons

In the ventral telencephalon, progenitors located in the GEs generate neurons that will migrate to multiple telencephalic areas, including the cortex, the basal ganglia, the olfactory bulb and limbic structures such as the amygdala and the nucleus accumbens (Fig.1.4, Wichterle et al., 2001; Nery et al., 2002; Wonders and Anderson, 2006), generating approximately 60 distinct transcriptomic neuron types (Tasic et al., 2018). These cell types are frequently located in distant and distinct brain regions, indicating that long-range migration and dispersion are common features among nearly all classes of telencephalic GABAergic neurons (van Velthoven et al., 2024). Among the different subpopulations of GABAergic neurons, most of somatostatin (Sst)-expressing neurons and all parvalbumin (Pvalb)-containing cells derive from the MGE whereas the majority of calretinin (Calb2)-containing cells and half of the neuropeptide y (Npy)-expressing neurons arise from the CGE (Gelman et al., 2011; Inan et al., 2012; Wonders et al., 2008). The different spiny projection neurons of the striatum originate in the LGE (Fentress et al., 1981). Several mechanisms have been shown to guide cell fate decisions in the ventral telencephalon, including spatial gradients of signaling factors (Flames et al., 2007; Xu et al., 2010; Brandão and Romcy-Pereira, 2015), cellular birthdates (Rymar and Sadikot, 2007; Bandler et al., 2017; Inan et al., 2012; Miyoshi and Fishell, 2011), and the mode of neurogenesis (Petros et al., 2015). Single-cell transcriptome studies have revealed that the initial gene expression

signatures of GABAergic neuron subtypes emerge soon after cells exit the cell cycle and before they migrate to their final locations within the telencephalon (Chen et al., 2017; Mayer et al., 2018; Mi et al., 2018). Furthermore, a clonal analysis with heritable DNA tags showed that during peak neurogenesis, individual mitotic progenitor cells in the GE possess the competence to generate inhibitory neurons with diverse transcriptomic signatures (Bandler et al., 2022). It remains debated whether different neuron subtypes are produced by distinct pools of committed progenitors or whether progenitors remain plastic and their competence is influenced by other factors that change during the course of neurogenesis (Hippenmeyer, 2023; Huilgol et al., 2023).

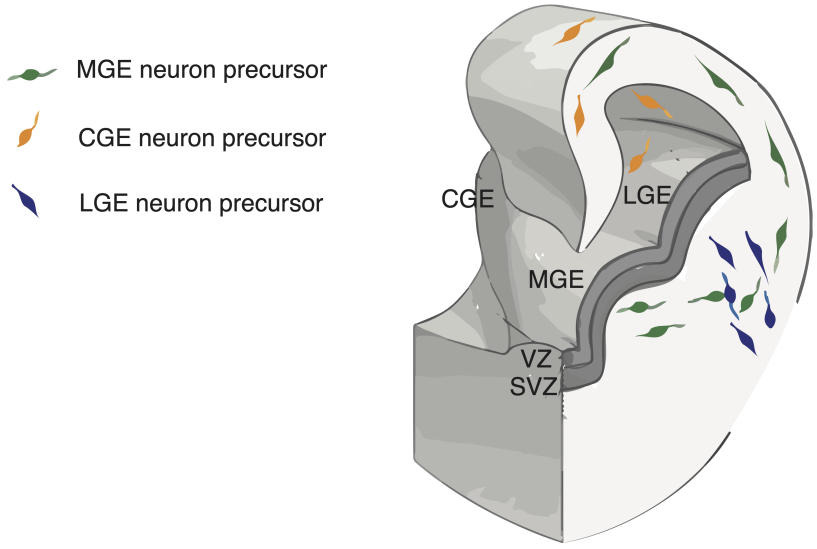

Figure 1.4: **Schematic of GABAergic neurons development.** Representation of the proliferative zones and neuronal precursors in the ventral telencephalon. MGE, CGE, LGE: medial, caudal, lateral ganglionic eminence; VZ: ventricular zone; SVZ: subventricular zone. Adapted from Turrero García and Harwell (2017).

1.3 Competence of neural progenitor cells

The developmental strategies of neuronal cell types are shaped by a combination of cell-intrinsic and cell-extrinsic properties. These properties define the competence of progenitor cells, which in turn influence the characteristics of their progeny (Vitali et al., 2018; Telley et al., 2019). Competence refers to a cell's ability to respond to various internal and external cues, determining how it will proceed in the differentiation and maturation processes. Differentiation is the procedure through which cells adopt specific fates, leading to the formation of distinct neuronal cell types. Maturation refers to the process by which a cell achieves its full functional potential and adaptability (Alvarez-Dominguez and Melton, 2022). Research showed that the competence of progenitor cells can shift over time; for example, dorsal neural progenitors gradually lose the ability to produce early-born cell types (competence restriction) and acquire the ability to produce later-born cells, meaning that each neural cell type in the cortex has a restricted time-frame for specification (Desai and McConnell, 2000).

1.3.1 Intrinsic factors

Intrinsic factors are cell-autonomous mechanisms that include genetic programs, transcription factors, and epigenetic modifications. They regulate the expression of specific protein sets that define the unique structure, activity, and response to signals of each neuronal type.

Specific transcription factors play key roles in determining the identity and competence of neuronal progenitors by activating or repressing lineage-specific genes. For example, basic helix-loop-helix (bHLH) factors like Neurog2, Ascl1, and Olig2 are key transcription factors that control whether progenitors become neurons, astrocytes, or oligodendrocytes (Bertrand et al., 2002; Ross et al., 2003; Meijer et al., 2012; Namihira and Nakashima, 2013).

Another finely regulated process in neurogenesis is the self-renewal versus differentiation of progenitor cells. Here, Hes1 is a bHLH factor that regulates self-renewal by directly repressing the expression of Neurog2 or Ascl1 (Bertrand et al., 2002; Hatakeyama et al., 2004; Imayoshi et al., 2008).

Epigenetic modifications include alterations in chromatin structure, DNA methylation, and histone modifications, which introduce an additional layer of regulation to gene expression. The transition from neuroepithelial cell to progenitor to postmitotic neuron involves considerable chromatin structure rearrangements, where a more open chromatin landscape (euchromatin) gradually transitions to cell-type-specific patterns of more closed chromatin (heterochromatin) (Stergachis et al., 2013). In this scenario, the consolidation of heterochromatin includes increased interactions on a large scale within topologically associating domains (TADs) that contain neuronal genes (Bonev et al., 2017). TADs are genomic regions characterized by a high level of self-interaction, therefore they are considered functional units of the genome. Multiple enhancers per gene can be found within each TAD, potentially allowing for more complex regulation of the timing and cell-type specificity of gene expression (Closser et al., 2022). Transcription factors can promote chromatin opening or closing and, in some cases, may perform both roles depending on their site of action. For instance, FOXP2 represses the expression of genes that characterize progenitor cells in the deeper layers of the cortex, and, in collaboration with NFI cofactors, it promotes euchromatin for genes related to cell maturation (Hickey et al., 2019).

Histone modifications link epigenetic changes at individual loci to larger-scale changes in chromatin, facilitating the fine-tuning of spatiotemporal gene expressions during neurogenesis. Distinct, reversible histone modifications, such as methylation and acetylation, are associated with the repressing or activating of genes at individual loci. For example, histone methylation can be considered an active mark or a repressive mark of transcription, depending on the methylated residue. Methylation of histone H3 on lysine 4 (H3K4),

lysine 36 (H3K36), lysine 79 (H3K79), or arginine 17 (H3R17) is largely involved in transcriptional activation (Di Nisio et al., 2021). Various histone-modifying enzymes catalyze the addition or removal of a specific histone modification (Kouzarides, 2007), and their expression is closely linked to the regulation of key neurogenesis processes. For instance, during the cerebral cortex development, the loss of EZH2, an H3K27 methyltransferase, disrupts neurogenesis timing and affects the proportions of different cell types, leading to premature neuronal differentiation (Pereira et al., 2010).

1.3.2 Extrinsic factors

Extrinsic factors include external signals from the environment—such as growth factors, signaling molecules, and cell-cell interactions—that influence the competence of neuronal progenitors. These extrinsic factors act both as fate determinants and as synchronizers of overall neurogenesis activity (Camacho-Aguilar and Warmflash, 2020). Signaling molecules or morphogens are released in a gradient from specific regions within the developing tissue. Progenitor cells respond differently to these signals depending on their proximity to the source and the duration of exposure (Sugimori et al., 2007). This mechanism enables a vast diversity of progenitor cell types to arise from a relatively small set of genes. For instance, during spinal cord development, progenitor pools commit to different fates in response to morphogen gradients, most notably Sonic hedgehog (Shh)(Briscoe et al., 2000; Placzek and Briscoe, 2005). Extracellular signaling molecules can also act as regulators of neuronal production, as in the case of Wnt activity (Chenn and Walsh, 2002; Machon et al., 2007). At early stages of corticogenesis, downregulation of WNT signaling primarily decreases precursor proliferation (Woodhead et al., 2006), while at later stages it also inhibits neuronal production (Munji et al., 2011).

1.4 Methods for analyzing cell development

To investigate cell development and commitment in complex organisms, numerous techniques have been developed over the years to label cells *in vivo* and analyze their contributions to embryonic development. Early approaches relied on non-transgenic methods, such as direct observation in transparent organisms (Sulston et al., 1983), injection of non-specific markers (Beddington, 1982; Grimm et al., 2017), and cell or tissue transplantation (Le Douarin, 1993; Pașca, 2024). Advances in genetic engineering have introduced more sophisticated techniques based on retroviral injection (Stuhlmann et al., 1984; Turner and Cepko, 1987; Yamashita and Emerman, 2006), genetic recombination (Nagy, 2000; Grindley et al., 2006; Jensen and Dymecki, 2014), or plasmid transfection (Figueres-Oñate et al., 2019). The use of these methods is designed to be temporally and spatially regulated while minimizing disruption to the organism's development. In recent years, the integration of cell development analysis with single-cell technologies (Tang et al., 2009; Trapnell et al., 2014; Stuart et al., 2019) and CRISPR systems (Dixit et al., 2016; Alemany et al., 2018) has enabled unprecedented levels of resolution and information. Computational methods for reconstructing lineage trajectories from cell transcriptomes have also considerably advanced (Cannoodt et al., 2016; Wagner and Klein, 2020). Various algorithms have been developed, based on dimensionality reduction, nearest neighbor graph, or hierarchical clustering (Kester and van Oudenaarden, 2018). In this study, a combination of transgenic and non-transgenic analysis approaches was utilized alongside single-cell methods and dimensionality reduction algorithms, to investigate the competence of GABAergic neuron progenitors in the telencephalon.

1.4.1 Clonal tracking: TrackerSeq

Clonal tracking techniques mark a progenitor cell and its descendants, allowing the construction of genealogical trees that trace increasingly committed cells as development progresses. The diversity of cell types found in the progeny is representative of the fate potential of the original cell and its commitment at the time of the experiment. In this study, a method known as TrackerSeq (Bandler et al., 2022) was utilized to explore the clonal relationships between GABAergic progenitors and their daughter cells. TrackerSeq is a technique where a library of genetic barcodes is utilized to mark cells and track their relationships as the organism develops. To obtain the barcodes, a high complexity library of 37–bp synthetic nucleotides is generated. Each barcode is cloned into the 3′ untranslated region of eGFP in a plasmid. Plasmids containing the barcoded eGFP reporter cassette and a piggyBac transposon are then electroporated into the cells where they integrate into the genome through the cut-and-paste mechanism of the transposon (Ding et al., 2005). This method is effective because it can tag mitotic progenitors in the ganglionic eminences and is highly efficient, leveraging the diverse barcode library (approximately 4.3 million lineage barcodes), the precision of electroporation (Saito and Nakatsuji, 2001), and the efficiency of the piggyBac transposon (Kim and Pyykko, 2011).

1.4.2 Birthdating method: FlashTag

Birthdating techniques monitor isochronic cell populations from the moment of their birth to the time of collection, providing insights into the temporal changes in their progenitors' competence. The most widely used birthdating methods are BrdU or EdU labeling, which are thymidine analogs incorporated into cells during DNA synthesis (S phase of the cell cycle; Miller and Nowakowski (1988); Zeng et al. (2010). Historically this method is used to trace cohorts of cells born at the same time, however, this definition is imprecise: labeling

during the S phase prevents tracking the exact moment when the targeted cells exit the cell cycle, as they might stay in a mitotic state and keep self-renewing. In this study, a birthdating technique called FlashTag (FT) was utilized, which labels cells that are adjacent to the ventricular surface during the M phase of the cell cycle due to the interkinetic nuclear migration (Govindan et al., 2018). The labeling works by injecting a carboxyfluorescein succinimidyl ester (CFSE) dye into the mouse ventricles. Once the CFSE enters the cell cytoplasm, it undergoes cleavage and emits fluorescence. It gets diluted with each cell division and is fully retained only in the newly born neurons that exit the cell cycle shortly after the dye injection. This allows a more precise tracing of isochronic cohorts of newborn neurons in comparison to other techniques.

1.4.3 Transplantation-based method

Fate mapping of neuronal progenitor cells consists of marking them in the embryo at a specific time and place and then determining what these cells and all their descendants become after development is complete. One way of achieving cell fate mapping is by transplantation of labeled cells into a host. This technique allows the monitoring of contributions of progenitor cells to the embryo and studying the influence of intrinsic versus extrinsic factors in processes such as cell migration and specification (Cunningham and McKay, 1994). Moving a cell to a different anatomical area (heterotopic transplantation) or into a different developmental time (heterochronic transplantation) can reveal the extent to which extrinsic cues act upon its competence. Transplantation of embryonic LGE and MGE progenitors to postnatal mouse cortex revealed that the unique migratory potentials of inhibitory cells are intrinsic and linked to the germinal zone they originate from (Campbell et al., 1995; Wichterle et al., 1999). However, transplantation of striatal precursors into distinct telencephalic regions led to distinct morphologies and axonal projections, specific to the area of their final location (Fishell, 1995). Pioneering studies that utilize

heterochronic transplantation of early and late cortical progenitors in ferrets revealed that their fate potential changes over time, and their competence to generate diverse cell types becomes gradually restricted (McConnell and Kaznowski, 1991; Frantz and McConnell, 1996). These findings were later confirmed by combining transplantation techniques with single-cell analysis, which enabled studying differences in competence for each progenitor subtype (Oberst et al., 2019).

2 Aims of the study

The objective of this study was to offer new insights into the competence of inhibitory neuron progenitors in the telencephalon, examining how it changes during neurogenesis and how it affects the downstream neurons they generate. To achieve this, this study is divided into four parts, each addressing a different question:

1. What is the genetic landscape of the inhibitory lineage in progenitors and precursors at different stages of neurogenesis, and how does it differ from the excitatory lineage? To answer this, transcriptome data that includes inhibitory progenitors and precursors at different stages of neurogenesis were explored and compared to their excitatory counterparts.

2. What is the clonal output and fate commitment of inhibitory progenitors? To answer this, two TrackerSeq datasets from early and late time points were compared, revealing the clonal relationships and the transcriptomes of inhibitory progenitors. The clonal analysis and the comparison between stages helped to shed light on the differentiation competence and fate commitment of inhibitory progenitor cells on a single-cell level.

3. How does progenitor competence evolve during neurogenesis, and how does this impact their neuronal daughter cells? To address this, isochronic cohorts of neurons were investigated. Different injection and collection times were employed to focus on the newly born neurons and the transcriptomic signatures transmitted from their progenitor cells. This analysis revealed important insights into the maturation competence of GABAergic progenitors.

4. What intrinsic and extrinsic factors influence the competence of inhibitory neuron progenitors? To explore the intrinsic information carried by progenitor cells beyond the transcriptome level, chromatin, and gene interactions were investigated. Furthermore, transplantation experiments were conducted to study extrinsic mechanisms that might act upon progenitor competence.

3 Materials and Methods

3.1 Animals

All experiments were conducted according to institutional guidelines of the Max Planck Society and the regulations of the Bavarian government ethical committee. Mice were group housed in isolated ventilated cages (room temperature $22 \pm 1°C$, relative humidity $55 \pm 5\%$) under a 12 h dark/light cycle with ad libitum access to food and water. Embryos were staged in days post-coitus, with embryonic day (E) 0.5 defined as 12:00 of the day a vaginal plug was detected after overnight mating.

Strain name	Common name	Reference
C57BL/6NRj	-	Janvier Labs
Tg(dlx6a-cre)1Mekk	Dlx6-Cre	JAX:008199 (Monory et al., 2006)
Rosa26LSL-tdTomato	Ai9	JAX:007909 (Madisen et al., 2010)

Table 3.1: List of mouse strains utilized in the study.

3.2 Single cell transcriptome datasets

3.2.1 Experiment design and sample preparation

Single-cell RNA sequencing

Brains from Dlx5/6-Cre::tdTomato mouse embryos were collected at E12.5, E14.5 or E16.5 in ice-cold L-15 medium (Thermo Fisher Scientific, 11415064) containing 5% FBS. Ganglionic eminences were manually dissected and dissociated with the Miltenyi BioTech Neural Tissue Dissociation Kit (P) (#130-092-628) on a gentleMACS Dissociator according to the manufacturer's protocol. From the same brains, cortical and striatal regions were dissected, dissociated, and FACS-enriched for tdTomato-positive cells using a SY3200 Cell Sorter (software WinList3D version 8.0.2) or BD FACSAria III Cell Sorter (BD FACSDiva Software, version 8.0.2) with a 100 µm nozzle. Finally, TdTomato-positive neurons from the cortex and striatum were pooled with neurons from the ganglionic eminences (GEs), and scRNA-seq was performed (Fig.3.1). Three embryos per replicate were utilized for a total of 6 embryos for E12.5 and E16.5 and 3 embryos for E14.5 (Table3.2).

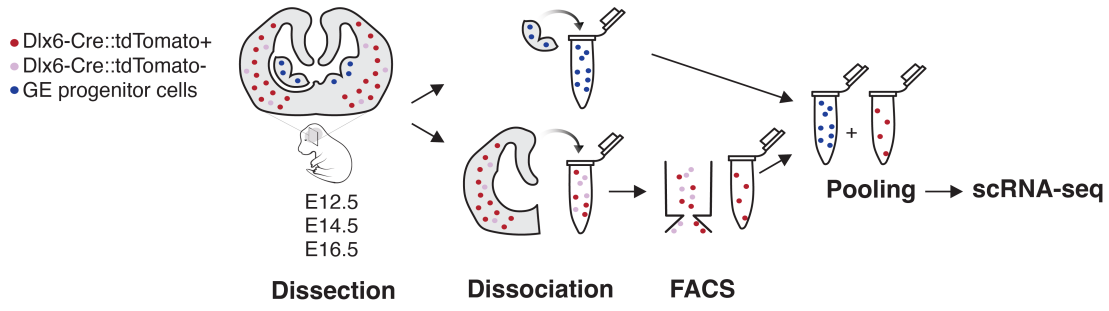

Figure 3.1: **Sample preparation and collection to generate the scRNA-seq datasets.** Embryonic brain areas are dissected and dissociated into a cell suspension at E12.5, E14.5, and E16.5. Fluorescence-activated cell sorting (FACS) is utilized to enrich cell states of interest. After cell pooling, single-cell RNA sequencing is performed.

Single-cell RNA sequencing combined with TrackerSeq

Timed pregnant mice were anesthetized with isoflurane (5% induction, 3% during the surgery) and treated with the analgesic Metamizol (WDT). The TrackerSeq library was prepared according to the protocol from Bandler et al. (2022). For *in utero* electroporation (IUE) at E16.5, embryos were injected unilaterally in the lateral ventricle with 700 nL of DNA plasmid solution made of 0.5 µg µL^{-1} pEF1a-pBase (piggyBac-transposase) and the TrackerSeq library 0.5 µg µL^{-1}, diluted in endo-free TE buffer and 0.002% Fast Green FCF (Sigma). Embryos were then electroporated with 5 electric pulses (50 V, 50 ms at 1 Hz) with a square-wave electroporator (BTX, ECM 830). GFP-positive cells were isolated with FACS 96 hours later, and scRNA-seq was performed (Fig.3.2).

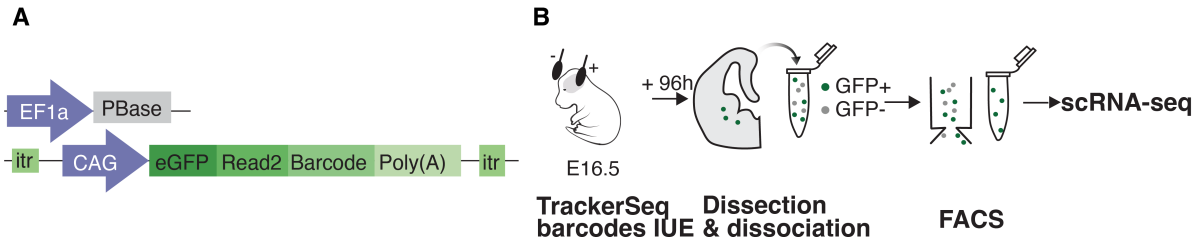

Figure 3.2: **Schematic representation of the experimental procedure to generate the TrackerSeq dataset. A.** Vector maps of TrackerSeq. PBase: piggyBac transposase. **B.** Experimental workflow to generate scRNA-seq datasets of clonally related cells. IUE: *in-utero* electroporation.

Single-cell RNA sequencing combined with FlashTag

Timed pregnant mice were anesthetized with isoflurane and treated with the analgesic Metamizol as previously described. A CFSE working solution was prepared by adding 8 µL of DMSO and 1 µL of Fast Green to one vial of CellTrace CFSE (CellTraceTM CFSE, Life Technologies, #C34554) for a final concentration of 10 mM, following the instructions from Govindan et al. (2018). To generate $\mathbf{FT_{E12.5\ +\ 6h}}$ **and** $\mathbf{FT_{E16.5\ +\ 6h}}$,

500 nL of CFSE working solution was injected into ventricles of wild-type C57BL/6NRj embryos at E12.5 and E16.5 respectively. The abdominal wall was then closed, and the embryos were left to develop until collection. After six hours, GEs were manually dissected and dissociated on the gentleMACS Dissociator according to the manufacturer's protocol (Fig.3.3A,B). FlashTag positive cells with high intensity ($> 10^5$) were sorted using FACS and scRNA-seq was performed (Fig.3.3C). **For $\mathbf{FT_{E12.5\ +\ 96h}}$**, 500 nL of CFSE working solution was injected into ventricles of Dlx5/6-Cre::tdTomato embryos at E12.5. After 96 hours, the striatum and cortex were dissected and dissociated on the gentleMACS Dissociator. FlashTag and tdTomato positive cells were sorted using FACS, and scRNA-seq was performed (Fig.3.3A,B).

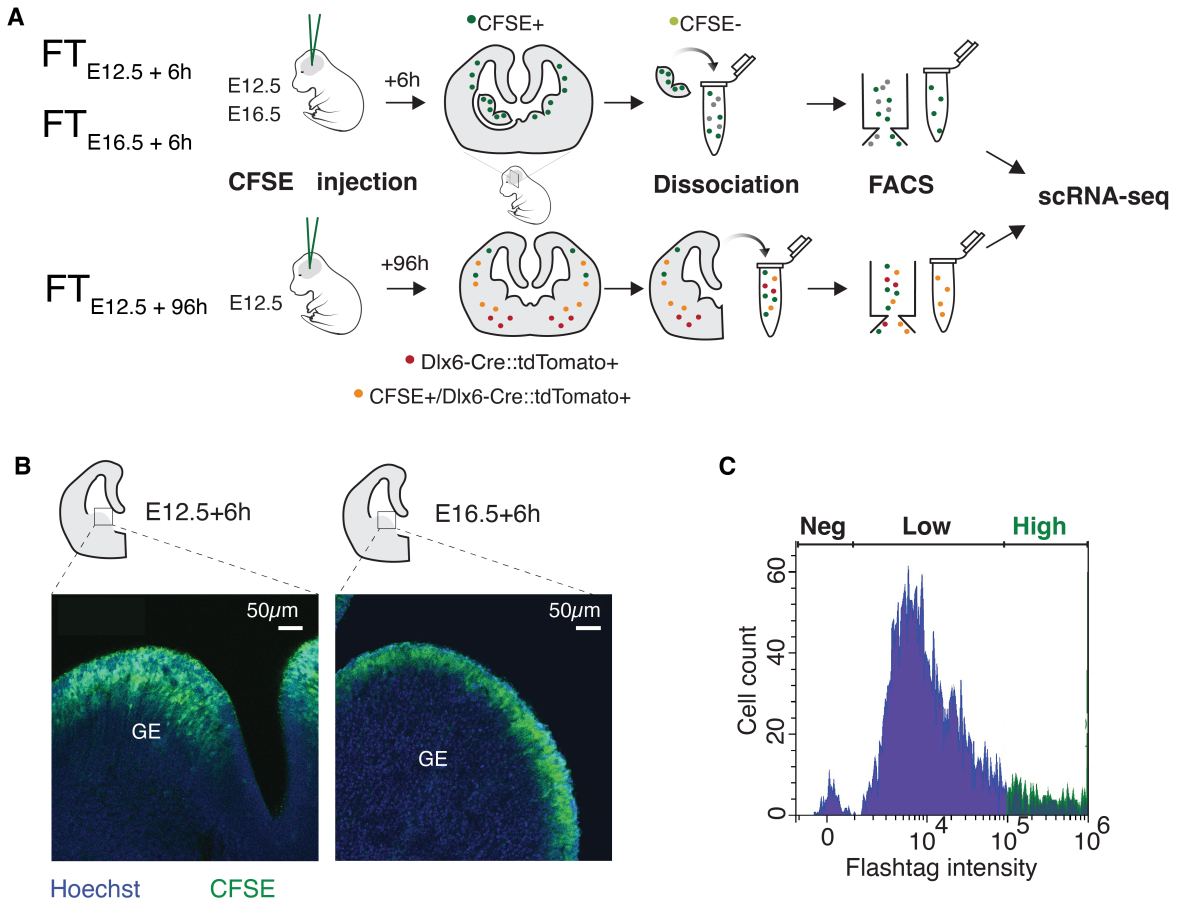

Figure 3.3: **Schematic representation of the experimental procedure to generate the FlashTag dataset. A**. Experimental procedure to create scRNA-seq datasets of cells labeled with FlashTag at different injection and collection time points. **B.** Coronal sections of ganglionic eminences at E12.5 and E16.5 six hours after injection with CFSE. GE: ganglionic eminence. **C.** FlashTag intensity cut-off utilized for fluorescence-activated cell sorting.

3.2.2 Library preparation

Single-cell RNA sequencing

For experiments employing the 10x Genomics platform, Chromium Single Cell 3' Library & Gel Bead Kit v3 (PN-1000075), Chromium Single Cell 3' Chip Kit v3 (PN-1000073),

Dataset type	Stage	Replicates	Embryos
scRNA-Seq	E12.5	2	6
scRNA-Seq	E14.5	1	3
scRNA-Seq	E16.5	2	6
TrackerSeq	E16.5+96h	1	1
FlashTag	E12.5+6h	2	6
FlashTag	E16.5+6h	2	6
FlashTag	E12.5+96h	1	3

Table 3.2: Overview of the datasets, the number replicates and the number of animals utilized in experiments involving scRNA-seq.

and Chromium i7 Multiplex Kit (PN-120262) were used according to the manufacturer's instructions. Additionally, Chromium Single Cell 3' Library & Gel Bead Kit v3.1 (PN-1000268), Chromium Single Cell 3' Chip Kit v3.1 (PN-1000127), and Dual Index Kit TT Set A (PN-1000215) were used according to the manufacturer's instructions in the Chromium Single Cell 3' Reagents Kits v3.1 User Guide (Dual Index). Libraries were quantified using a BioAnalyzer (Agilent) and sequenced either on an Illumina NextSeq500 or Novaseq at the Genomics Core Facility of the Helmholtz Center, at the Next Generation Facility of the Max Planck Institute of Biochemistry, or at MLL Münchner Leukämielabor GmbH.

TrackerSeq

The lineage barcode library retrieved from RNA was amplified with a standard NEB protocol for Q5 Hot Start High-Fidelity 2X Master Mix (#M094S) in a 50 µL reaction, using 10 µL of cDNA as a template. 2 PCR Mix:

- 25 µL Q5 High-fidelity 2X Master Mix
- 2.5 µL 10 µmol P7 indexed reverse primer
- 2.5 µL 10 µmol i5 indexed forward primer
- 10 µL molecular-grade H2O

- 10 µL cDNA

PCR protocol:

1. 98 °C for 30 s
2. 98 °C for 10 s
3. 63 °C for 20 s
4. 72 °C for 10 s
5. repeat steps 2–4 for 11 to 18 times
6. 72 °C for 2 min
7. 4 °C hold

Libraries were purified with a dual-sided SPRI selection using Beckman Coulter Agencourt RNAClean XP beads (Beckman Coulter, A63987) and quantified with a BioAnalyzer.

3.2.3 Analysis

Sequencing reads were processed using CellRanger v3.0.2 or v6.1.2 (Zheng et al., 2017), using the mouse reference genome mm10 v2.1.0. Resulting count matrices were analyzed using the Seurat package v4.3.0 (Hao et al., 2021) in R v4.1.0. For each dataset, high-quality cells were filtered by the number of genes and mitochondrial read fraction (Fig.3.4). Subsequently, counts were normalized and corrected for sequencing depth using Seurat's *NormalizeData* function. Cell-cycle assignments for each cell were calculated using the cell-cycle gene list from (Tirosh et al., 2016).

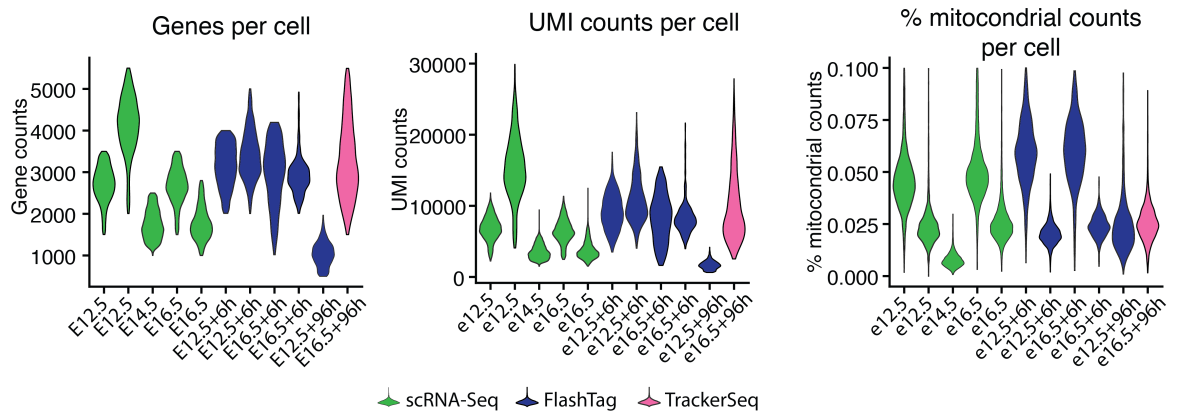

Figure 3.4: **Summary of data quality metrics.**Violin plot illustrating the number of genes, counts, and mitochondrial gene fraction per cell for each replicate.

After identification of highly variable features as described in (Butler et al., 2018), scaled gene-expression values were calculated by applying z-normalisation to the 2000 most variable genes, whilst simultaneously regressing out unwanted sources of variation: sequencing-depth, feature-depth, mitochondrial read fraction, and estimated difference between cell-cycle phases with the *ScaleData* function (Fig.3.4). The *FindClusters* function was used to identify cell clusters. The *FindAllMarkers* function was used to identify cluster marker genes. Clusters with marker genes of excitatory neurons (e.g. Neurod1, Neurod6, Tbr2) or non-neuronal cells (e.g. Apoe, Olig1, Flt1, Pdgfra) were filtered out and excluded from the following steps. Raw counts of samples from scRNASeq, TrackerSeq, and FlashTag datasets were merged using the Seurat package and aligned using Monocle3 v1.0.0 (Trapnell et al., 2014; Qiu et al., 2017; Cao et al., 2019; Fig.3.5A). For this purpose, the scaled matrix from the Seurat object was converted into a Monocle3 object of the cell_data_set class and preprocessed without the default normalisation, as the dataset was already normalised. Batch-correction was performed using Batchelor v1.8.1 (Haghverdi et al., 2018) followed by Leiden-clustering (using fine resolution) and dimensional reduction using UMAP (McInnes et al., 2020). A developmental trajectory was fitted as a

principal graph through fine clusters based on the UMAP-embedding. The root of the trajectory was defined as the cells with the highest Nestin gene expression, identified in the "Fabp7" cluster. A pseudotime score was assigned to each cell based on its projected position on the trajectoryFig (3.5B). Leiden clustering (using coarser resolution in Monocle3) identified distinct clusters of cell states. Marker genes specific to each cluster were identified by running differential expression analysis (in Seurat) using the *FindAllMarkers* function. Clusters were manually annotated based on marker gene expression. The transition between mitotic and postmitotic cells was defined by selecting the highest pseudotime score of mitotic clusters as the threshold (3.5C).

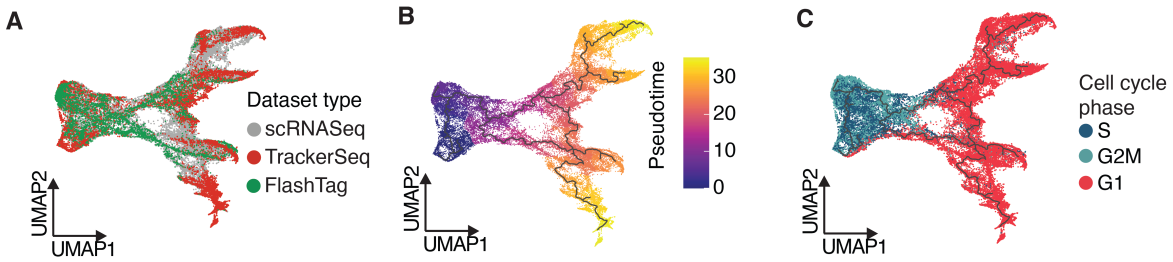

Figure 3.5: **Summary of datasets collected with different methods to investigate the competence of progenitors located in the ganglionic eminences.** UMAP plot depicting single cells derived from scRNAseq, TrackerSeq, and FlashTag datasets aligned in Monocle3. Cells are coloured by **A.** Dataset type, **B.** Pseudotime score, **C.** Cell cycle phase.

Merging the transcriptome data to publicly available datasets

For this analysis, publicly available datasets were utilized: raw counts of e13.5 and e15.5 datasets from (Bandler et al., 2022) (GSE IDs: GSM5684874, GSM5684875, GSM5684876, GSM5684877, GSM5684878, and GSM5684879) and raw counts from the developing mouse somatosensory cortex (Di Bella et al., 2021) at stages E12.5 to E16.5 (GSE IDs: GSM4635073, GSM4635074, GSM4635075, GSM4635076, and GSM4635077). The count matrices were merged with the scRNASeq datasets to create a combined Seurat object (Fig.3.6A). Cells

were filtered based on the mitochondrial read fraction ($\leq 10\%$). Normalization, scaling, batch correction, dimensionality reduction, and clustering were performed as previously described (Fig.3.6B,C). Clusters were manually annotated based on top marker gene expression. For cells originating from Di Bella *et al.*, we utilized the annotations available from the original paper (Di Bella et al., 2021).

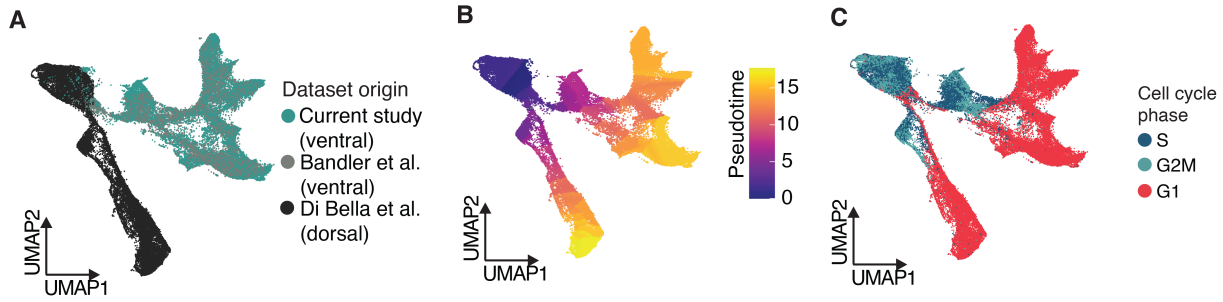

Figure 3.6: **Summary of merged scRNA-seq datasets of inhibitory and excitatory cells.** UMAP plot depicting single cells derived from datasets of this study, from Bandler et al. (2022) and from Di Bella et al. (2021). The datasets are aligned in Monocle3 and coloured by **A.** Dataset origin, **B.** Pseudotime score, **C.** Cell cycle phase.

To screen for variable genes along the pseudotime trajectory in inhibitory and excitatory lineages, the following steps were performed:

(1) For each lineage, cells were binned from each stage into ten sections based on their inferred pseudotime.

(2) Enriched genes were selected based on two criteria: high expression and high gene abundance. High expression was inferred by calculating the fold change between the expression in all cells inside the bin compared to all cells outside the bin. High gene abundance was calculated by comparing the fraction of cells that express a gene inside versus outside the bin (a gene was considered to be expressed in a cell if its scaled expression value was higher than 0.5).

(3) A normal distribution was fitted to the changes in expression and abundance. Significantly enriched genes were selected when the difference in expression and abundance was

higher than the corresponding average difference plus two times the standard deviation of the corresponding fitted distribution.

(4) Steps two and three were repeated for each bin.

(5) The trajectory of inhibitory neurons branches out as cells leave the cell cycle, therefore this algorithm was run for each branch independently and only genes that appeared in at least two out of five branches were selected.

TrackerSeq analysis

TrackerSeq barcode reads were pre-processed as described in (Bandler et al., 2022). To assess the clonal coupling between cell states, z-scores between clusters were calculated (Wagner et al., 2018). The z-score is defined as the number of shared barcodes relative to randomized data, with values ranging from positive (coupled clusters) to negative (anti-coupled clusters). These random permutations were used to calculate empirical P-values. For coupled pairs of clusters, the null hypothesis is that the observed coupling is not higher than random coupling. Conversely, for anticoupled pairs, the null hypothesis is that the observed coupling is not lower than random couplings. A random coupling is in contradiction to the null hypothesis when a permutation for one pair of clusters scores above the observed coupling (for positively coupled pairs), or below the observed coupling (for negatively coupled pairs). The relative fraction is reflected in the empirical P-value, which was consequently corrected for multiple comparisons using the Benjamini-Hochberg (FDR) method (Benjamini and Hochberg, 1995).

Clones were identified as “dispersing” or “non-dispersing” depending on whether their cells were distributed in multiple or just one branch tip, respectively. To test whether the transcriptome of mitotic progenitors in “non-dispersing” clones was predictive of their postmitotic state, “non-dispersing” clones were grouped by their postmitotic cell state in

both $\text{TrackerSeq}_{\text{E12.5 + 96h}}$ and $\text{TrackerSeq}_{\text{E16.5 + 96h}}$ combined. Separate data frames were created for mitotic and postmitotic subsets of each group. Pearson correlation coefficients were calculated between pairs of gene expression within different subsets, generating all the possible combinations of pairs within the columns of the data frames. The subsets of postmitotic clones, mitotic clones, and randomly selected mitotic cells were all correlated to the postmitotic reference group.

3.3 Chromatin accessibility datasets

3.3.1 Sample and library preparation

Sample preparation was performed following the same procedure as for $\text{FT}_{\text{E12.5 + 6h}}$ and $\text{FT}_{\text{E16.5 + 6h}}$ in the previous section. Single-cell ATAC-seq was performed according to the Chromium Single Cell ATAC Reagent Kits v1 user guide (10x Genomics). FACS sorted cells were centrifuged at 500 rcf for 5 min at 4 °C and resuspended in 100 µL chilled diluted lysis buffer and incubated for 5 min at 4 °C. 1 ml of chilled wash buffer was added to the lysed cells and mixed five times with a pipette, followed by centrifugation at 500 rcf for 5 min at 4°C. The isolated nuclei were counted (using a c-chip hemocytometer) and resuspended in an appropriate volume of chilled diluted nuclei buffer to reach the desired final nuclei concentration. The nuclei were immediately used to generate single-cell ATAC libraries, followed by paired-end sequencing on the Illumina NextSeq 500 platform (Fig.3.7.

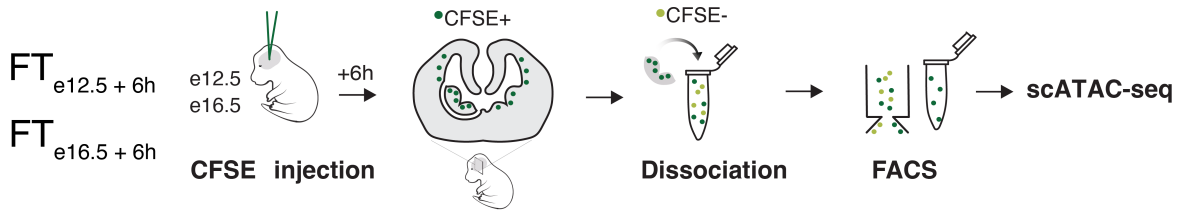

Figure 3.7: **Schematic of the experimental steps to obtain the FlashTag-labelled scATAC-seq datasets.**

3.3.2 Analysis

The analysis of scATAC-seq data in this study was carried out in collaboration with Dr. Ann Rose Bright

The raw sequencing data (BCL file) were converted to the fastq format using *cellranger-atac mkfastq* function from Cell Ranger ATAC v1.2.0 (Satpathy et al., 2019). The reads were aligned to the mm10 (GRCm38) mouse reference genome and fragment files were generated using the *cellranger-atac count* function. Both time points included 2 replicates, and the aligned fragment files were converted to arrow files and analyzed further using the ArchR package v1.0.1 (Granja et al., 2021). Dimensionality reduction was performed using latent semantic indexing (LSI), followed by batch correction using Harmony v0.1.1 (Korsunsky et al., 2019). To extract the trajectories of interest and integrate them into an ArchRProject, the *getTrajectory* and *addTrajectory* functions were run. Pseudotime heatmaps were generated to visualize enriched motifs.

Temporal dynamics and coverage plots

Peak calling was performed using *addReproduciblePeakSet* function, which runs MACS2 (Zhang et al., 2008) to identify marker peaks for $\mathrm{FT}_{\mathrm{E12.5\ +\ 6h}}$ and $\mathrm{FT}_{\mathrm{E16.5\ +\ 6h}}$ datasets. To

categorize peak sets into unique and overlapping peaks, the *findoverlap* function was used. For both scATAC-seq and H3K4me3 ChIP-seq datasets, coverage for each peak category was calculated using the *ScoreMatrixList* function.

Transcription factor footprint analysis

Footprint analysis was carried out on $FT_{E12.5 + 6h}$ and $FT_{E16.5 + 6h}$ datasets using transcription factor occupancy prediction tool: TOBIAS v0.14.0 (Bentsen et al., 2020). We employed the Jaspar non-redundant motif database (Castro-Mondragon et al., 2022) as the primary reference source for motif data. Bias correction was performed to generate corrected bigwig files using the *ATACorrect* function with default parameters. Footprint scores were calculated on corrected bigwig files using the *FootprintScores* function, and differential binding TFs were detected using *BINDetect* function. Predicted TFs were categorised as significant based on two criteria: their differential binding score (greater than 0.2 for E12.5 and less than –0.4 for E16.5:referred to as change) and the –log10 of the p-value from the statistical test against a background model. The footprints were visualized using the *PlotAggregate* and *PlotHeatmap* functions.

Co-binding analysis

To detect co-occurring TF binding sites, we utilized TF-COMB v1.1 (Bentsen et al., 2022). A distinct CombObj was created by loading unique peak sets (E12.5 and E16.5) identified previously. Transcription factor binding sites were identified within the peak regions followed by market basket analysis. TFs co-occurring with NFIB were then subsetted and further assessed for their co-binding (cosine score) and binding events via dot plot.

3.3.3 Gene regulatory network prediction

The analysis of eGRN data in this study was carried out in collaboration with Florian Neuhaus

We used Scenic+ (v0.1) (Gonzalez-Blas et al., 2023) to predict enhancer-driven gene regulatory networks (eGRNs) for CFSE-labelled cells at E12.5 and E16.5. As scRNA-seq and scATAC-seq data were unpaired we created a common annotation, by defining broad cell states (AP, BP, and precursor) in the transcriptomic data, merging clusters based on marker gene expression. Annotations in the scATAC-seq data were created by applying label transfer, based on gene-scores predicted by ArchR. These broad cell states were split by stage, resulting in 6 stage-specific cell states (Fig. S**??**a). Scenicplus performs co-accessibility analysis of regions and links regions to upstream TFs by searching for enriched TF motifs in regions. To make this analysis more coherent with prior results, we used the previously calculated peak set from ArchR as input for Scenicplus, instead of recalculating a new peak set using pycisTopic (Bravo González-Blas et al., 2019). Following the Scenicplus workflow, we created topics of co-accessible regions and performed binarization and motif enrichment of regions in the 20 most important topics. Networks were created by aggregating 10 cells from both modalities of corresponding cell states into pseudocells and then inferring TFs and regions that are predictive of a gene, based on co-accessibility and motif enrichment. The regions considered for a gene have to lie within a genomic interval of 150 kb up- and downstream of the gene. The results are so-called "eRegulons", i.e. regulatory triplets of one TF, bound regions, and corresponding target genes. For each eRegulon the activity in each cell was calculated using AUC-scores (Aibar et al., 2017). Each eRegulon was filtered using standard filtering (*apply_std_filtering_to_eRegulons* function) and high-quality eRegulons were selected by filtering for eRegulons where TF-expression and

AUC scores correlated more than 0.5 or less than -0.5.

We reconstructed cell-state specific subnetworks by running AUC-binarization (*binarize_AUC*-function). Here, we filtered for (1) eRegulons that are active in at least 50% of cells within a corresponding cell state and for (2) corresponding target genes that have a higher normalized expression than 0.5 (normalized expression is log1p transformed after correcting for sequencing depth). Cell state-specific networks (APs, BPs, and precursors) were created by merging the corresponding E12.5- and E16.5-subnetwork using the igraph library v1.5.0 (Csardi and Nepusz, 2006). Stage-specific networks (E12.5 and E16.5) are similarly created by merging subnetworks of APs, BPs, and precursors of the same stage. In both approaches, the merged networks consisted of the union of vertices and edges. GO-enrichment analysis of target genes was performed using DAVID with default parameters (Dennis et al., 2003).

3.4 Transplantation datasets

3.4.1 Sample and library preparation

To generate the $AP_{E12.5 \rightarrow E12.5}$, $AP_{E12.5 \rightarrow E16.5}$, $AP_{E16.5 \rightarrow E16.5}$, and $AP_{E16.5 \rightarrow e13.5}$ datasets, timed pregnant mice were anesthetized with isoflurane and treated with the analgesic Metamizol as previously described. To target APs, injection of CFSE working solution was performed into wild-type C57BL/6NRj embryos at E12.5 and E16.5. One hour later, APs were FT^+ and three to six embryonic brains were collected. After manual dissections of the ganglionic eminences in ice-cold L-15 medium containing 5% FBS, the tissue was dissociated on a gentleMACS dissociator according to the manufacturer's protocol. Cells were resuspended in ice-cold HBSS containing 10mmol EGTA and 0.1% Fast Green to a final concentration of 40000 cells/µL to 80000 cells/µL. The cell suspension was split into

two separate pools, and 1 µL was injected homo- or hetero-chronically into the ventricles of embryonic brains at E12.5 or E16.5. Forty-eight hours later, ganglionic eminences were dissected and dissociated as described above. CFSE-labelled cells were isolated with flow cytometry and centrifuged 500 rpm, 5min, 4°C. Total RNA-seq libraries were prepared using the SMART-Seq® Stranded Kit (634442, Takara), according to standard manufacturer's protocol (Low-input Workflow, PCR 1: 5 cycles and PCR 2: 12–15 cycles; Fig.3.8). The library quality was assessed by using a Qubit™ Flex Fluorometer (Q33327, Thermo Fisher Scientific) and a 4200 TapeStation (G2991BA, Agilent). A total of 10 samples were multiplexed and sequenced in a lane of a NovaSeq 6000 SP flow cell with the 100 cycles kit for paired-end sequencing (2× 60 bp) to reduce sequencing batch effects (100 pM final loading, 42 M reads per sample on average). BCL raw data were converted to FASTQ data and demultiplexed by the bcl2fastq Conversion Software (Illumina).

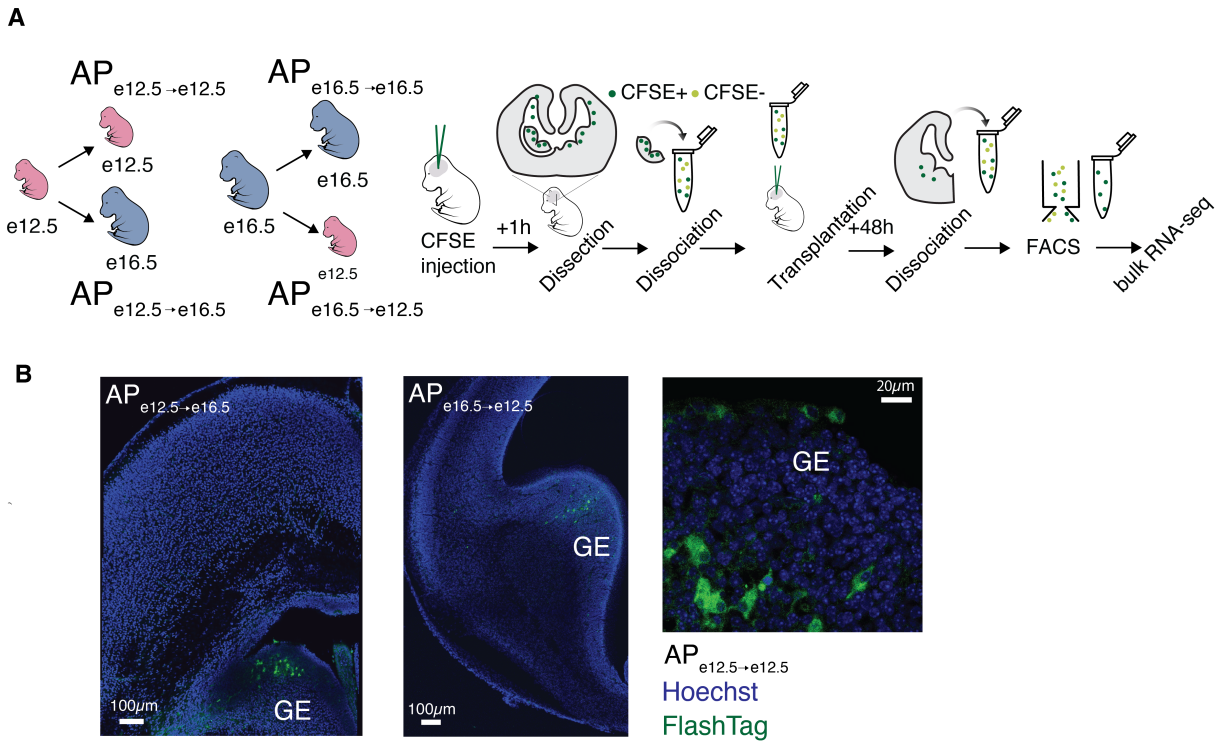

Figure 3.8: **Overview schematics of the transplantation experiment. A.** Schematic of the different transplantation conditions and the experiment steps. **B.** Coronal sections of ganglionic eminences 48 hours after transplantation. GE: ganglionic eminence.

3.4.2 Analysis

The Galaxy web platform on the public server at *usegalaxy.eu* was employed to analyze the data (Afgan et al., 2018). Paired end reads were trimmed with the Trimmomatic tool and quality control was performed with FastQC. Reads were mapped to the mouse reference genome using the HISAT2 algorithm (Kim et al., 2019) and the number of reads per annotated genes was counted using featureCounts (Liao et al., 2014). After Fragments Per Kilobase of transcript per Million mapped reads (FPKM) normalization of the count matrices, the proportion of single cell states within each replicate was inferred with Bisque v1.0.5 (Jew et al., 2020) by using the annotated combined single-cell clusters as reference.

A weighted pseudotime score was assigned to each replicate by calculating the median of the pseudotime score per cluster from the combined single-cell datasets. For differential gene expression analysis, the count matrices were subset by variable genes of inhibitory neuron datasets, and DESeq2 v1.42.0 was utilized (Love et al., 2014).

4 Results

4.1 Patterning of neurogenesis in dorsal and ventral lineages

4.1.1 Classification of GABAergic precursor states

In this study, various datasets were used, including transcriptome data (scRNA-seq), along with clonal tracking (TrackerSeq) and birthdating (FlashTag) information for individual cells. These datasets were pre-processed and integrated into a single combined dataset (Materials and Methods; Fig.4.1A,B). A trajectory of gene expression changes between cell states was inferred using Monocle3 on the combined dataset and a pseudotime score was assigned to each cell (Fig.4.1C). Cells with high Nestin (Nes) expression, a marker for radial glial progenitors, were used to initiate the trajectory (Fig.4.1D,E).

To obtain consistency throughout the study, clusters were identified in the combined dataset (Fig.4.2A,B) and, similar to previous publications , they represented a continuum of cell state transitions during cellular maturation and differentiation Mayer et al. (2018); Bandler et al. (2022); Lee et al. (2022); Rhodes et al. (2022); Lim et al. (2018). Following the mitotic apical and basal progenitors (APs and BPs), the trajectory branched into distinct precursor states, giving rise to GABAergic projection neurons (PNs) and interneurons (INs; Fig.4.2A,B). The clusters representing the different cell states along

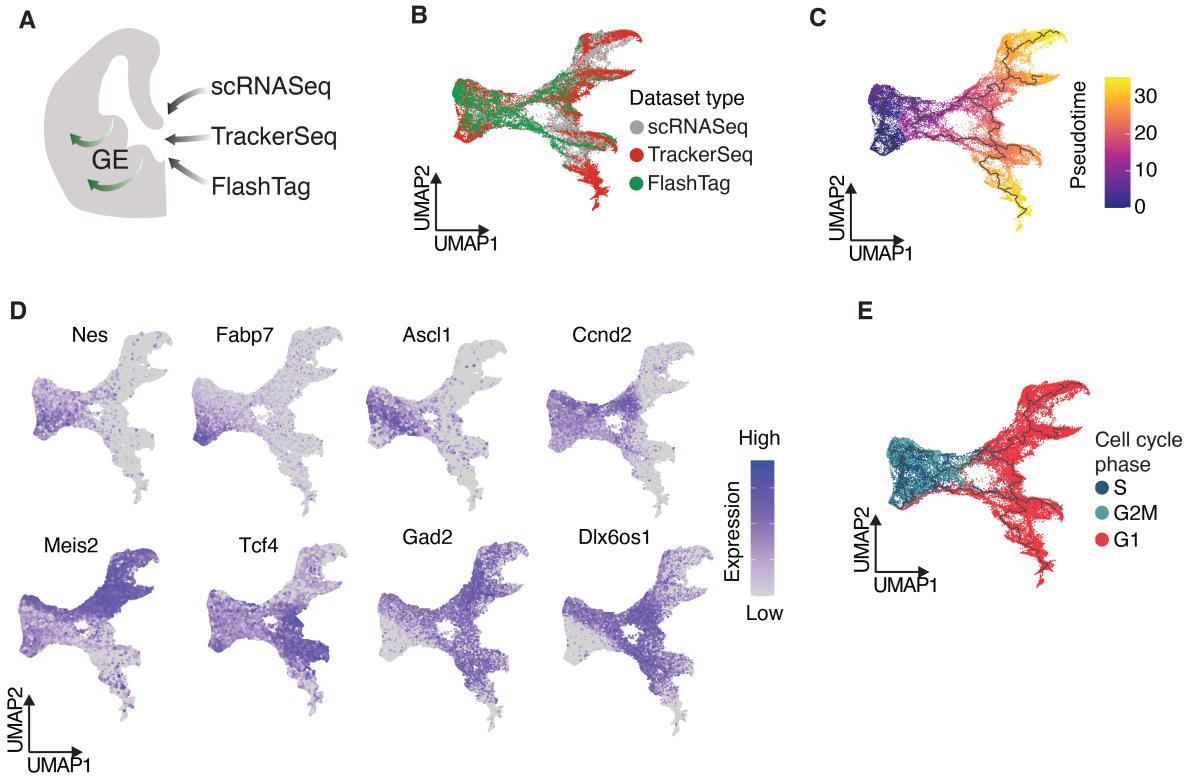

Figure 4.1: **Integration and processing of the transcriptome datasets. A**. Summary of the methods utilized to investigate the competence of GABAergic progenitors located in the ganglionic eminences (GEs). **B**. UMAP plot showing single cells derived from scRNA-seq, TrackerSeq, and FlashTag datasets aligned in Monocle3 in a combined dataset. **C**. UMAP plot of the combined dataset with the inferred Monocle3 trajectory. Cells are colored by the assigned pseudotime score. **D**. Expression of marker genes in the combined dataset. Nes and Fabp7 label APs, Ascl1 and Ccnd2 are markers for BPs. Postmitotic inhibitory neurons express Gad2 and Dlx6os1. Meis2 labels PNs and Tcf4 labels INs. **E**. UMAP plot of combined dataset annotated by cell cycle phase.

the trajectory were manually annotated based on the expression of the top five marker genes. The identified groups were: apical progenitors (APs; Fabp7), basal progenitors (BPs; Fabp7/Ccnd1, Top2a, and Ube2c), GABAergic projection neuron precursors (PNs: Abracl, Tshz1, Six3/Gucy1a3, Gucy1a3, and Ebf1/Isl1), and GABAergic interneuron precursors (INs: Nkx2-1, Npy, Maf/Sst, and Snhg11; Fig.4.2C).

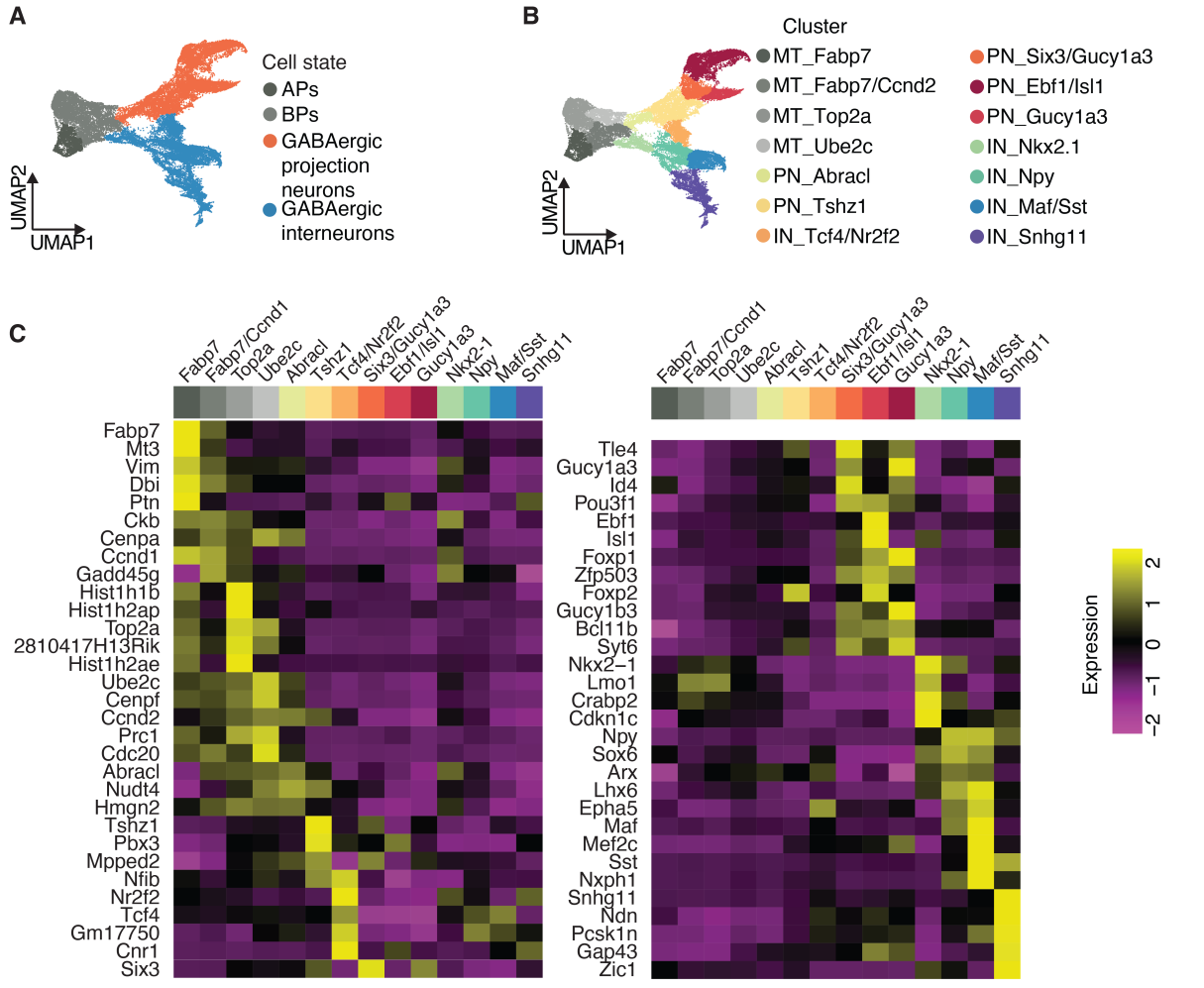

Figure 4.2: **Clustering and cell state identification in the transcriptome datasets.** **A**. UMAP plot of combined dataset annotated by broad cluster identity (APs: apical progenitors, BPs: basal progenitors). **B**. UMAP plot of combined dataset clustered and annotated based on top marker genes and broad cluster identity (MT: mitotic, PN: projection neuron, IN: interneuron). **C**. Heatmap of differentially expressed genes in GABAergic cell clusters.

4.1.2 Developmental pattern of GABAergic neurons

To study the patterning in the development of GABAergic neurons, the analysis focused initially on the scRNA-seq datasets (Fig.4.3A). The transcriptome-only datasets contained the cell states previously identified in the combined dataset analysis (Fig.4.2B, Fig.4.3B).

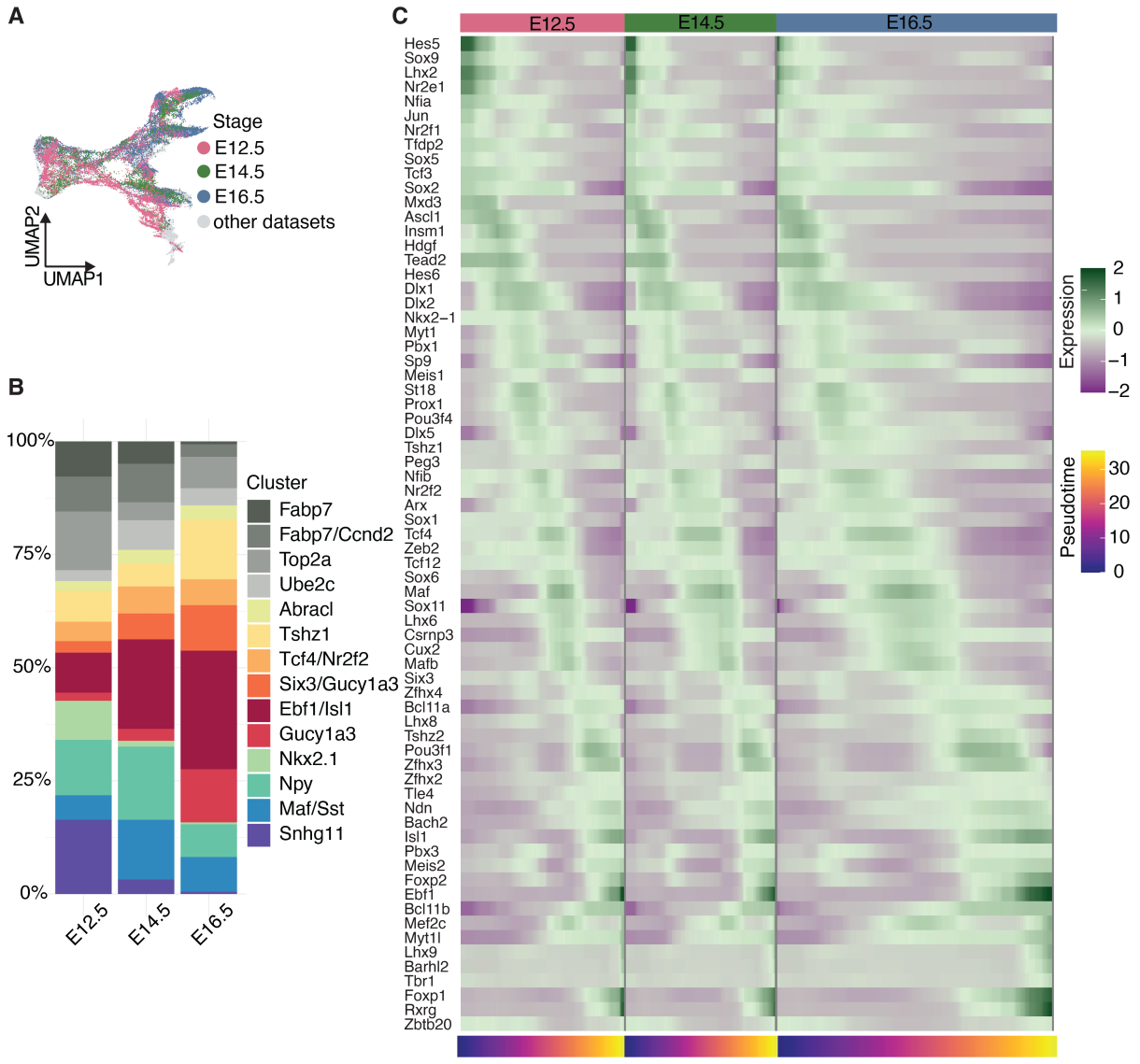

Figure 4.3: **Characterization of genetic patterns in the development of GABAergic neurons. A**. UMAP plot of the combined dataset. The scRNA-seq datasets coloured by collection stage are highlighted. **B**. Distribution of cell states at different developmental stages in scRNA-seq datasets. **C**. Scaled and smoothed expression of dynamic TFs in GABAergic cells. TFs are ordered by their maximum expression along the pseudotime trajectory.

The cell state ratio varied from E12.5 to E14.5 and E16.5 developmental stages (Fig.4.3B). To assess the gene expression changes that are key for inhibitory neuron maturation and differentiation, transcription factors (TFs) with a dynamic expression along the Monocle3

trajectory were identified (Fig.4.3C). Interestingly, the dynamic TFs were consistently expressed across all the time points (E12.5, E14.5, and E16.5). This finding suggests a genetic program of inhibitory neurons that is conserved across developmental stages. This developmental pattern differs from previous observations in dorsal lineages, where temporally patterned genes unfold sequentially during neurogenesis (Di Bella et al., 2021; Telley et al., 2019).

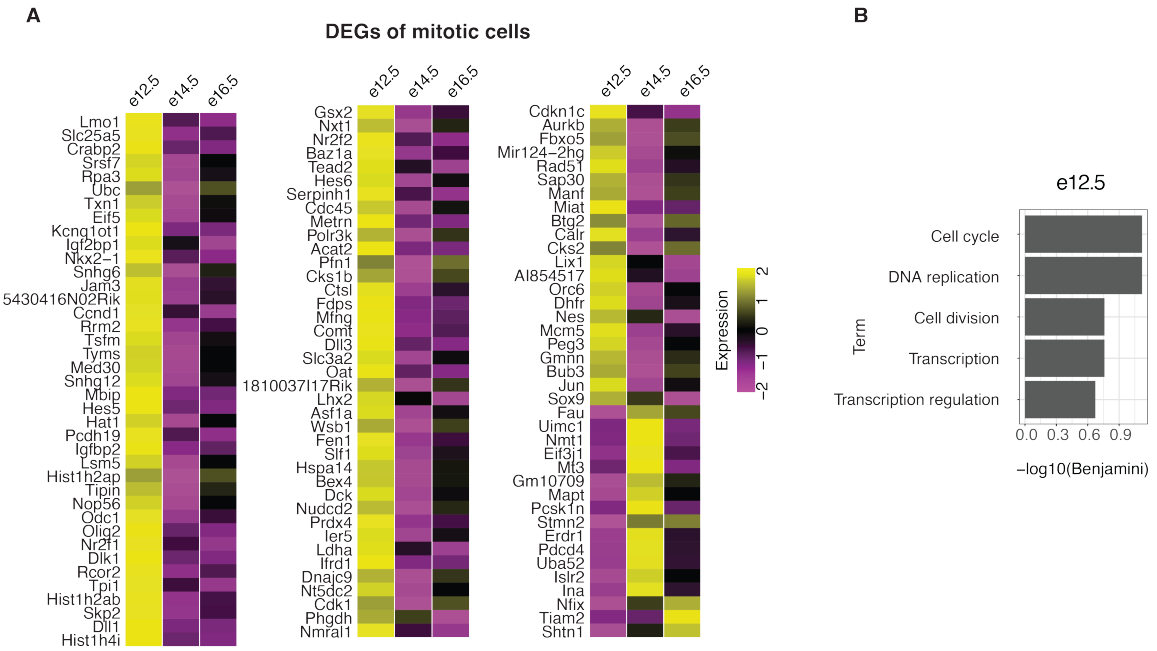

Figure 4.4: **Differential gene expression in GABAergic progenitors. A**. Average gene expression heatmap of differentially expressed genes in mitotic progenitors at E12.5, E14.5, and E16.5 in the scRNA-seq datasets. **B**. Functional annotation of differentially expressed genes in E12.5 APs. Top five GO terms ranked by Benjamini-Hochberg corrected *P*-values (DAVID).

Differential gene expression analysis between the different stages in the mitotic subset of cells was performed in the scRNA-seq datasets. Only a few genes were upregulated at later time points, while genes that were downregulated were primarily related to self-renewal (Fig.4.4A,B). This finding aligns with a change in the balance between cell proliferation and differentiation during neurogenesis (Götz and Huttner, 2005).

4.1.3 Comparison between dorsal and ventral lineages

To compare directly the developmental patterns between ventral and dorsal lineages, datasets of GABAergic and glutamatergic neurons from equivalent time points were projected into the same subspace. Specifically, the datasets from this study that underwent only scRNA-seq were enriched by merging them and aligning them with published data of GABAergic neurons from e13.5 and e15.5 (Bandler et al., 2022). Glutamatergic neurons from E12.5 to E16.5 (Di Bella et al., 2021) were merged and aligned as well to the ventral datasets (Fig. 4.5A). On the UMAP plot, dorsal and ventral lineages were in proximity at the level of APs and dispersed into different directions at more mature cell states, i.e. BPs and postmitotic precursors, similarly to previously described patterns (Moreau et al., 2021; Fig. 4.5B,C). When comparing successive developmental stages, cells of the dorsal lineage showed a sequential shift in the UMAP positioning, consistent with findings from previous studies (Telley et al., 2016; Di Bella et al., 2021). In contrast, cells of the ventral lineage largely overlapped across developmental stages (Fig. 4.5D).

To quantify the temporal progression of dorsal and ventral progenitors, the mitotic cells were subset from the common pool of dorsal and ventral lineages and Pearson correlation coefficients were calculated between the different stages. Ventral progenitors showed higher correlation coefficients between successive stages of neurogenesis than dorsal progenitors, indicating generally less change in their gene expression profiles (Fig. 4.6A).

Next, postmitotic cells were annotated: marker gene expression was utilized for the ventral lineage and published annotations (based also on marker genes expression) were utilized for dorsal lineage (Di Bella et al., 2021). The following groups were part of the published annotations: SCPN for subcerebral projection neurons, CThPN for corticothalamic projection neurons, DL CPN for deep layer callosal projection neurons, and UL CPN for upper layer callosal projection neurons (Fig. 4.6B).

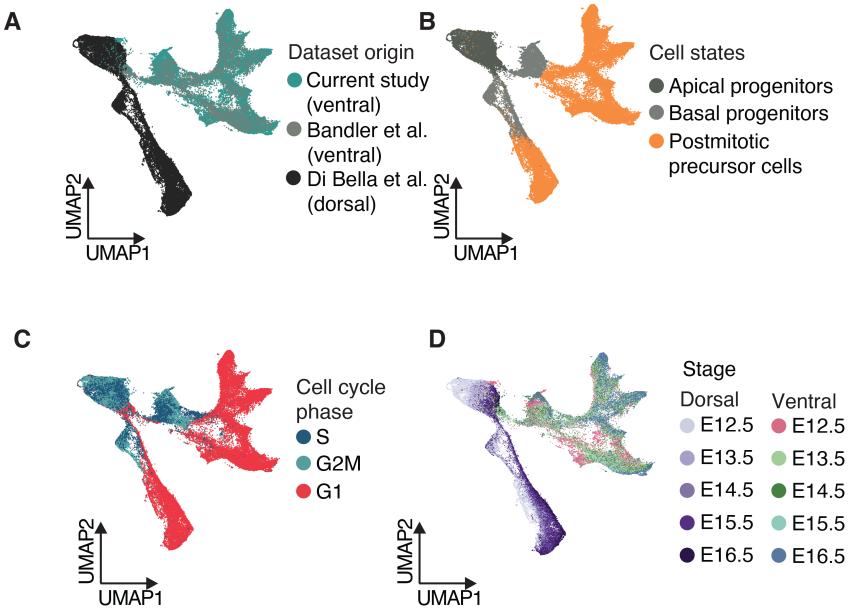

Figure 4.5: **Integration and processing of ventral and lineage datasets. A**. UMAP plot of ventral and dorsal lineage datasets from different publications. **b-d**, UMAP plot of ventral and dorsal lineage datasets, with cells coloured by broad cell state (**B**), cell cycle phase (**C**) and collection stage (**D**).

The proportion of cells in postmitotic precursor states across different developmental stages was quantified (Fig. 4.6C). While the relative distribution of precursor states was similar across stages in ventral cells, it sequentially shifted in dorsal cells (SCPN → CThPN → DL CPN → UP CPN). The observations suggest that the differentiation competence of GABAergic progenitors is stable throughout neurogenesis, and the generation of GABAergic precursor states does not adhere to a stage-specific sequence. This contrasts the sequential generation of precursor states in dorsal lineages.

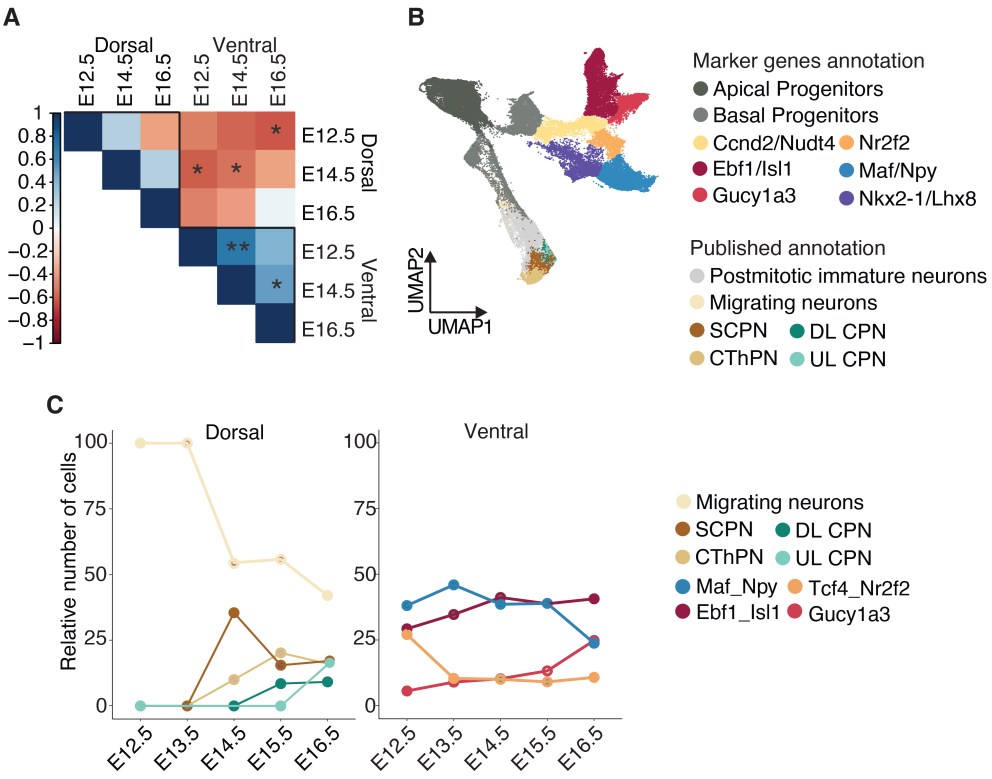

Figure 4.6: **Developmental patterning of ventral and dorsal lineages. A**. Pearson's correlation plot between dorsal and ventral progenitors at different developmental stages; $*P < 0.05$, $**P < 0.01$. **B**. UMAP plot of ventral and dorsal lineage datasets, with cells coloured by marker gene annotation (ventral) or published annotation (dorsal). **C**. Line plot showing relative cell number of dorsal (left) and ventral (right) postmitotic neuronal states across stages.

4.2 Clonal relationships in GABAergic neurons across neurogenesis

4.2.1 Clonal distribution in the ventral lineage

To assess the competence of GABAergic progenitors to generate different cell states at different points of neurogenesis, a barcode lineage tracing method called TrackerSeq was utilized. TrackerSeq uses heritable DNA barcodes to label individual progenitors and their

progeny and can be combined with different methods such as scRNA-seq (Bandler et al., 2022). Progenitors in the GE were targeted at E16.5 with TrackerSeq plasmids via *in utero* electroporation (IUE), electroporated cells were FACS-enriched 96 hours later, and scRNA-seq was performed ($\text{TrackerSeq}_{\text{E16.5 + 96h}}$). For a comparison between multiple stages of neurogenesis, a TrackerSeq dataset published by Bandler et al. (2022) was also included in the analysis. Specifically, the published dataset contained progenitors electroporated with TrackerSeq plasmids at E12.5 and collected 96 hours later ($\text{TrackerSeq}_{\text{E12.5 + 96h}}$; Fig.4.7A).

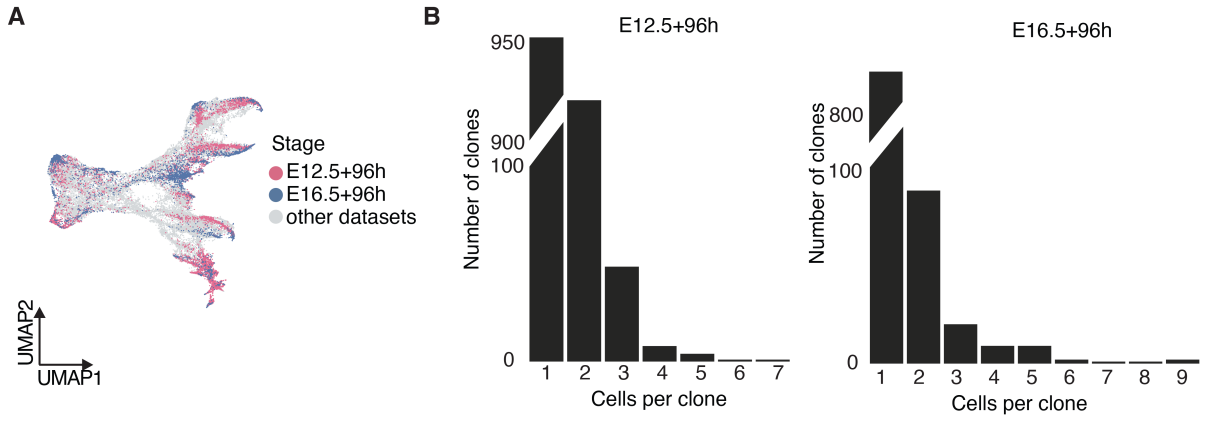

Figure 4.7: **Quality control analysis of the TrackerSeq datasets. A**. UMAP plot of TrackerSeq barcoded cells colored by IUE stage; IUE at E12.5 and E16.5, scRNA-seq after 96 hours. **B**. Clonal groups quantification in $\text{TrackerSeq}_{\text{E12.5 + 96h}}$ (left) and $\text{TrackerSeq}_{\text{E16.5 + 96h}}$ (right).

In the following steps, only multicellular clones with cells in the branch tips of the Monocle3 trajectory were selected to ensure a robust and comparable analysis to previous publications (Fig.4.7B, Fig.4.8A; Bandler et al., 2022). Clones were distributed throughout all the different neuronal states at both stages ($\text{TrackerSeq}_{\text{E12.5 + 96h}}$ and $\text{TrackerSeq}_{\text{E16.5 + 96h}}$), indicating that progenitors in the GEs can give rise to a similar set of precursor states throughout neurogenesis (Fig.4.8B). The clonal groups were categorized into two types, based on the distribution of their cells in one ("non-dispersing" clones) or several ("dispersing" clones) branch tips. Consistent with Bandler *et al.*, $\text{TrackerSeq}_{\text{E12.5 + 96h}}$ clones dispersed into multiple branch tips. Notably, a comparable fraction of "dispersing" clones

was found in TrackerSeq$_{\text{E16.5 + 96h}}$ (Fig.4.8C). The true proportion of "dispersing" clones is likely higher than observed, as TrackerSeq only partially recovers clones due to substantial cell loss during sample preparation (Bandler et al., 2022).

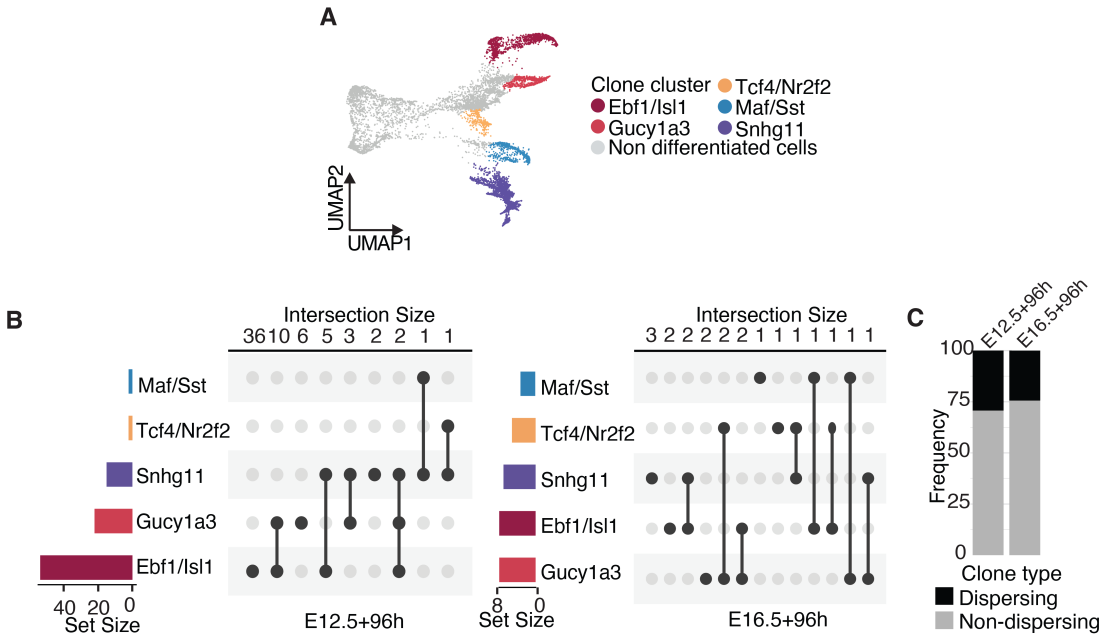

Figure 4.8: **Clonal distribution analysis TrackerSeq datasets.** **A**. UMAP plot of cell states at the branch tips utilized to group clones. **B**. Upset plot displaying clonal intersections in $_{\text{E12.5 + 96h}}$ (left) and in TrackerSeq$_{\text{E16.5 + 96h}}$ (right). **C**. Barplot displaying the frequency of dispersing and non-dispersing clones in TrackerSeq$_{\text{E12.5 + 96h}}$ and TrackerSeq$_{\text{E16.5 + 96h}}$.

4.2.2 Competence of mitotic progenitors to generate different neuronal fates

Clonal resolution enables linking individual mitotic progenitor cells to the fate of their postmitotic progeny. To test whether the transcriptome of mitotic cells correlates to the transcriptome of their postmitotic sister cells within the same clone, correlation analysis between single cells of "non-dispersing" clones was utilized. Cells from each fate, represented by the branch tip, were correlated to randomly chosen mitotic cells, fate-specific

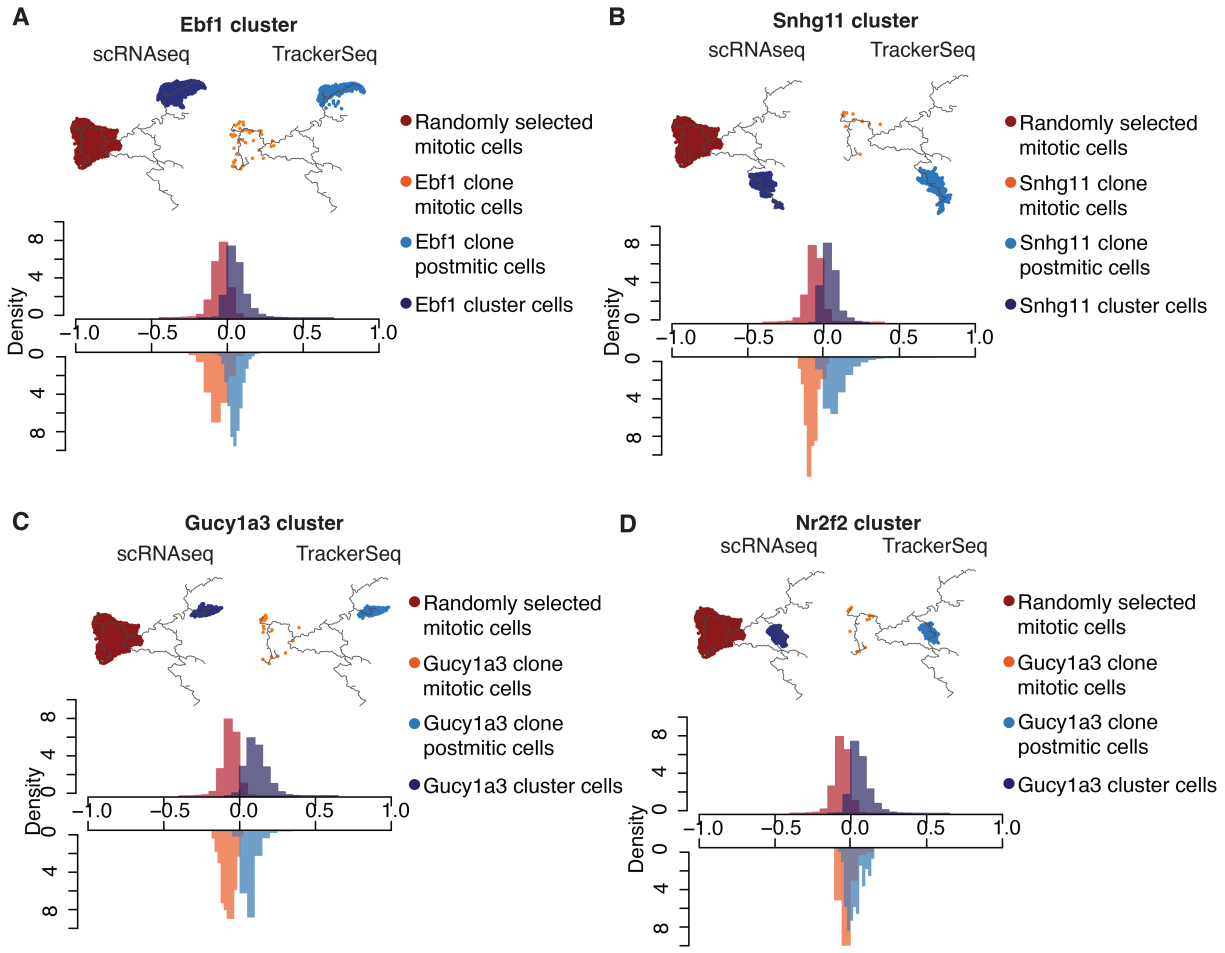

Figure 4.9: **Correlation score distribution between random and TrackerSeq-labelled cells. A-D**. Permutation of correlation analysis of TrackerSeq-labelled clones in branch tip clusters. **A**. Ebf1 cluster. **B**. Snhg11 cluster. **C**. Gucy1a3 cluster. **D**. Nr2f2 cluster.

mitotic cells, fate-specific postmitotic cells, and the cells from the branch tip itself. The goal was to assess the similarity of randomly selected mitotic cells, mitotic clones, and postmitotic clones to the genetic program of differentiated cells in the branch tip.

Interestingly, mitotic progenitor cells that were part of "non-dispersing" clones did not correlate more strongly with their clonal output than did randomly selected progenitor cells (Fig.4.9A-D). Overall, the clonal analysis indicates that progenitor cells maintained a stable level of differentiation competence throughout neurogenesis.

4.3 Maturation dynamics in early and late-born neurons

Single-cell sequencing and clonal analysis revealed stability in the differentiation competence of GABAergic neuron progenitor cells. Mitotic cells in the GEs have the potential to generate multiple neuronal cell states until the latest point of neurogenesis (E16.5). However, these methods have limitations in answering what type of influence progenitor cells have on the properties of their daughter cells at different time points. To answer this question a birthading technique called FlashTag (FT) was utilized. FT labels isochronic cohorts of cells with the fluorescent dye carboxyfluorescein succinimidyl ester (CFSE) (Govindan et al., 2018). In this method, mitotic cells layering the ventricle are labeled during the M phase of the cell cycle and maintain high fluorescence when leaving the cell cycle. Three datasets that differed in injection or collection time points were generated with the FT technique. CFSE was injected into the ventricles of E12.5 and E16.5 wild-type embryos, GEs were anatomically dissected six hours later and FT labeled (FT^+) cells FACS enriched to perform scRNA-seq ($FT_{E12.5\ +\ 6h}$ and $FT_{E16.5\ +\ 6h}$ respectively). CFSE was injected into the ventricles of E12.5 Dlx5/6-Cre::tdTomato mouse embryos, where Dlx5 and Dlx6 serve as markers for inhibitory neurons (Monory et al., 2006). Inhibitory neurons were then collected after migration from anatomically dissected cortex and striatum at 96 hours post-injection. $TdTomato^+$ and FT^+ cells were enriched by FACS, and scRNA-seq was performed ($FT_{E12.5\ +\ 96h}$; Materials & Methods).

$FT_{E12.5\ +\ 6h}$ and $FT_{E16.5\ +\ 6h}$ contained mitotic progenitors as well as early postmitotic neuronal precursors. $FT_{E12.5\ +\ 96h}$ cohorts contained exclusively postmitotic cells (Fig.4.10A,B), consistent with the notion that FT marks isochronic cohorts of cells that exit the cell cycle shortly after CFSE application (Telley et al., 2016; Mayer et al., 2018). No-

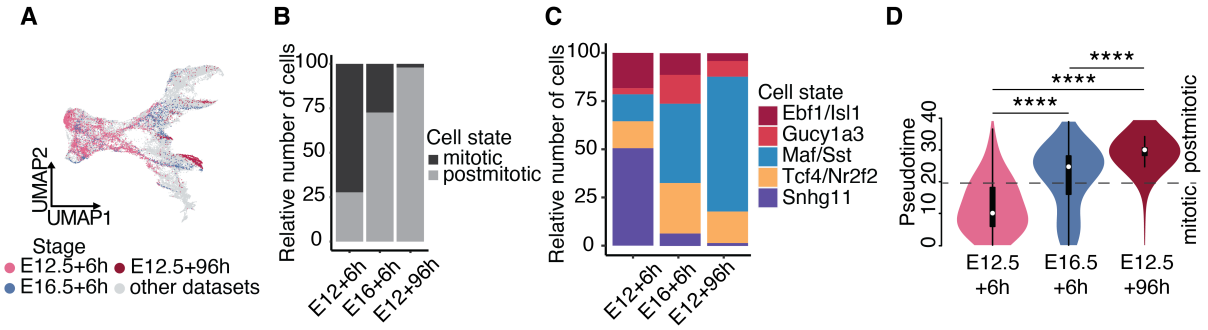

Figure 4.10: **Cell-state and pseudotime score in FlashTag-labelled cohorts of cells. A**. UMAP plot of FlashTag (FT) datasets coloured by injection and collection stage; injection at E12.5 and E16.5, scRNA-seq after 6 hours or 96 hours. **B**. Barplot depicting relative fractions of mitotic and postmitotic cell states in $FT_{E12.5 + 6h}$, $FT_{E16.5 + 6h}$, and $FT_{E12.5 + 96h}$. **C**. Barplot depicting the relative number of cells in postmitotic neuronal states of $FT_{E12.5 + 6h}$, $FT_{E16.5 + 6h}$, and $FT_{E12.5 + 96h}$. **D**. Violin plots representing the distribution of FT+ cells along the combined pseudotime trajectory, displayed for each condition; Wilcoxon rank sum test ($****adjustedP < 0.001$).

tably, the postmitotic fraction of all three conditions ($FT_{E12.5 + 6h}$, $FT_{E12.5 + 96h}$, $FT_{E16.5 + 6h}$) differentiated into all precursor states, albeit in different proportions (Fig.4.10C). Monocle3 pseudotime (PT) scores were quantified as a proxy for the degree of maturation acquired by the different FT^+ cohorts. As expected, given its later collection, $FT_{E12.5 + 96h}$ showed higher PT scores than $FT_{E12.5 + 6h}$. Strikingly, the PT score of $FT_{E16.5 + 6h}$ was markedly higher than that of $FT_{E12.5 + 6h}$, even though both were collected after six hours (Fig.4.10D).

To examine the different properties of the FT^+ daughter cells, a differential gene expression (DGE) analysis was performed between postmitotic cells of the cohorts collected after 6 hours ($FT_{E12.5 + 6h}$ vs. $FT_{E16.5 + 6h}$; Fig.4.11A). Genes upregulated in $FT_{E16.5 + 6h}$ overlapped with the gene expression found in $FT_{E12.5 + 96h}$ (Fig.4.11B). This suggests that late-born neurons reach a similar gene expression profile within six hours as early born neurons within 96 hours. Many of the genes upregulated in $FT_{E16.5 + 6h}$ were associated with the promotion of neuronal proliferation and migration (4.1). Some of these genes were

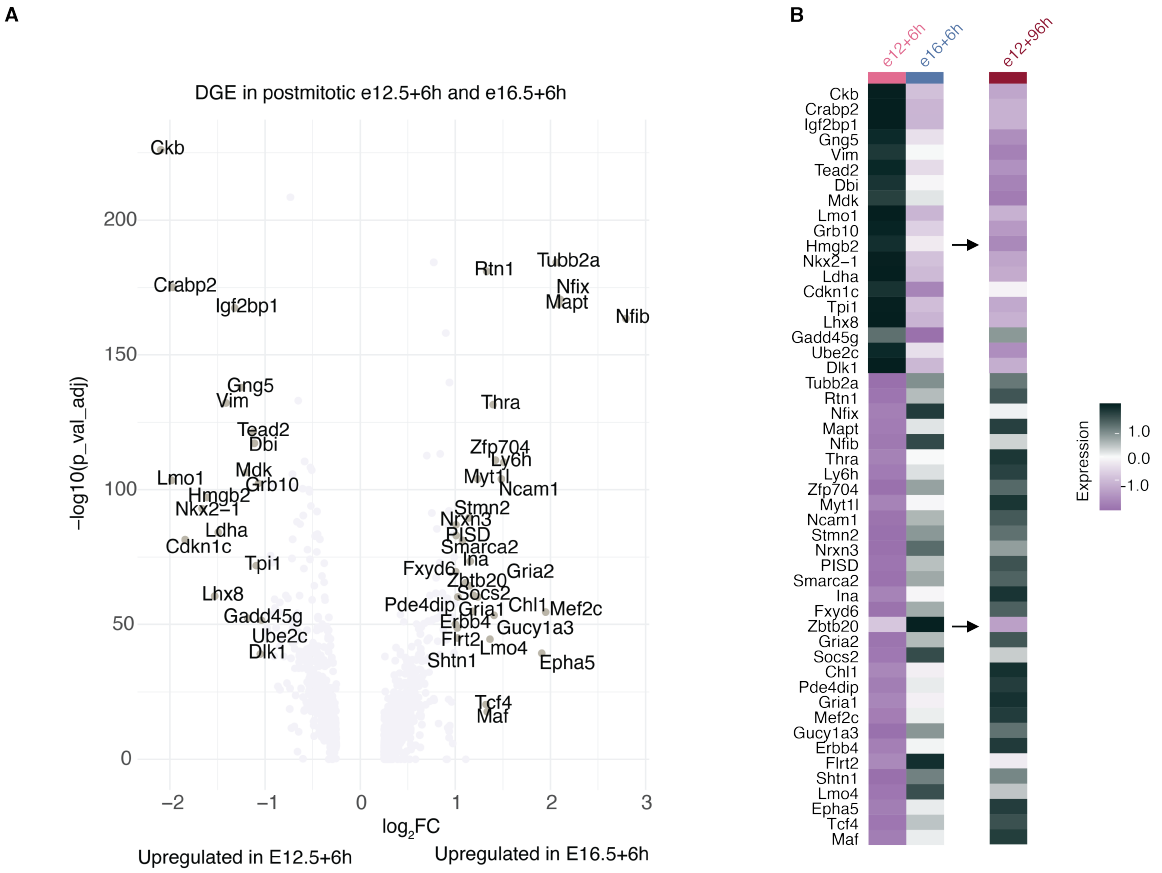

Figure 4.11: **Differential gene expression analysis in postmitotic neuronal states.** **A**. Volcano plot showing differentially expressed genes between the postmitotic cell states of $\mathrm{FT}_{\mathrm{E12.5+6h}}$ and $\mathrm{FT}_{\mathrm{E16.5+6h}}$. **B**. Heatmap showing average scaled expression of differential genes in $\mathrm{FT}_{\mathrm{E12.5+6h}}$ and $\mathrm{FT}_{\mathrm{E16.5+6h}}$ postmitotic cells; the expression of the identified genes is visualized in $\mathrm{FT}_{\mathrm{E12.5+96h}}$.

specifically linked to neuronal signaling pathways. Overall, the results using FT birthdating suggest that although newborn neurons at different stages differentiate similarly into precursor states, they differ in their maturation dynamics.

Gene symbol	log_2FC	Function during neurogenesis	Reference (PMID)
Tubb2a	2,06	Microtubule protein involved in neuronal migration and proliferation; mutation linked to brain malformation and epilepsy.	24702957
Rtn1	1,33	Reticulon protein localized in ER and neuronal dendrites, regulates ER activity and cytosolic calcium dynamics.	23454728, 23559015
Nfix	2,10	Transcription factor essential for normal brain development, regulates progenitor cell differentiation in the hippocampus.	23042739, 18477394
Mapt	2,08	Microtubule-associated protein with role in brain development and neurogenesis as well as detrimental role in neurodegeneration at later age.	29202785
Nfib	2,79	Transcription factor involved in neuronal radial glia differentiation and cortical development regulation.	23749646, 32166136
Thra	1,40	Nuclear hormone receptor required for normal neural progenitor cell proliferation in human cerebral cortical development.	31628250
Ly6h	1,42	Endogenous neurotoxin-like protein, inhibits alpha7 nicotinic acetylcholine receptor currents at the plasma membrane.	25716842, 32686737
Zfp704	1,51	C2H2 zinc finger protein expressed in several NC-derived lineages.	17693064
Myt1l	1,23	CCHC zinc finger TF involved in neuronal identity and maturation.	21617644, 34614421
Ncam1	1,48	Neural cell adhesion molecule important for neuronal migration, neurite develoopent, synaptogenesis and neural stem cells regulation.	19788570, 20038681, 17682066
Stmn2	1,14	Microtubule regulator, necessary for normal axonal outgrowth , regeneration and protection.	30643292
Nrxn3	1,01	Presynaptic transmembrane protein with role in synapse development and function.	34879268, 2847265
PISD	1,01	Mitocondrial-localized enzyme, associated with impaired mitochondrial protein homeostasis.	30858161
Smarca2	1,08	Subunit of chromatin remodelling complexes, involved in neural progenitor differentiation.	31375262
Ina	1,16	Neuronal intermediate filament protein that influence morphology and physiology of axonx.	11739575
Fxyd6	1,00	Transmembrane protein involved in Na/K pump function modulation.	33231612
Zbtb20	1,11	Transcription factor with role in neurogenesis and astrocytogenesis modulation.	27282384, 27000654
Gria2	1,15	Subunit of AMPA receptor, LOF leads to neurodevelopmental disorders.	31300657
Socs2	1,19	Intracellular protein that regulates neuron embryonic development and the neurotrophin signaling.	12368809, 24860421
Chl1	1,24	Neural recognition molecule that begatively regulates neuronal proliferation and differentiation.	20933598
Pde4dip	1,03	Protein anchoring components of the cAMP-dependent pathway in the ER to Golgi trafficking.	35346821
Gria1	1,18	Subunit of AMPA receptor, LOF leads to neurodevelopmental disorders.	35675825
Mef2c	1,95	Transcripton factor involved in interneurons fate and maturation and is linked to various neuropsychiatric and neurodevelopmental disorders.	27779093, 18579729, 32452758
Gucy1a3	1,41	Subunit of guanylate cyclase enzyme regulating MGE neurons migration and marker of indirect striatal medium spiny neurons.	24155296, 36081908
Erbb4	1,00	Receptor tyrosine kinase required for interneuron migration and inhibitory synapse formation.	15473965, 34226493
Flrt2	1,02	cell adhesion molecules with role in Tangential Migratory Streams of Cortical Interneurons.	34301831
Shtn1	1,02	Protein coding gene involved in neuronal polarization and axonogenesis.	17030985, 30733148
Lmo4	1,36	Transcriptional regulator essential for normal patterns of proliferation ans survival of neuroepithelial cells.	15691703
Epha5	1,91	Ephrin receptor protein, involved in axon guidance and synaptogenesis during development.	19326470, 20824214
Tcf4	1,32	Transcription factor regulating cortical interneuron neurogenesis.	35965434
Maf	1,34	Transcription factor regulating cortical interneuorn fate and maturation.	30699346, 32452758

Table 4.1: Functional summary of e16.5 enriched genes differentially expressed between $FT_{e12.5 + 6h}$ and $FT_{e16.5 + 6h}$.

4.4 Chromatin accessibility and network underlying maturation competence

The analysis of scATAC-seq and eGRN data in this study was carried out in collaboration with Dr. Ann Rose Bright and Florian Neuhaus

To explore whether the different maturation dynamics at embryonic stages are associated with changes at the chromatin level, single-cell chromatin accessibility using the assay for transposase-accessible chromatin using sequencing (scATAC–seq; Buenrostro et al., 2015) was profiled on samples derived from FT^+ cohorts in the GEs. Similarly to the FT^+ cohorts collected for the transcriptome, CFSE was injected into the ventricles of E12.5 and E16.5 wild-type embryos, and GEs were anatomically dissected 6 hours later ($FT_{E12.5\ +\ 6h}$, $FT_{E16.5\ +\ 6h}$, respectively). From the dissected tissue, FT^+ cells were enriched via FACS, and scATAC-seq was performed (Materials & Methods). Following sequencing, the paired-end reads were mapped to an mm10 reference genome, and the ArchR (Granja et al., 2021) framework was employed for quality control, dimensionality reduction, clustering, and peak calling.

In contrast to the isochronic cohorts observed in the scRNA-seq experiments (Fig.4.10A), $FT_{E12.5\ +\ 6h}$ and $FT_{E16.5\ +\ 6h}$ in the scATAC-seq experiment were separate on the UMAP plot (Fig.4.12A). Gene body accessibility patterns of marker genes confirmed the presence of the mitotic and postmitotic cell states that were identified in the transcriptome of the FT^+ cohorts collected after 6 hours (Fig.4.12B). To identify and quantify the cis-regulatory elements (CREs) responsible for this separation, peak calling was conducted separately on $FT_{E12.5\ +\ 6h}$ and $FT_{E16.5\ +\ 6h}$. The resulting peaks were categorized to identify genomic sites with E12.5-specific peaks, E16.5-specific peaks, and sites with overlapping peaks (E12.5-sites, E16.5-sites and overlapping-sites, respectively; Fig.4.12C). Subsequently, the ATAC-

seq fragment distribution was computed and displayed in coverage plots (Fig.4.12D). At E12.5-sites higher accessibility was present in $FT_{E12.5 + 6h}$ in respect to $FT_{E16.5 + 6h}$. Conversely, E16.5-sites had higher accessibility in $FT_{E16.5 + 6h}$ than $FT_{E12.5 + 6h}$.

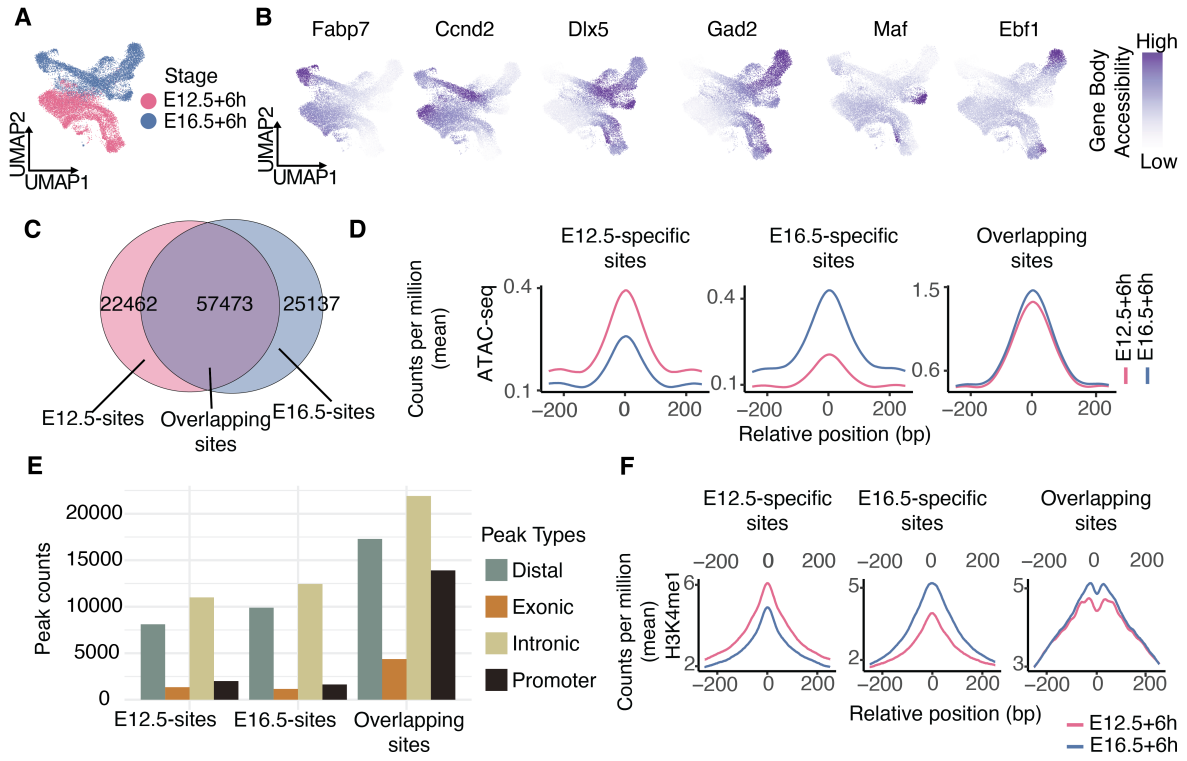

Figure 4.12: **Chromatin accessibility and peak types in scATAC-seq datasets. A**. UMAP plot showing scATAC-seq datasets; FT injection at E12.5 and E16.5, followed by scATAC-seq after 6 hours. **B**. UMAP depiction of gene body accessibility for marker genes. Fabp7 for APs, Ccnd2 for BPs, Dlx5 and Gad2 for postmitotic inhibitory neurons, Maf for INs and Ebf1 for PNs. **C**. Venn diagram showing the three categories of sites (E12.5 sites, E16.5 sites and overlapping sites) and the number of non-overlapping and overlapping sites. **D**. Coverage plot displaying ATAC-seq signal intensity for peak categories. X-axis is relative position (base pairs) and y-axis is counts per million (mean). **E**. Barplot quantifying peak types (distal, exonic, intronic, and promoter) at E12.5, E16.5, and overlapping sites. **F**. Coverage plot displaying H3K4me1 signal intensity for peak categories. X-axis is relative position (base pairs) and y-axis is counts per million (mean).

The peak sets were divided by genomic region into promoters, distal, exonic, and intergenic regions (Fig.4.12E). Differently from the overlapping sites, at E12.5-sites and E16.5-sites, distal and intergenic regions represented a larger proportion of peaks with respect

to promoters and exonic ones. Together, this indicates that chromatin accessibility undergoes marked changes between different stages of development, implying a dynamic process of chromatin remodeling that predominantly occurs at distal and intronic regulatory elements. To define the functional status of identified sites as poised-active distal regulatory elements, the distribution of H3K4me1 fragments was analyzed. H3K4me1 is commonly associated to distal enhancers (Heintzman et al., 2007) and could be analyzed utilizing forebrain ChIP-seq data from ENCODE (Gorkin et al., 2020). H3K4me1 profiles closely aligned with chromatin accessibility profiles (Fig.4.12F). Specifically, E12.5-sites exhibited a stronger H3K4me1 signal at E12.5 compared to E16.5, and the contrary was observed for E16.5-sites. These observations suggest that distal regulatory elements are potentially maintained in a poised-active state and likely drive the stage-specific dynamics in chromatin accessibility.

To explore how the stage-specific accessibility of CREs relates to the maturation process, a PT score was assigned to cells along a maturation trajectory (from APs to BPs to precursor cells; Fig.4.13A). Peak calling was performed along the inferred trajectory and the identified CREs were grouped into three main categories based on their accessibility profiles along the pseudotime: “initial”, “intermediate”, and “late” CREs, corresponding broadly to APs, BPs, and precursor cells. In the “initial” CREs group more peaks were found in $FT_{E16.5\ +\ 6h}$ in respect to $FT_{E12.5\ +\ 6h}$, suggesting an early opening of additional regulatory elements in E16.5 progenitors (Fig.4.13B). To identify the TFs associated to all the identified CREs, a motif scanning was conducted at both stages. Both common and stage-specific motifs could be identified (Fig.4.13A). Motifs of TFs associated with inhibitory neuron development, such as Tcf4, Meis2, Ebf1, and Isl1, were detected at both stages. Conversely, several motifs from the NFI family (Nfia, Nfib, Nfic) were linked exclusively to “initial” CREs in $FT_{E16.5\ +\ 6h}$. The NFI TFs are known for regulating key steps during brain development (Zenker et al., 2019), such as neural and glial cell differentiation

(Bunt et al., 2017), neuronal migration (Heng et al., 2012), and maturation (Hickey et al., 2019).

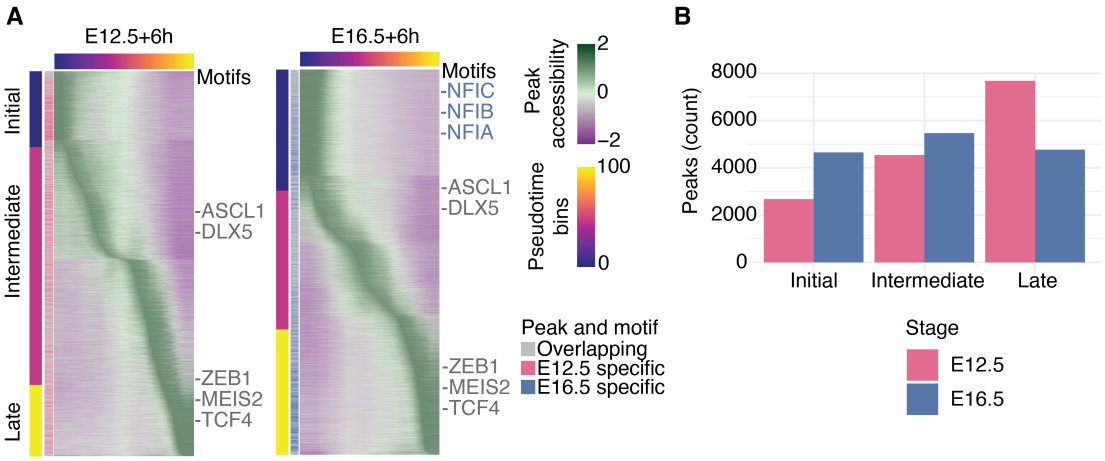

Figure 4.13: **Peak accessibility distribution analysis in pseudotime. A**. Heatmap displaying the accessibility of cis-regulatory elements across pseudotime for $FT_{E12.5 + 6h}$ and $FT_{E16.5 + 6h}$. Peaks are divided into "initial", "intermediate" and "late" based on accessibility profiles along pseudotime bins. Overlapping peaks are annotated in grey and unique peaks are annotated by stage-specific colours. Motifs common to both stages are written in grey while unique motifs are in blue. **B**. Barplot quantifying peak distribution across initial, intermediate, and late phases of pseudotime.

DNA-binding proteins, like TFs, protect genomic regions from Tn5 integration during ATAC-seq sample preparation, hindering the cleavage of DNA and creating a measurable footprint that reflects the binding patterns of TFs on chromatin. These footprints, thus predict the strength of TF binding (i.e. TF activity) and binding locations. A footprint analysis was conducted on the FT^{+} cohorts, using TOBIAS (Bentsen et al., 2020), followed by differential binding analysis. Among the differential factors, the NFI family demonstrated the most substantial and statistically significant increase of TF binding activity in $FT_{E16.5 + 6h}$ compared to $FT_{E12.5 + 6h}$(Fig.4.14A). To visualize and evaluate this finding, stage-specific aggregate footprint profiles were generated for select TFs (Fig.4.14B). Nfix, Nfic, and Nfia displayed TF activity only in $FT_{E16.5 + 6h}$ while Nfib displayed TF activity already in $FT_{E12.5 + 6h}$, which significantly increased in $FT_{E16.5 + 6h}$ (Fig.4.14B).

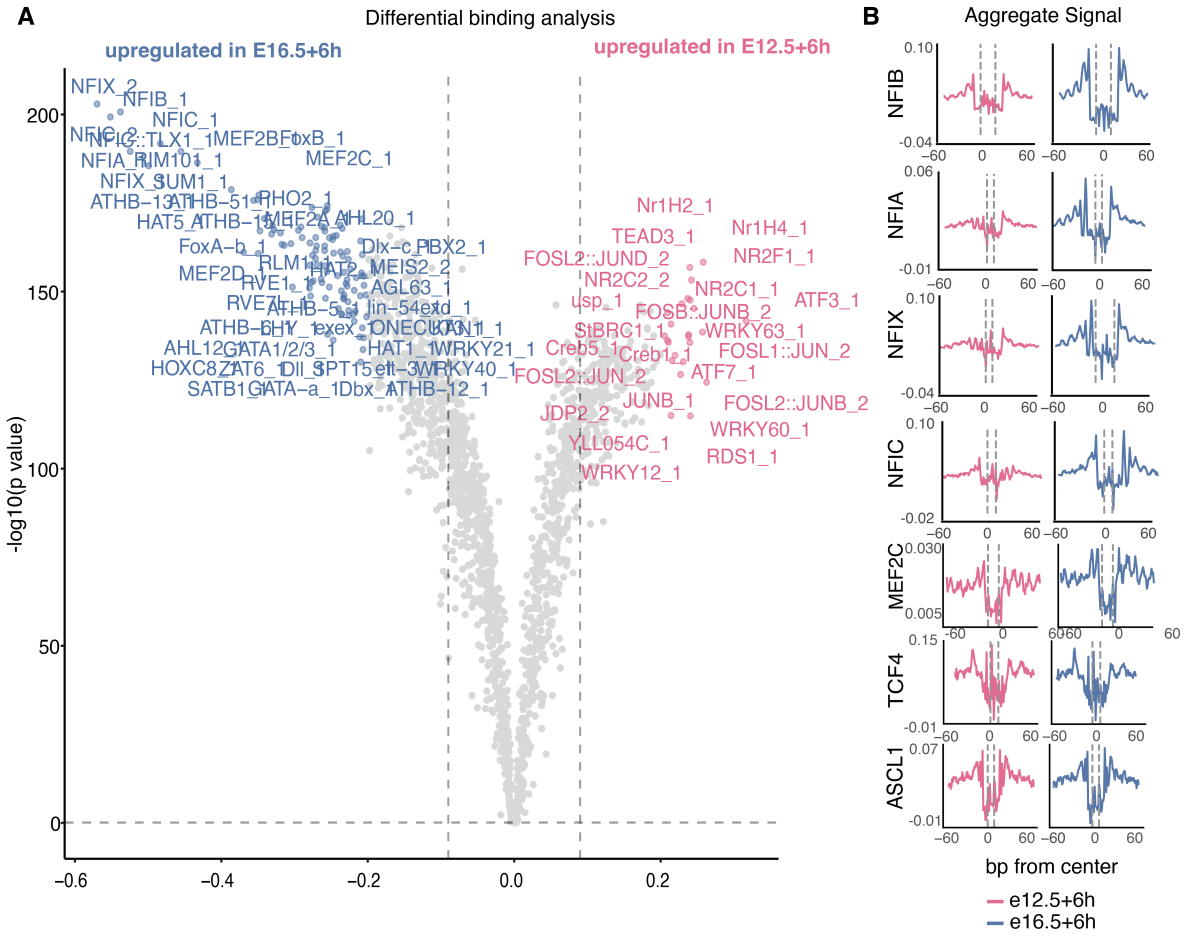

Figure 4.14: **Differential binding analysis in early and late cohort of GABAergic cells.** **A**. Volcano plot displaying –log10(P-value)(x-axis) and differential binding score (y-axis) of significant transcription factors. Each dot represents a motif. **B**. Aggregate footprint profiles of select transcription factors in $\mathrm{FT}_{\mathrm{E12.5\,+\,6h}}$ and $\mathrm{FT}_{\mathrm{E16.5\,+\,6h}}$. **C**. Boxplot showing normalized gene expression levels at E12.5, E14.5 and E16.5; scRNA-seq dataset. Cells with no expression of the selected genes are not displayed. **D**. Coverage plot showing chromatin accessibility dynamics at Nfib, Nfia, Nfic and Nfix footprint sites in $\mathrm{FT}_{\mathrm{E12.5\,+\,6h}}$ and $\mathrm{FT}_{\mathrm{E16.5\,+\,6h}}$ datasets.

The footprint profiles align with the gradual increase in gene expression patterns of the NFI family of TFs observed in the transcriptomic data (Fig.4.15A). Next, to assess whether regions, where the NFI family TFs binds (footprint sites), exhibit dynamic changes in accessibility, the fragment distribution within these regions was calculated (Fig.4.14B). Coverage plots displayed a temporal increase in accessibility from $\mathrm{FT}_{\mathrm{E12.5\,+\,6h}}$ to $\mathrm{FT}_{\mathrm{E16.5\,+\,6h}}$ at Nfib,

Nfia, Nfic, and Nfix footprint sites. These results indicate a potential association of these factors with the observed chromatin dynamics, highlighting their likely role in chromatin remodeling.

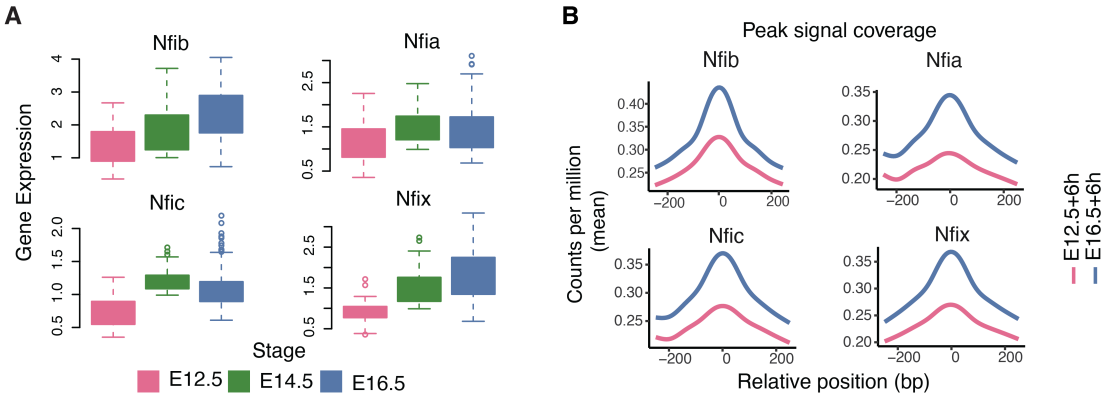

Figure 4.15: **Gene expression and footprint analysis of NFI transcription factors.** **A**. Boxplot showing normalised gene expression levels of Nfib, Nfia, Nfic, and Nfix at E12.5, E14.5, and E16.5; scRNA-seq dataset. Cells with no expression of the selected genes are not displayed. **B**. Coverage plot showing chromatin accessibility dynamics at Nfib, Nfia, Nfic, and Nfix footprint sites in scATAC-seq $\mathrm{FT}_{\mathrm{E12.5+6h}}$ and $\mathrm{FT}_{\mathrm{E16.5+6h}}$ datasets.

Taken together, these findings demonstrate that FT^{+} cohorts exhibit stage-specific chromatin accessibility, driven mainly by CREs. Furthermore, the NFI family of TFs plays a crucial role in characterizing $\mathrm{FT}_{\mathrm{E16.5+6h}}$ cells based on their expression, early activation of regulatory elements, and footprint. When comparing scATAC-seq profiles between $\mathrm{FT}_{\mathrm{E12.5+6h}}$ and $\mathrm{FT}_{\mathrm{E16.5+6h}}$, distal regulatory elements (i.e. enhancers) were identified to be the prime source of heterogeneity.

To comprehensively infer enhancer-driven regulatory interactions, SCENIC+ package (Gonzalez-Blas et al., 2023) was utilized. Gene expression and chromatin accessibility datasets of $\mathrm{FT}_{\mathrm{E12.5+6h}}$ and $\mathrm{FT}_{\mathrm{E16.5+6h}}$ were combined to link genomic binding events (i.e. a TF binding to a regulatory site) to downstream target genes. The analysis was performed on cells grouped by collection stage (E12.5 and E16.5) and broad cell-state (APs, BPs, and precursors), obtaining six groups in total (Fig.4.16A). After running the

SCENIC+ pipeline with standard filtering, the resulting GRN contained 147 TFs that bound on average 168 sites, with each site regulating one to three target genes (mean = 1.1; Fig.4.16B-D). The activity of regulatory modules (i.e. expression of TF and associated

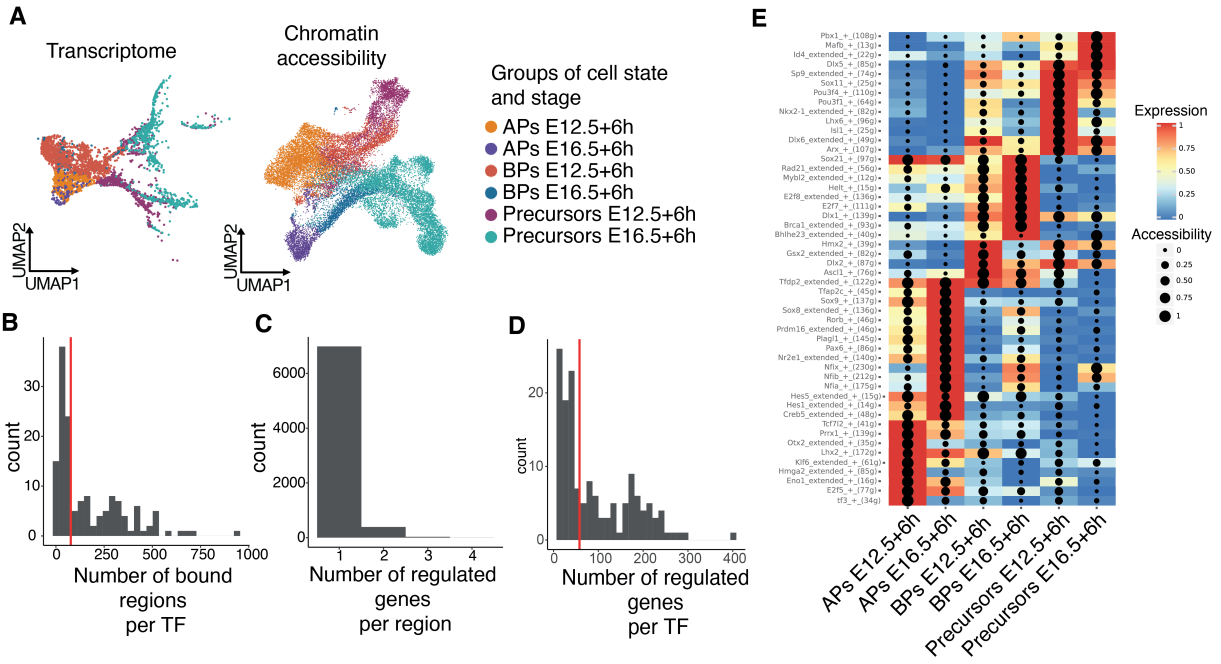

Figure 4.16: **Combination of transcriptome and chromatin in gene regulatory network analysis. A**. UMAP embedding of cells from scRNA-seq (left) and scATAC-seq (right). Cells are annotated based on broad cell state and stage. **B-D**. Distribution of the number of bound regions per TF (**B**), regulated genes per region (**C**), and target genes per TF (**D**). Red horizontal lines in (**B**) and (**D**) indicate the median of the corresponding distribution. **E**. Heatmap displaying active marker modules for stage-specific cell states. The color indicates the scaled average expression of the module (i.e. TF expression and target genes expression). Dot size indicates scaled accessibility of associated regulatory regions. Modules are named after the TF, type of regulation (here only positive), and number of target genes.

target genes) was scored in each cell (Aibar et al., 2017), and enriched modules for each group were identified (Fig.4.16E). Modules of canonical cell state marker genes exhibited enrichment in the respective groups: modules of Hes5, Hes1, and Pax6 in APs (Ohtsuka et al., 2001; Thakurela et al., 2016), Ascl1 and Dlx2 modules in BPs (Raposo et al., 2015; Lindtner et al., 2019), and modules of either Dlx5 or Lhx6 in neuronal precursors (Lindtner

et al., 2019; Liodis et al., 2007). Modules exhibiting patterns specific to certain cell states or developmental stages were observed. For example, Nkx2-1 was active in BPs and precursor states, yet remained restricted to $FT_{E12.5 + 6h}$. Modules of NFI family TFs were active across all cell states in $FT_{E16.5 + 6h}$, with the highest activity in APs compared to BPs and precursor cells. Next, active gene regulatory interactions specific to the six groups were

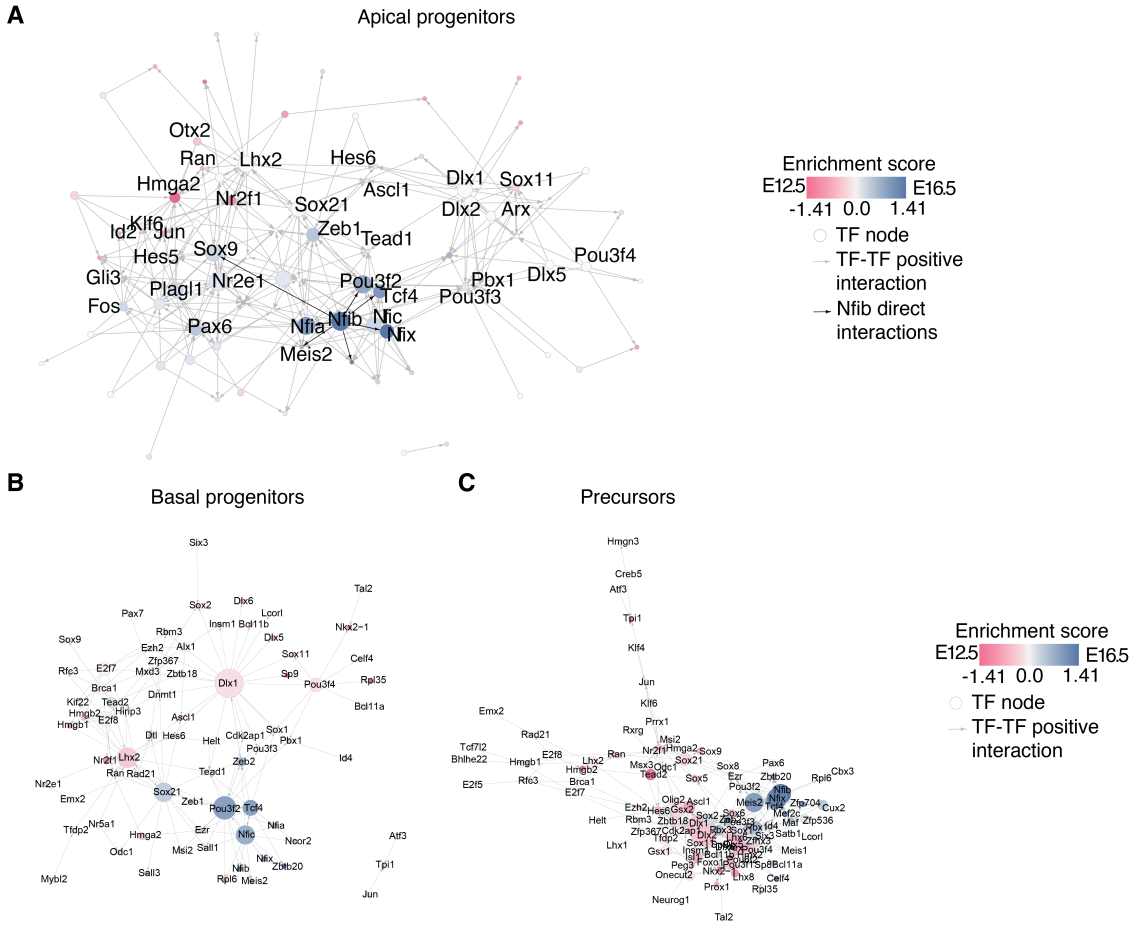

Figure 4.17: **Enhancer-driven gene regulatory networks in broad clusters of GABAergic cells. A-C**, Subnetwork for APs (**A**), BPs (**B**) and precursors (**C**). Each subnetwork is merged across E12.5 and E16.5, with node color indicating the difference in expression between stages. The size of nodes reflects the number of downstream targets per TF. Subnetworks show only positive interaction between TFs.

inferred by filtering the GRN for modules active in over 50% of cells per group and applying an additional filter on downstream target genes based on gene expression level (normalized

expression > 0.5). A subnetwork for every group was obtained, each containing state- and stage-specific modules of active TFs and target genes (Fig.4.17A-C). The analysis focused specifically on subnetworks of APs to identify modules that maintain or modulate progenitor competence (Fig.4.17A). Modules of canonical inhibitory neuron markers like Dlx1, Dlx2, and Arx were maintained throughout all stages (Lindtner et al., 2019; Colasante et al., 2015), whereas modules linked to progenitor self-renewal, like Hmga2, Nr2f1, and Nr2f2 (Nishino et al., 2008; Bertacchi et al., 2020), were enriched in E12.5 APs. APs at E16.5 were characterized by enriched activity of Nfib, together with Nfia, Nfix, Pou3f2, Meis2, and Tcf4. In line with previous studies, Nfib acts as an upstream regulator of Nfix (Matuzelski et al., 2017), but also as an upstream regulator of Nfia, Pou3f2, Meis2, and Tcf4.

Of particular interest was the interaction of Nfib with Meis2 and Tcf4, which are TFs specific to the development of inhibitory projection neurons and interneurons, respectively (Su et al., 2022; Wang et al., 2022). These three TFs share common direct target genes in different cell states of $FT_{E16.5\ +\ 6h}$ (Fig.4.17A), suggesting combinatorial binding of Nfib with Tcf4 or Meis2. To test this hypothesis, TFCOMB (Bentsen et al., 2022) was utilized to analyse peaks from $FT_{E12.5\ +\ 6h}$ and $FT_{E16.5\ +\ 6h}$ scATAC-seq datasets (Fig.4.18A). Interestingly, collaboration of Nfib with these factors was observed at both stages, with higher cosine scores and more binding events for Nfib-Tcf4 and Nfib-Meis2 in E16.5 peaks (Fig.4.18B). Additionally, Nfib, Meis2 and Tcf4 shared direct downstream target genes (Fig.4.18C). Gene ontology (GO) enrichment analysis of the downstream genes indicated involvement in processes related to brain development, neuron fate specification, and positive regulation of cell proliferation (Fig.4.18D).

In summary, regulatory clusters specific to mitotic and postmitotic cells of the E16.5 cohort were identified. One of these clusters is led by Nfib which regulates and interacts with Meis2 and Tcf4 via direct targeting and combinatorial binding. Together, these genes

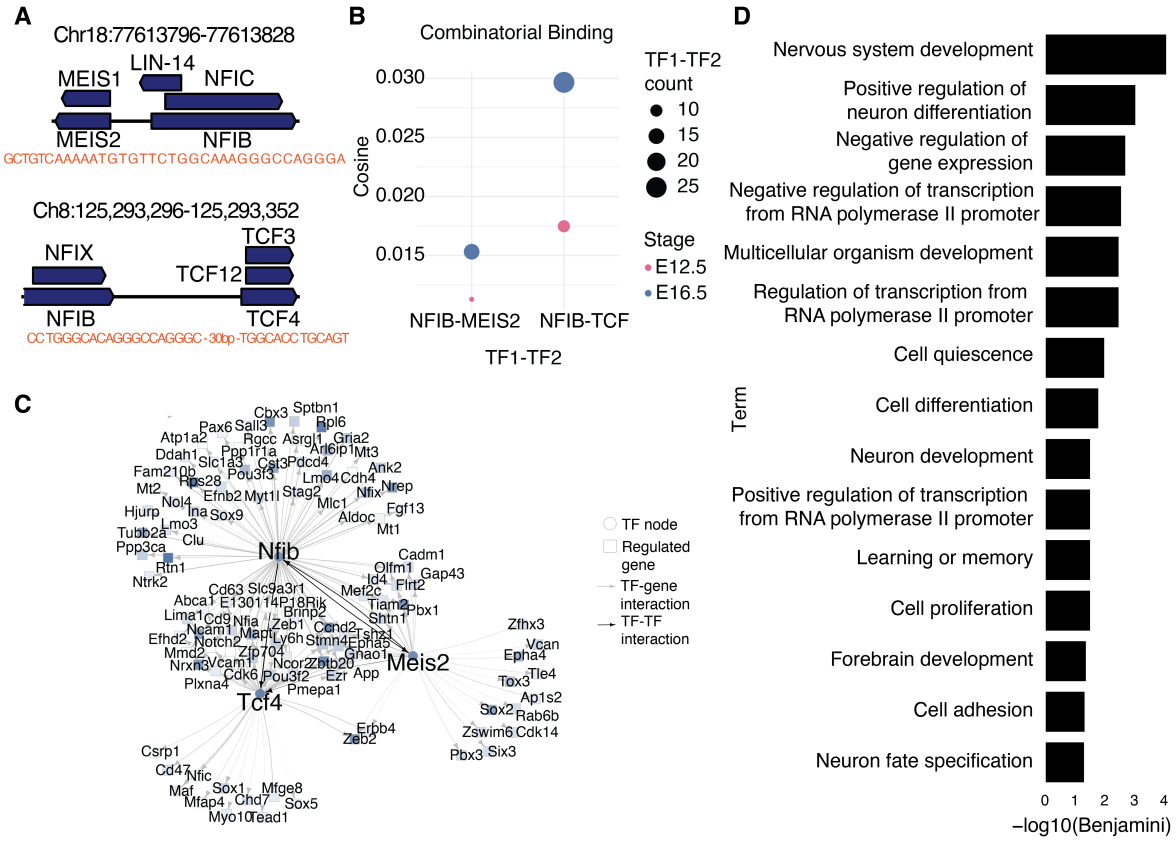

Figure 4.18: **Combinatorial binding analysis. A**. Genomic view of transcription factor binding sites for Nfib-Meis2 and Nfib-Tcf4. **B**. Dot plot showing cosine score on the y-axis and TF pairs on the x-axis. Colour and size indicate the stage and the number of occurrences of TF1-TF2, respectively. **C**. GRN subgraph highlighting downstream targets of Nfib, Tcf4 and Meis2 at E16.5. Nfib, Tcf4 and Meis2 nodes are indicated by node shape. Interactions between Nfib, Tcf4 and Meis2 are highlighted. Node color reflects the enrichment score by stage. **D**. Significantly enriched GO-terms (Benjamini-Hochberg corrected $P < 0.05$) for target genes of Nfib and Nfix and/or Tcf4 in E16.5 cells.

regulate pathways that promote the maturation from progenitor cell to neuron.

In summary, these findings suggest that this eGRN is linked to the shift in the maturation competence of GABAergic progenitors.

4.5 Influence of extrinsic environment on maturation competence

To investigate whether the extrinsic environment affects maturation competence in APs at different stages, homo- and hetero-chronic transplantation experiments were performed and the PT scores along with the expression of genes downstream of Nfib, Tcf4, and Meis2 were assessed.

For the transplantation experiment, CFSE was injected into the ventricles of donor mouse embryos at E12.5 and E16.5. One hour later, GEs were dissected and dissociated, resulting in a cell suspension comprising FT-labelled APs, unlabelled BPs, and unlabelled precursor cells. The cell suspension was transplanted homo- and hetero-chronically into host embryos via intraventricular injection. Forty-eight hours after transplantation, the GEs were collected from the host embryos, FT^+ cells were isolated by FACS, and their transcriptome was assessed via bulk RNA sequencing ($AP_{E12.5 \rightarrow E12.5}$ and $AP_{E12.5 \rightarrow E16.5}$ for early APs and $AP_{E16.5 \rightarrow E16.5}$ and $AP_{E16.5 \rightarrow E12.5}$ for late APs). At the collection stage, cells have entered the tissue and started to migrate away from the ventricular zone (Materials & Methods). FPKM normalization was utilized on the collected bulk RNA-seq datasets (Fig.4.19A). Employing clusters of the combined scRNA-seq data as reference, the proportions of different neuronal states were estimated in transplantation datasets utilizing Bisque (Jew et al., 2020; Fig.4.19B,C). Next, a PT score was assigned to each replicate by using the average PT score per reference cluster and weighting it according to the inferred cell state proportions. The PT scores were higher when APs were transplanted into an E16.5 environment ($AP_{E12.5 \rightarrow E16.5}$, $AP_{E16.5 \rightarrow E16.5}$) compared to an E12.5 environment ($AP_{E12.5 \rightarrow E12.5}$, $AP_{E16.5 \rightarrow E12.5}$; Fig.4.20A,B). To identify the transcriptomic differences resulting from transplantation, the count matrix was filtered by highly variable

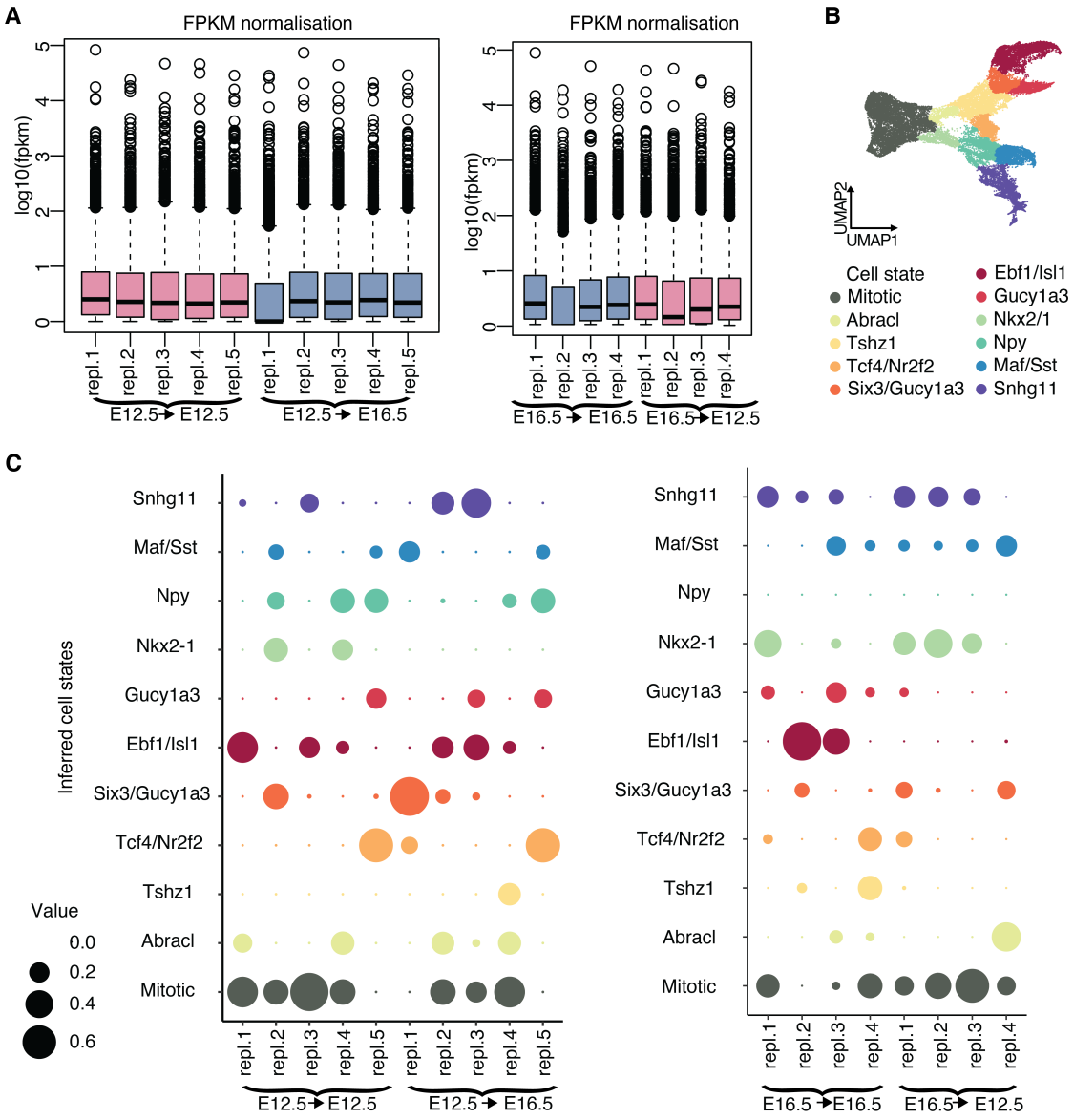

Figure 4.19: **Cell state inference in the transplanted cohorts of cells.** **A**. FPKM normalization of count matrices of the transplantation bulk RNAseq datasets. **B**. UMAP plot of the combined dataset utilized for cluster reference. **C**. Predicted cell state composition in each replicate of transplantation bulk RNAseq datasets.

genes from the combined transcriptome dataset and DeSeq2 (Love et al., 2014) was used for differential expression analysis (Fig.4.20C,D). Notably, Nfib and many of its downstream genes (among other genes) exhibited increased expression in $AP_{E12.5 \rightarrow E16.5}$ compared to

$AP_{E12.5 \rightarrow E12.5}$. However, no significantly downregulated genes were observed (Fig.4.20C). Furthermore, only two genes downstream of Nfib (Mlc1 and Aldoc) were significantly downregulated in $AP_{E16.5 \rightarrow E12.5}$ compared to $AP_{E16.5 \rightarrow E16.5}$ (Fig.4.20D).

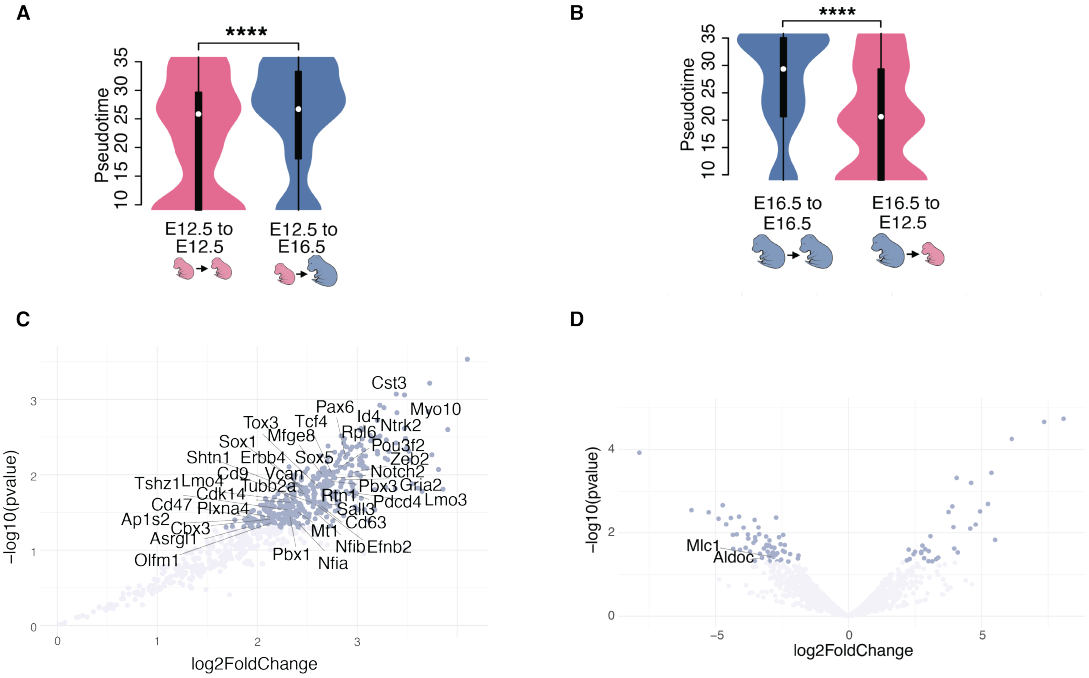

Figure 4.20: **Pseudotime scoring and differential gene expression in transplanted cells.** **A**. Distribution of transplanted cells along pseudotime in $AP_{E12.5 \rightarrow E12.5}$ and $AP_{E12.5 \rightarrow E16.5}$; two-sided Wilcoxon rank sum test ($****adjustedP < 0.001$). **B**. Distribution of transplanted cells along pseudotime in $AP_{E16.5 \rightarrow E16.5}$ and $AP_{E16.5 \rightarrow E12.5}$; two-sided Wilcoxon rank sum test ($****adjustedP < 0.001$). **C**. Differentially expressed genes between $AP_{E12.5 \rightarrow E12.5}$ and $AP_{E12.5 \rightarrow E16.5}$; $1 < log_2FC < -1$, $P < 0.05$. Only genes downstream of Nfib, Meis2 and Tcf4 are labelled. **D**. Differentially expressed genes between $AP_{E16.5 \rightarrow E16.5}$ and $AP_{E16.5 \rightarrow E12.5}$; $1 < log_2FC < -1$, $P < 0.05$. Only genes downstream of Nfib, Meis2 and Tcf4 are labelled.

These findings indicate an involvement of the extrinsic environment in shaping the maturation competence of transplanted cells. The patterns of PT and gene expression were reminiscent of the recipient stage. The gene expression change after transplantation suggests that maturation competence is likely a mechanism that operates through acquisition rather than loss of specific genes.

5 Discussion

5.1 Developmental patterns differ in ventral and dorsal lineages

In this study, the developmental patterning of the inhibitory lineage was examined by tracking the progression from progenitor cells to precursors at different stages of neurogenesis and comparing the results with existing patterns described in the literature.

The developmental trajectory of inhibitory neurons was observed to diverge after the exit from the cell cycle and branch into transcriptomically distinct postmitotic cell states. At embryonic days 12.5, 14.5, and 16.5, a similar repertoire of neuron subtypes was generated, irrespective of developmental stage, suggesting a stable developmental pattern. Furthermore, analysis of transcription factors expressed along the maturation trajectory revealed a conserved genetic cascade across neurogenesis.

Several models have been proposed in the past to explain the fate specification of GABAergic neurons, including the "progenitor specification" and "progressive specification" hypotheses (Wamsley and Fishell, 2017). The progenitor specification hypothesis posits that cell fate is determined at the progenitor state level. Fate-mapping studies have supported this view by identifying spatial and temporal cues that bias the development of specific cell types, such as chandelier cells (Taniguchi et al., 2013), somatostatin- and

parvalbumin-expressing interneurons (Inan et al., 2012), and striosome and matrix compartments of the striatum (Kelly et al., 2018). However, while multiple studies described temporal and spatial differentiation patterns in GABAergic neurons (Wonders et al., 2008; Butt et al., 2008; Flames et al., 2007; Miyoshi et al., 2007), there is no evidence of a fate birthmark transmitted from apical progenitors to their daughter cells. In contrast, the progressive specification hypothesis suggests that inhibitory subtype specification occurs later, after cell cycle exit. This model suggests that the refinement of inhibitory cells subtypes occurs gradually over an extended period, during which they interact with transcription factors that transduce patterning signals (Rubenstein and Puelles, 1994; Shimamura et al., 1995; Wichterle et al., 2001; Nery et al., 2002; Xu et al., 2004; Wonders and Anderson, 2006; Flames et al., 2007; Sandberg et al., 2016), migrate (Lim et al., 2018), and mature in morphology (De Marco Garcia et al., 2011) and synapse formation (De Felipe et al., 1997; Katz and Shatz, 1996).

In this study, differential gene expression analysis in inhibitory progenitors at E12.5 and E16.5 revealed that stage-specific marker genes primarily regulate the balance between cell proliferation and differentiation. This suggests that progenitors differ mainly in genes related to broader cellular behaviors rather than specific fate-determining factors. This pattern of inhibitory neuron development contrasts with the sequential shift in progenitor fate competence observed in excitatory neurons (Telley et al., 2019; Vitali et al., 2018; Di Bella et al., 2021). The temporal competence of dorsal RGCs changes over time, as evidenced by the stage-specific transcriptomic profiles regulated by multifactorial gene networks (Telley et al., 2016, 2019), leading to the progressive generation of distinct cell types (Di Bella et al., 2021). In summary, this research shows that ganglionic eminences generate inhibitory cell states from a consistent pool of progenitors across developmental stages. This pool of progenitors remains largely unchanged over time, suggesting that the diversification into distinct GABAergic subtypes is a later developmental event.

5.2 Clonally related inhibitory neurons share mixed transcriptomic signatures

To further investigate inhibitory neuron progenitor competence and commitment, a clonal tracking technique called TrackerSeq was utilized. This method labels single cells with heritable barcodes, allowing to trace sister cells that have differentiated into specialized cell states and analyze their transcriptome. Two datasets with similar characteristics were compared: one involving injection of TrackerSeq barcodes at E12.5 (from Bandler et al., 2022), and one at E16.5 (generated in this study).

Both datasets revealed the presence of clones distributed across all the various inhibitory cell states, demonstrating that clonal relationships can be studied in comparable cell populations at different stages. Clonally related cells can be classified as "dispersing" or "non-dispersing" based on their grouping into multiple or only one cell state clusters respectively. In this study, the number of "dispersing" clones was comparable at both early and late stages, indicating that a similar subset of progenitors remains multipotent. This is in contrast to what was observed for excitatory progenitors, which undergo progressive fate restriction (Frantz and McConnell, 1996; Oberst et al., 2019). Therefore, ventral RGCs exhibited a "mixed" competence, where some progenitors grouped with a single differentiated cell type, while others shared barcodes with multiple cell types. It is important to note that due to the nature of the experiment, some cells may have been lost during dissection, meaning the actual proportion of dispersing clones could be much larger. Other studies that have utilized clonal analysis demonstrated the production of both Pvalb and Sst interneurons by individual progenitor cells in the MGE, supporting the multipotent progenitor hypothesis (Mayer et al., 2015; Harwell et al., 2015). Furthermore, MGE progenitors have been demonstrated to retain a high degree of plasticity during neurogenesis

and capability to convert into CGE-like cells (Xu et al., 2010).

Correlation analysis revealed that mitotic cells differ from fate-specified differentiated cells whether selected randomly or as sister cells of the analyzed fate. This suggests that although these progenitors are clonally connected with only one progenitor cell state, they did not exhibit a distinct transcriptomic signature. This finding does not exclude that chromatin-level regulation, rather than transcriptomic differences, may be driving the fate specification at this neurogenic period. Multiple genetic fate mapping studies, paired with mathematical modeling, have tried to address the complexity of cellular diversity within specific brain structures (see Zechner et al., 2020 for review). While the vast heterogeneity within the CNS is widely accepted, there remains no consensus on how this diversity emerges. On the progenitor competence level, some research suggests that progenitor subtype diversity is key to understanding this variability (van Heusden et al., 2021). In contrast, other studies propose that the brain may harbor multipotent progenitors whose fate choices are largely stochastic (Clément and Olayé, 2024). Advances in single-cell transcriptomics, particularly studies of radial glial cells (RGCs) in the mouse cortex, have revisited this debate. For instance, Cux2-positive RGCs are intrinsically programmed to generate upper-layer neurons, independent of birthdate or niche, suggesting that molecular fate specification dictates the birth order (Franco et al., 2012). However, subsequent findings have identified multipotent progenitors that can give rise to both deep- and upper-layer neurons, challenging the deterministic framework (Guo et al., 2013). This interplay of stochastic and deterministic mechanisms is observed in other CNS structures, such as the zebrafish telencephalon and retina. In the retina, for instance, early neurogenesis appears to follow stochastic fate decisions, but as development progresses, deterministic patterns begin to dominate, particularly for cell types like Müller glia (He et al., 2012; Rulands et al., 2018).

In this study, the presence of both “dispersing” and “non-dispersing” clones within the

same cell population suggests that the progenitor fate competence in the GE might be governed by a dynamic mix of stochastic and deterministic processes working in concert.

5.3 Early- and late-born GABAergic neurons exhibit diverse levels of transcriptomic maturation

After exploring the competence of inhibitory progenitors in terms of their neuronal differentiation and clonal output, this study aimed to investigate the stage-specific gene expression profile in progenitors and their daughter cells and identify possible patterns. Cell birthdating techniques were employed to gain a more precise understanding of the transcriptomic signatures that progenitor cells may pass on to their daughter cells at various developmental time points. FlashTag labeling led to the screening of both progenitors and newly-born neuron precursors. Cells born at E12.5, and collected either 6 hours or 96 hours after, exhibited distinct gene expression profiles, consistent with the distinct experimental conditions. The E12.5 + 6 hours group mapped to the beginning of the pseudotime trajectory, while the cells collected 96 hours later mapped to the end of it, reflecting the cell maturation that occurred during this time period. A comparison of gene expression between newly-born precursors (collected 6 hours after labeling) at E12.5 and E16.5 revealed no differences in genes specific to cell fate. However, differences in genes indicative of varying maturation levels were observed. Interestingly, cells born at E16.5 exhibited gene expression patterns similar to the E12 + 96 hours group and mapped to an intermediate position on the pseudotime trajectory, between the two early-born groups (E12.5 + 6 hours and E12.5 + 96 hours). This demonstrated that inhibitory neurons give rise to progeny with varying maturation levels depending on the developmental time point, with late-born cells reaching similar maturation levels as early-born cells that had 96 hours to develop.

This variation in maturation likely functions as a regulatory mechanism to synchronize

neurogenesis across different stages of development, which is crucial for organizing the implicated processes in a precise sequence and at a specific pace to ensure proper embryonic development (Ebisuya and Briscoe, 2018). In this study, the variation in the maturation of precursor cells emerges immediately after the cell cycle exit, suggesting the involvement of a developmental clock mechanism already at the level of RGCs. Developmental cues may be transmitted as a "birthmark" from ventral progenitors to their daughter cells, similar to what was observed in birthdating studies in the dorsal telencephalon (Telley et al., 2019; Pollen et al., 2015). Excitatory progenitors exhibit a temporal progression in their competence from an internally directed "introverted" status to a more exteroceptive "extraverted" status (Vitali et al., 2018). This shift is characterized by the prevalence of cell-cycle-related and chromatin-related processes in early RGCs, and signaling molecules essential for responding to external stimuli in the late RGCs (Vitali et al., 2018; Telley et al., 2019). A similar pattern was observed in the present study, where cell-cycle and cell-division-related processes are inferred from the gene ontology analysis of E12.5 progenitors, while differentiation and extracellular communication pathways are notably enriched in the E16.5 cohort of labeled cells.

The findings in this study are consistent with the concept of a global developmental clock, integrating both intrinsic cellular programs and extrinsic signals, ensuring that progenitors pass on stage-specific maturation cues (Busby and Steventon, 2021). Different clock mechanisms have been proposed to explain distinct developmental maturation times in neurons both inter- and intra-species. Some examples are the rate of metabolic activity in mitochondria (Iwata et al., 2023) or selective translation of epigenetic modifiers (Wu et al., 2022). In particular, the depletion of Fbl reduces the translation of Ezh2, a member of the polycomb repressive complex 2 (PRC2), affecting the differentiation of neuronal stem cells (Wu et al., 2022). Furthermore, it has been shown that the release of epigenetic barriers also sets the timing of maturation in neural progenitor cells, with key

factors including EZH2, EHMT1/2, and DOT1L (Ciceri et al., 2024; Appiah et al., 2023). Consistent with this, the loss of Ring1B, a component of the polycomb group (PcG) complex, in cortical progenitors results in the prolonged generation of early neuronal subtypes (Morimoto-Suzki et al., 2014). In general, the progression of distinct cell types during development is inherently tied to the timing at which cells are competent to receive either the inhibition or activation of intrinsic and extrinsic signals (Barry et al., 2017; Marchetto et al., 2019).

In this study, different maturation levels characterize neurons born at different stages from a transcriptomically homogeneous pool of progenitor cells. This suggests a possible involvement of intrinsic and/or extrinsic factors, that influence the progenitor competence in a stage-specific manner. Both of these hypotheses were explored through chromatin analysis and transplantation experiments.

5.4 Chromatin accessibility and network dynamics reveal temporal changes in gene regulation

To explore the cell-intrinsic aspects of inhibitory progenitor competence, chromatin accessibility has been analyzed in progenitors and precursors at different stages.

Analysis of E12.5 and E16.5 cohorts revealed significant temporal differences in the epigenetic landscape, beginning at the level of the progenitor cells. In chromatin regions accessible at both time points, the ratio between distal and promoter sites was similar, while stage-specific peaks showed a stronger bias toward distal regions rather than promoters. This suggests that the variability in the chromatin of early and late cohorts is driven by changes at the levels of enhancers rather than promoters or gene body accessibility. Furthermore, E12.5 and E16.5 specific peaks did not exhibit a clear-cut distinction between the stages, but a gradual opening or closing pattern. This observation was confirmed by

the analysis of H3Kme1, a marker for enhancers, that displayed the same pattern of counts per million as the differential peaks and indicates that rather than drastic changes in gene expression, the observed heterogeneity may be driven by the differential regulation of genes through enhancer activity, a phenomenon already observed in the development process (Wang et al., 2015; Falo-Sanjuan et al., 2019).

The chromatin accessibility and the enhancer-driven gene regulatory network (eGRN) highlighted the relation of the NFI family of transcription factors with a significant number of peaks mapped to the beginning of the pseudotime trajectory, corresponding to apical progenitor regions. In particular, Nfib and Nfix were predicted to positively interact at both stages with genes essential for the proper identity of ventral lineages (Anderson et al., 1997; Lindtner et al., 2019). Connections observed specifically at E12.5 included Nr2f1, Hmga2, Jun, and Otx2 genes, which are known to be involved in early neural patterning and progenitor maintenance (Nishino et al., 2008; Bertacchi et al., 2020). At E16.5, the network was dominated by interactions with transcription factors crucial for the specification of inhibitory projection neurons - Meis2 - and interneurons - Tcf4 (Wang et al., 2022; Su et al., 2022; Dvoretskova et al., 2023).

NFI factors are known to regulate both neuronal and glial lineages during central nervous system development (Bunt et al., 2017). In their absence, radial glial cells fail to differentiate, leading to an accumulation of undifferentiated cells by the end of neurogenesis (Betancourt et al., 2014; Harris et al., 2016; Clark et al., 2019). Recent research has identified a link between the NFI family and a high number of transcription factor activities, emphasizing their extensive role in organism regulation (Göös et al., 2022). Furthermore, the NFI family of factors has been shown to promote the progression of neurogenesis in human subplate and deep-layer cortical neurons by acting as cofactors with FOXP2. This partnership facilitates chromatin opening and activates neuronal maturation genes (Hickey et al., 2019).

Based on these findings, this study hypothesizes that the interaction between the NFI family, in particular the Nfib and Nfix transcription factors, with essential regulators of GABAergic interneurons and projection neurons, leads to more mature neurons. The gradual expression and binding patterns of these transcription factors are consistent with the accumulation-based mechanism typical of developmental clocks (Ebisuya and Briscoe, 2018). Furthermore, since the main source of heterogeneity in the chromatin landscape was enhancer-driven, Nfib and Nfix may prime enhancer regions in APs of the GEs, initiating chromatin remodeling and leading to stage-specific maturation competence. However, further chromatin immunoprecipitation and genetic perturbation studies are needed to confirm this hypothesis.

5.5 Extrinsic environment and progenitor competence are linked

To investigate whether cell-extrinsic mechanisms influence the competence of inhibitory neuron progenitors, heterochronic and homochronic transplantation were utilized. Apical progenitors in the GE were transplanted in host brain ventricles at early and late embryonic stages of neurogenesis and collected after their integration in the GE tissue.

The cells that were transplanted in later-stage brains exhibited higher maturation scores based on their cell type composition. This could indicate that the environment surrounding apical progenitors at embryonic time points contains stage-specific cues that influence their development and maturation.

Pioneering transplantation studies in ferret brains have provided valuable insights into how environmental cues influence the plasticity and fate determination of cortical progenitors (McConnell and Kaznowski, 1991). More recent single-cell analyses in the mouse cortex have revealed that early-stage radial glial cells (RGCs) exhibit fate plasticity, with

their ability to generate neurons shifting over time to match the specific needs of later developmental stages (Oberst et al., 2019). In contrast, late-stage progenitors demonstrate a more restricted fate potential, with their plasticity significantly diminished (Kohwi and Doe, 2013; Oberst et al., 2019). It has been demonstrated that the diversification of cortical neurons and glia can be recapitulated in vitro (Gaspard et al., 2008; Shen et al., 2006; Eiraku et al., 2008). However, numerous studies identified additional regulation provided by environmental factors, such as signals in cerebrospinal fluid (Lehtinen et al., 2011) and feedback from BPs and postmitotic neurons to APs (Parthasarathy et al., 2014; Seuntjens et al., 2009; Nelson et al., 2013). For example, during cortex development, sequential derepression and negative feedback from deep-layer neurons to APs may scale the production of upper-layer neurons (Toma et al., 2014).

In this study, APs from E12.5 and E16.5 responded differently after transplantation to a heterochronic environment. Early APs in late environments exhibited higher levels in the expression of genes that were part of the NFI family regulatory network, but no significantly downregulated neuronal genes were observed. Late APs in an early environment, on the other side, exhibited both upregulation and downregulation of genes, but only a few of the genes interacting in the NFI-led eGRN-specific network were significantly downregulated. This suggests that ventral progenitors may exhibit a progressive restriction in their plasticity to generate cells with different maturation levels and adjust to their host environment through the acquisition rather than loss of specific genes.

In summary, not only stage-specific cues are present in the ganglionic eminences progenitor environment, but also that apical progenitors might be more or less competent to respond to these signals. Further investigation is needed to reveal the mechanisms by which the transplanted cells interact and synchronize with the host environment.

6 Conclusion

6.1 Conclusion and outlook of the study

The question of how cell diversity arises from progenitor cells has been a central issue in developmental neurobiology. Waddington's "epigenetic landscape" model, proposed in 1957, suggests that fate decisions are represented as paths or valleys in a dynamic landscape, where cells roll down predetermined paths toward specific fates (Waddington, 1957). However, this model does not address whether these decisions are imprinted in fate-committed progenitors or whether they are progressively steered by intrinsic and/or extrinsic factors as they advance through their developmental pathway.

This study explores the developmental pathways of inhibitory progenitor cells during neurogenesis, the factors that influence their competence, and how these processes impact the differentiation and maturation of their progeny. Through a combination of clonal analysis, transcriptomics, chromatin accessibility, and transplantation techniques, several key insights were gained into the unique characteristics that govern neurogenesis in the ventral telencephalon. The transcriptomic analysis revealed that during the transition from progenitors to early neuron precursors, the differentiation of inhibitory neurons follows similar gene expression cascades, irrespective of developmental stage. This pattern contrasts with excitatory neurons, which undergo a tightly regulated sequential fate specification. Clonal tracking further demonstrated that progenitor cells in the ventral telencephalon retain

considerable plasticity at different developmental stages, with some progenitors remaining largely multipotent until later stages of neurogenesis. Notably, gene expression profiling of newly-born neurons identified significant variations in their maturation across different stages of neurogenesis. This finding supports the idea of a molecular timer mechanism that coordinates the maturation of progenitors, ensuring synchronization of neurogenesis at various stages of development. This idea was further explored by investigating chromatin accessibility, enhancer-driven gene regulatory networks, and the influence of external cues on progenitor cells. The NFI family of transcription factors, particularly Nfib and Nfix, has been identified as playing a key role in the maturation of inhibitory neurons through enhancer-driven regulation. Furthermore, stage-specific cues from the environment play a critical role in shaping progenitor behavior and neuronal maturation.

These insights deepen the understanding of the molecular mechanisms governing inhibitory neuron development and the generation of neuronal diversity in the ventral telencephalon. Furthermore, they highlight key differences between ventral and dorsal neurogenesis, revealing a heterogeneity in the mechanisms and patterns that shape development in the telencephalon. However, the research presents important limitations, including the lack of direct experimental correlation between the increase in NFI factors and changes in maturation levels, as well as the need for a more detailed investigation into the extrinsic factors that shape the stage-specific environment and synchronize progenitor cell behavior.

The findings suggest that the differentiation competence of ventral progenitors (i.e. their ability to generate transcriptomically distinct cell states) remains similar during development. Contrarily, their maturation competence (i.e. their capacity to generate neurons with distinct maturation levels) gradually narrows over time, driven by a combination of accumulating molecular cues and stage-specific environmental contexts.

In conclusion, the study highlights the dynamic interplay between intrinsic genetic programs and extrinsic environmental factors in regulating inhibitory progenitor competence.

Abbreviations

AP	Apical Progenitor
BP	Basal Progenitor
CFSE	Carboxyfluorescein Succinimidyl Ester
CRE	Cis-Regulatory Element
CthPN	Corticothalamic Projection Neuron
DL CPN	Deep Layer Callosal Projection Neuron
eGRN	Enhancer-driven Gene Regulatory Network
FACS	Fluorescence-Activated Cell Sorting
FPKM	Fragments Per Kilobase of transcript per Million mapped reads
FT	FlashTag
GE	Ganglionic Eminence
IN	Interneuron
IUE	In Utero Electroporation
PN	Projection Neuron

PT	Pseudotime
SCPN	Subcerebral Projection Neuron
scATAC-seq	Single-Cell Assay for Transposase-Accessible Chromatin using sequencing
scRNA-seq	Single-Cell RNA Sequencing
TF	Transcription Factor
UL CPN	Upper Layer Callosal Projection Neuron

Bibliography

Aaku-Saraste, E., Hellwig, A., and Huttner, W. B. (1996). Loss of occludin and functional tight junctions, but not zo-1, during neural tube closure–remodeling of the neuroepithelium prior to neurogenesis. *Dev Biol*, 180(2):664–79.

Afgan, E., Baker, D., Batut, B., van den Beek, M., Bouvier, D., Cech, M., Chilton, J., Clements, D., Coraor, N., Grüning, B. A., Guerler, A., Hillman-Jackson, J., Hiltemann, S., Jalili, V., Rasche, H., Soranzo, N., Goecks, J., Taylor, J., Nekrutenko, A., and Blankenberg, D. (2018). The galaxy platform for accessible, reproducible and collaborative biomedical analyses: 2018 update. *Nucleic Acids Res*, 46(W1):W537–W544.

Aibar, S., González-Blas, C. B., Moerman, T., Huynh-Thu, V. A., Imrichova, H., Hulselmans, G., Rambow, F., Marine, J.-C., Geurts, P., Aerts, J., van den Oord, J., Atak, Z. K., Wouters, J., and Aerts, S. (2017). Scenic: single-cell regulatory network inference and clustering. *Nat Methods*, 14(11):1083–1086.

Alemany, A., Florescu, M., Baron, C. S., Peterson-Maduro, J., and van Oudenaarden, A. (2018). Whole-organism clone tracing using single-cell sequencing. *Nature*, 556(7699):108–112.

Alvarez-Dominguez, J. R. and Melton, D. A. (2022). Cell maturation: Hallmarks, triggers, and manipulation. *Cell*, 185(2):235–249.

Anderson, S. A., Eisenstat, D. D., Shi, L., and Rubenstein, J. L. (1997). Interneuron migration from basal forebrain to neocortex: dependence on dlx genes. *Science*, 278(5337):474–6.

Anderson, S. A., Marin, O., Horn, C., Jennings, K., and Rubenstein, J. L. (2001). Distinct cortical migrations from the medial and lateral ganglionic eminences. *Development*, 128(3):353–63.

Appiah, B., Fullio, C. L., Ossola, C., Bertani, I., Restelli, E., Cheffer, A., Polenghi, M., Haffner, C., Garcia-Miralles, M., Zeis, P., Treppner, M., Bovio, P., Schlichtholz, L., Mas-Sanchez, A., Zografidou, L., Winter, J., Binder, H., Grün, D., Kalebic, N., Taverna, E., and Vogel, T. (2023). Dot1l activity affects neural stem cell division mode and reduces differentiation and asns expression. *EMBO Rep*, 24(8):e56233.

Bandler, R. C., Mayer, C., and Fishell, G. (2017). Cortical interneuron specification: the juncture of genes, time and geometry. *Curr Opin Neurobiol*, 42:17–24.

Bandler, R. C., Vitali, I., Delgado, R. N., Ho, M. C., Dvoretskova, E., Ibarra Molinas, J. S., Frazel, P. W., Mohammadkhani, M., Machold, R., Maedler, S., Liddelow, S. A., Nowakowski, T. J., Fishell, G., and Mayer, C. (2022). Single-cell delineation of lineage and genetic identity in the mouse brain. *Nature*, 601(7893):404–409.

Barry, C., Schmitz, M. T., Jiang, P., Schwartz, M. P., Duffin, B. M., Swanson, S., Bacher, R., Bolin, J. M., Elwell, A. L., McIntosh, B. E., Stewart, R., and Thomson, J. A. (2017). Species-specific developmental timing is maintained by pluripotent stem cells ex utero. *Dev Biol*, 423(2):101–110.

Beddington, R. S. (1982). An autoradiographic analysis of tissue potency in different regions of the embryonic ectoderm during gastrulation in the mouse. *J Embryol Exp Morphol*, 69:265–85.

Benjamini, Y. and Hochberg, Y. (1995). Controlling the False Discovery Rate: A Practical and Powerful Approach to Multiple Testing. *Journal of the Royal Statistical Society: Series B (Methodological)*, 57(1):289–300. _eprint: https://onlinelibrary.wiley.com/doi/pdf/10.1111/j.2517-6161.1995.tb02031.x.

Bentsen, M., Goymann, P., Schultheis, H., Klee, K., Petrova, A., Wiegandt, R., Fust, A., Preussner, J., Kuenne, C., Braun, T., Kim, J., and Looso, M. (2020). Atac-seq footprinting unravels kinetics of transcription factor binding during zygotic genome activation. *Nat Commun*, 11(1):4267.

Bentsen, M., Heger, V., Schultheis, H., Kuenne, C., and Looso, M. (2022). Tf-comb - discovering grammar of transcription factor binding sites. *Comput Struct Biotechnol J*, 20:4040–4051.

Bertacchi, M., Romano, A. L., Loubat, A., Tran Mau-Them, F., Willems, M., Faivre, L., Khau van Kien, P., Perrin, L., Devillard, F., Sorlin, A., Kuentz, P., Philippe, C., Garde, A., Neri, F., Di Giaimo, R., Oliviero, S., Cappello, S., D'Incerti, L., Frassoni, C., and Studer, M. (2020). NR2F1 regulates regional progenitor dynamics in the mouse neocortex and cortical gyrification in BBSOAS patients. *The EMBO Journal*, 39(13):e104163.

Bertrand, N., Castro, D. S., and Guillemot, F. (2002). Proneural genes and the specification of neural cell types. *Nat Rev Neurosci*, 3(7):517–30.

Betancourt, J., Katzman, S., and Chen, B. (2014). Nuclear factor one b regulates neural stem cell differentiation and axonal projection of corticofugal neurons. *J Comp Neurol*, 522(1):6–35.

Bonev, B., Mendelson Cohen, N., Szabo, Q., Fritsch, L., Papadopoulos, G. L., Lubling, Y., Xu, X., Lv, X., Hugnot, J.-P., Tanay, A., and Cavalli, G. (2017). Multiscale 3d genome rewiring during mouse neural development. *Cell*, 171(3):557–572.e24.

Borrell, V. and Reillo, I. (2012). Emerging roles of neural stem cells in cerebral cortex development and evolution. *Dev Neurobiol*, 72(7):955–71.

Brandão, J. A. and Romcy-Pereira, R. N. (2015). Interplay of environmental signals and progenitor diversity on fate specification of cortical gabaergic neurons. *Front Cell Neurosci*, 9:149.

Bravo González-Blas, C., Minnoye, L., Papasokrati, D., Aibar, S., Hulselmans, G., Christiaens, V., Davie, K., Wouters, J., and Aerts, S. (2019). cisTopic: cis-regulatory topic modeling on single-cell ATAC-seq data. *Nature Methods*, 16(5):397–400. Number: 5 Publisher: Nature Publishing Group.

Briscoe, J., Pierani, A., Jessell, T. M., and Ericson, J. (2000). A homeodomain protein code specifies progenitor cell identity and neuronal fate in the ventral neural tube. *Cell*, 101(4):435–45.

Buenrostro, J. D., Wu, B., Chang, H. Y., and Greenleaf, W. J. (2015). Atac-seq: A method for assaying chromatin accessibility genome-wide. *Curr Protoc Mol Biol*, 109:21.29.1–21.29.9.

Bunt, J., Osinski, J. M., Lim, J. W., Vidovic, D., Ye, Y., Zalucki, O., O'Connor, T. R., Harris, L., Gronostajski, R. M., Richards, L. J., and Piper, M. (2017). Combined allelic dosage of nfia and nfib regulates cortical development. *Brain Neurosci Adv*, 1:2398212817739433.

Busby, L. and Steventon, B. (2021). Tissue tectonics and the multi-scale regulation of developmental timing. *Interface Focus*, 11(3):20200057.

Butler, A., Hoffman, P., Smibert, P., Papalexi, E., and Satija, R. (2018). Integrating single-cell transcriptomic data across different conditions, technologies, and species. *Nature biotechnology*, 36(5):411–420.

Butt, S. J. B., Sousa, V. H., Fuccillo, M. V., Hjerling-Leffler, J., Miyoshi, G., Kimura, S., and Fishell, G. (2008). The requirement of nkx2-1 in the temporal specification of cortical interneuron subtypes. *Neuron*, 59(5):722–32.

Cai, J., Wu, Y., Mirua, T., Pierce, J. L., Lucero, M. T., Albertine, K. H., Spangrude, G. J., and Rao, M. S. (2002). Properties of a fetal multipotent neural stem cell (nep cell). *Dev Biol*, 251(2):221–40.

Camacho-Aguilar, E. and Warmflash, A. (2020). Insights into mammalian morphogen dynamics from embryonic stem cell systems. *Curr Top Dev Biol*, 137:279–305.

Campbell, K., Olsson, M., and Björklund, A. (1995). Regional incorporation and site-specific differentiation of striatal precursors transplanted to the embryonic forebrain ventricle. *Neuron*, 15(6):1259–73.

Cannoodt, R., Saelens, W., and Saeys, Y. (2016). Computational methods for trajectory inference from single-cell transcriptomics. *Eur J Immunol*, 46(11):2496–2506.

Cao, J., Spielmann, M., Qiu, X., Huang, X., Ibrahim, D. M., Hill, A. J., Zhang, F., Mundlos, S., Christiansen, L., Steemers, F. J., Trapnell, C., and Shendure, J. (2019). The single-cell transcriptional landscape of mammalian organogenesis. *Nature*, 566(7745):496–502.

Castro, D. S., Martynoga, B., Parras, C., Ramesh, V., Pacary, E., Johnston, C., Drechsel, D., Lebel-Potter, M., Garcia, L. G., Hunt, C., Dolle, D., Bithell, A., Ettwiller, L., Buckley, N., and Guillemot, F. (2011). A novel function of the proneural factor ascl1 in progenitor proliferation identified by genome-wide characterization of its targets. *Genes Dev*, 25(9):930–45.

Castro-Mondragon, J. A., Riudavets-Puig, R., Rauluseviciute, I., Lemma, R. B., Turchi, L., Blanc-Mathieu, R., Lucas, J., Boddie, P., Khan, A., Manosalva Pérez, N., Fornes,

O., Leung, T. Y., Aguirre, A., Hammal, F., Schmelter, D., Baranasic, D., Ballester, B., Sandelin, A., Lenhard, B., Vandepoele, K., Wasserman, W. W., Parcy, F., and Mathelier, A. (2022). Jaspar 2022: the 9th release of the open-access database of transcription factor binding profiles. *Nucleic Acids Res*, 50(D1):D165–D173.

Caviness, Jr, V. S., Goto, T., Tarui, T., Takahashi, T., Bhide, P. G., and Nowakowski, R. S. (2003). Cell output, cell cycle duration and neuronal specification: a model of integrated mechanisms of the neocortical proliferative process. *Cereb Cortex*, 13(6):592–8.

Caviness, Jr, V. S., Takahashi, T., and Nowakowski, R. S. (1995). Numbers, time and neocortical neuronogenesis: a general developmental and evolutionary model. *Trends Neurosci*, 18(9):379–83.

Chen, R., Wu, X., Jiang, L., and Zhang, Y. (2017). Single-cell rna-seq reveals hypothalamic cell diversity. *Cell Rep*, 18(13):3227–3241.

Chenn, A. and Walsh, C. A. (2002). Regulation of cerebral cortical size by control of cell cycle exit in neural precursors. *Science*, 297(5580):365–9.

Ciceri, G., Baggiolini, A., Cho, H. S., Kshirsagar, M., Benito-Kwiecinski, S., Walsh, R. M., Aromolaran, K. A., Gonzalez-Hernandez, A. J., Munguba, H., Koo, S. Y., Xu, N., Sevilla, K. J., Goldstein, P. A., Levitz, J., Leslie, C. S., Koche, R. P., and Studer, L. (2024). An epigenetic barrier sets the timing of human neuronal maturation. *Nature*.

Clancy, B., Darlington, R. B., and Finlay, B. L. (2001). Translating developmental time across mammalian species. *Neuroscience*, 105(1):7–17.

Clark, B. S., Stein-O'Brien, G. L., Shiau, F., Cannon, G. H., Davis-Marcisak, E., Sherman, T., Santiago, C. P., Hoang, T. V., Rajaii, F., James-Esposito, R. E., Gronostajski, R. M., Fertig, E. J., Goff, L. A., and Blackshaw, S. (2019). Single-cell rna-seq analysis

of retinal development identifies nfi factors as regulating mitotic exit and late-born cell specification. *Neuron*, 102(6):1111–1126.e5.

Clément, F. and Olayé, J. (2024). A stochastic model for neural progenitor dynamics in the mouse cerebral cortex. *Math Biosci*, 372:109185.

Closser, M., Guo, Y., Wang, P., Patel, T., Jang, S., Hammelman, J., De Nooij, J. C., Kopunova, R., Mazzoni, E. O., Ruan, Y., Gifford, D. K., and Wichterle, H. (2022). An expansion of the non-coding genome and its regulatory potential underlies vertebrate neuronal diversity. *Neuron*, 110(1):70–85.e6.

Colasante, G., Simonet, J. C., Calogero, R., Crispi, S., Sessa, A., Cho, G., Golden, J. A., and Broccoli, V. (2015). ARX Regulates Cortical Intermediate Progenitor Cell Expansion and Upper Layer Neuron Formation Through Repression of Cdkn1c. *Cerebral Cortex*, 25(2):322–335.

Csardi, G. and Nepusz, T. (2006). The igraph software package for complex network research. *InterJournal*, Complex Systems:1695.

Cunningham, M. and McKay, R. (1994). Transplantation strategies for the analysis of brain development and repair. *J Neurol*, 242(1 Suppl 1):S40–2.

De Felipe, J., Marco, P., Fairen, A., and Jones, E. G. (1997). Inhibitory synaptogenesis in mouse somatosensory cortex. *Cereb Cortex*, 7(7):619–34.

De Marco Garcia, N. V., Karayannis, T., and Fishell, G. (2011). Neuronal activity is required for the development of specific cortical interneuron subtypes. *Nature*, 472(7343):351–5.

Dennis, G., Sherman, B. T., Hosack, D. A., Yang, J., Gao, W., Lane, H. C., and Lempicki,

R. A. (2003). DAVID: Database for Annotation, Visualization, and Integrated Discovery. *Genome Biology*, 4(5):P3.

Desai, A. R. and McConnell, S. K. (2000). Progressive restriction in fate potential by neural progenitors during cerebral cortical development. *Development*, 127(13):2863–72.

Di Bella, D. J., Habibi, E., Stickels, R. R., Scalia, G., Brown, J., Yadollahpour, P., Yang, S. M., Abbate, C., Biancalani, T., Macosko, E. Z., Chen, F., Regev, A., and Arlotta, P. (2021). Molecular logic of cellular diversification in the mouse cerebral cortex. *Nature*, 595(7868):554–559.

Di Nisio, E., Lupo, G., Licursi, V., and Negri, R. (2021). The role of histone lysine methylation in the response of mammalian cells to ionizing radiation. *Front Genet*, 12:639602.

Ding, S., Wu, X., Li, G., Han, M., Zhuang, Y., and Xu, T. (2005). Efficient transposition of the piggybac (pb) transposon in mammalian cells and mice. *Cell*, 122(3):473–83.

Dixit, A., Parnas, O., Li, B., Chen, J., Fulco, C. P., Jerby-Arnon, L., Marjanovic, N. D., Dionne, D., Burks, T., Raychowdhury, R., Adamson, B., Norman, T. M., Lander, E. S., Weissman, J. S., Friedman, N., and Regev, A. (2016). Perturb-seq: Dissecting molecular circuits with scalable single-cell rna profiling of pooled genetic screens. *Cell*, 167(7):1853–1866.e17.

Dvoretskova, E., Ho, M. C., Kittke, V., Vitali, I., Delgado, I., Feng, C., Torres, M., Winkelmann, J., and Mayer, C. (2023). Spatial-specific enhancer activation determines inhibitory identity. *bioRxiv*.

Ebisuya, M. and Briscoe, J. (2018). What does time mean in development? *Development*, 145(12).

Eiraku, M., Watanabe, K., Matsuo-Takasaki, M., Kawada, M., Yonemura, S., Matsumura, M., Wataya, T., Nishiyama, A., Muguruma, K., and Sasai, Y. (2008). Self-organized formation of polarized cortical tissues from escs and its active manipulation by extrinsic signals. *Cell Stem Cell*, 3(5):519–32.

Englund, C., Fink, A., Lau, C., Pham, D., Daza, R. A. M., Bulfone, A., Kowalczyk, T., and Hevner, R. F. (2005). Pax6, tbr2, and tbr1 are expressed sequentially by radial glia, intermediate progenitor cells, and postmitotic neurons in developing neocortex. *J Neurosci*, 25(1):247–51.

Erlander, M. G., Tillakaratne, N. J., Feldblum, S., Patel, N., and Tobin, A. J. (1991). Two genes encode distinct glutamate decarboxylases. *Neuron*, 7(1):91–100.

Falo-Sanjuan, J., Lammers, N. C., Garcia, H. G., and Bray, S. J. (2019). Enhancer priming enables fast and sustained transcriptional responses to notch signaling. *Dev Cell*, 50(4):411–425.e8.

Fentress, J. C., Stanfield, B. B., and Cowan, W. M. (1981). Observation on the development of the striatum in mice and rats. *Anat Embryol (Berl)*, 163(3):275–98.

Fietz, S. A., Kelava, I., Vogt, J., Wilsch-Bräuninger, M., Stenzel, D., Fish, J. L., Corbeil, D., Riehn, A., Distler, W., Nitsch, R., and Huttner, W. B. (2010). Osvz progenitors of human and ferret neocortex are epithelial-like and expand by integrin signaling. *Nat Neurosci*, 13(6):690–9.

Figueres-Oñate, M., Sánchez-Villalón, M., Sánchez-González, R., and López-Mascaraque, L. (2019). Lineage tracing and cell potential of postnatal single progenitor cells in vivo. *Stem Cell Reports*, 13(4):700–712.

Fishell, G. (1995). Striatal precursors adopt cortical identities in response to local cues. *Development*, 121(3):803–12.

Flames, N., Pla, R., Gelman, D. M., Rubenstein, J. L. R., Puelles, L., and Marín, O. (2007). Delineation of multiple subpallial progenitor domains by the combinatorial expression of transcriptional codes. *J Neurosci*, 27(36):9682–95.

Florio, M. and Huttner, W. B. (2014). Neural progenitors, neurogenesis and the evolution of the neocortex. *Development*, 141(11):2182–94.

Franco, S. J., Gil-Sanz, C., Martinez-Garay, I., Espinosa, A., Harkins-Perry, S. R., Ramos, C., and Müller, U. (2012). Fate-restricted neural progenitors in the mammalian cerebral cortex. *Science*, 337(6095):746–9.

Frantz, G. D. and McConnell, S. K. (1996). Restriction of late cerebral cortical progenitors to an upper-layer fate. *Neuron*, 17(1):55–61.

Gaspard, N., Bouschet, T., Hourez, R., Dimidschstein, J., Naeije, G., van den Ameele, J., Espuny-Camacho, I., Herpoel, A., Passante, L., Schiffmann, S. N., Gaillard, A., and Vanderhaeghen, P. (2008). An intrinsic mechanism of corticogenesis from embryonic stem cells. *Nature*, 455(7211):351–7.

Gelman, D., Griveau, A., Dehorter, N., Teissier, A., Varela, C., Pla, R., Pierani, A., and Marín, O. (2011). A wide diversity of cortical gabaergic interneurons derives from the embryonic preoptic area. *J Neurosci*, 31(46):16570–80.

Ghimire, S., Mantziou, V., Moris, N., and Martinez Arias, A. (2021). Human gastrulation: The embryo and its models. *Dev Biol*, 474:100–108.

Golgi, C. (1885). *Sulla fina anatomia degli organi centrali del sistema nervoso*. S. Calderini.

Gonzalez-Blas, C. B., De Winter, S., Hulselmans, G., Hecker, N., Matetovici, I., Christiaens, V., Poovathingal, S., Wouters, J., Aibar, S., and Aerts, S. (2023). Scenic+:

single-cell multiomic inference of enhancers and gene regulatory networks. *Nature Methods*.

Göös, H., Kinnunen, M., Salokas, K., Tan, Z., Liu, X., Yadav, L., Zhang, Q., Wei, G.-H., and Varjosalo, M. (2022). Human transcription factor protein interaction networks. *Nat Commun*, 13(1):766.

Gorkin, D. U., Barozzi, I., Zhao, Y., Zhang, Y., Huang, H., Lee, A. Y., Li, B., Chiou, J., Wildberg, A., Ding, B., Zhang, B., Wang, M., Strattan, J. S., Davidson, J. M., Qiu, Y., Afzal, V., Akiyama, J. A., Plajzer-Frick, I., Novak, C. S., Kato, M., Garvin, T. H., Pham, Q. T., Harrington, A. N., Mannion, B. J., Lee, E. A., Fukuda-Yuzawa, Y., He, Y., Preissl, S., Chee, S., Han, J. Y., Williams, B. A., Trout, D., Amrhein, H., Yang, H., Cherry, J. M., Wang, W., Gaulton, K., Ecker, J. R., Shen, Y., Dickel, D. E., Visel, A., Pennacchio, L. A., and Ren, B. (2020). An atlas of dynamic chromatin landscapes in mouse fetal development. *Nature*, 583(7818):744–751.

Götz, M. and Huttner, W. B. (2005). The cell biology of neurogenesis. *Nat Rev Mol Cell Biol*, 6(10):777–88.

Götz, M., Stoykova, A., and Gruss, P. (1998). Pax6 controls radial glia differentiation in the cerebral cortex. *Neuron*, 21(5):1031–44.

Govindan, S. and Jabaudon, D. (2017). Coupling progenitor and neuronal diversity in the developing neocortex. *FEBS Lett*, 591(24):3960–3977.

Govindan, S., Oberst, P., and Jabaudon, D. (2018). In vivo pulse labeling of isochronic cohorts of cells in the central nervous system using flashtag. *Nat Protoc*, 13(10):2297–2311.

Granja, J. M., Corces, M. R., Pierce, S. E., Bagdatli, S. T., Choudhry, H., Chang, H. Y.,

and Greenleaf, W. J. (2021). Archr is a scalable software package for integrative single-cell chromatin accessibility analysis. *Nat Genet*, 53(3):403–411.

Grimm, J. B., Muthusamy, A. K., Liang, Y., Brown, T. A., Lemon, W. C., Patel, R., Lu, R., Macklin, J. J., Keller, P. J., Ji, N., and Lavis, L. D. (2017). A general method to fine-tune fluorophores for live-cell and in vivo imaging. *Nat Methods*, 14(10):987–994.

Grindley, N. D. F., Whiteson, K. L., and Rice, P. A. (2006). Mechanisms of site-specific recombination. *Annu Rev Biochem*, 75:567–605.

Guo, C., Eckler, M. J., McKenna, W. L., McKinsey, G. L., Rubenstein, J. L. R., and Chen, B. (2013). Fezf2 expression identifies a multipotent progenitor for neocortical projection neurons, astrocytes, and oligodendrocytes. *Neuron*, 80(5):1167–74.

Haghverdi, L., Lun, A. T. L., Morgan, M. D., and Marioni, J. C. (2018). Batch effects in single-cell RNA sequencing data are corrected by matching mutual nearest neighbours. *Nature biotechnology*, 36(5):421–427.

Hao, Y., Hao, S., Andersen-Nissen, E., Mauck, W. M., Zheng, S., Butler, A., Lee, M. J., Wilk, A. J., Darby, C., Zager, M., Hoffman, P., Stoeckius, M., Papalexi, E., Mimitou, E. P., Jain, J., Srivastava, A., Stuart, T., Fleming, L. M., Yeung, B., Rogers, A. J., McElrath, J. M., Blish, C. A., Gottardo, R., Smibert, P., and Satija, R. (2021). Integrated analysis of multimodal single-cell data. *Cell*, 184(13):3573–3587.e29.

Harris, L., Zalucki, O., Gobius, I., McDonald, H., Osinki, J., Harvey, T. J., Essebier, A., Vidovic, D., Gladwyn-Ng, I., Burne, T. H., Heng, J. I., Richards, L. J., Gronostajski, R. M., and Piper, M. (2016). Transcriptional regulation of intermediate progenitor cell generation during hippocampal development. *Development*, 143(24):4620–4630.

Hartfuss, E., Galli, R., Heins, N., and Götz, M. (2001). Characterization of cns precursor subtypes and radial glia. *Dev Biol*, 229(1):15–30.

Harwell, C. C., Fuentealba, L. C., Gonzalez-Cerrillo, A., Parker, P. R. L., Gertz, C. C., Mazzola, E., Garcia, M. T., Alvarez-Buylla, A., Cepko, C. L., and Kriegstein, A. R. (2015). Wide dispersion and diversity of clonally related inhibitory interneurons. *Neuron*, 87(5):999–1007.

Hatakeyama, J., Bessho, Y., Katoh, K., Ookawara, S., Fujioka, M., Guillemot, F., and Kageyama, R. (2004). Hes genes regulate size, shape and histogenesis of the nervous system by control of the timing of neural stem cell differentiation. *Development*, 131(22):5539–50.

Haubensak, W., Attardo, A., Denk, W., and Huttner, W. B. (2004). Neurons arise in the basal neuroepithelium of the early mammalian telencephalon: a major site of neurogenesis. *Proc Natl Acad Sci U S A*, 101(9):3196–201.

He, J., Zhang, G., Almeida, A. D., Cayouette, M., Simons, B. D., and Harris, W. A. (2012). How variable clones build an invariant retina. *Neuron*, 75(5):786–98.

Heintzman, N. D., Stuart, R. K., Hon, G., Fu, Y., Ching, C. W., Hawkins, R. D., Barrera, L. O., Van Calcar, S., Qu, C., Ching, K. A., Wang, W., Weng, Z., Green, R. D., Crawford, G. E., and Ren, B. (2007). Distinct and predictive chromatin signatures of transcriptional promoters and enhancers in the human genome. *Nat Genet*, 39(3):311–8.

Heng, Y. H. E., Barry, G., Richards, L. J., and Piper, M. (2012). Nuclear factor i genes regulate neuronal migration. *Neurosignals*, 20(3):159–67.

Hickey, S. L., Berto, S., and Konopka, G. (2019). Chromatin decondensation by foxp2 promotes human neuron maturation and expression of neurodevelopmental disease genes. *Cell Rep*, 27(6):1699–1711.e9.

Hippenmeyer, S. (2023). Principles of neural stem cell lineage progression: Insights from developing cerebral cortex. *Curr Opin Neurobiol*, 79:102695.

Hockfield, S. and McKay, R. D. (1985). Identification of major cell classes in the developing mammalian nervous system. *J Neurosci*, 5(12):3310–28.

Hu, J. S., Vogt, D., Sandberg, M., and Rubenstein, J. L. (2017). Cortical interneuron development: a tale of time and space. *Development*, 144(21):3867–3878.

Huilgol, D., Russ, J. B., Srivas, S., and Huang, Z. J. (2023). The progenitor basis of cortical projection neuron diversity. *Curr Opin Neurobiol*, 81:102726.

Imayoshi, I., Shimogori, T., Ohtsuka, T., and Kageyama, R. (2008). Hes genes and neurogenin regulate non-neural versus neural fate specification in the dorsal telencephalic midline. *Development*, 135(15):2531–41.

Inan, M., Welagen, J., and Anderson, S. A. (2012). Spatial and temporal bias in the mitotic origins of somatostatin- and parvalbumin-expressing interneuron subgroups and the chandelier subtype in the medial ganglionic eminence. *Cereb Cortex*, 22(4):820–7.

Iwata, R., Casimir, P., Erkol, E., Boubakar, L., Planque, M., Gallego López, I. M., Ditkowska, M., Gaspariunaite, V., Beckers, S., Remans, D., Vints, K., Vandekeere, A., Poovathingal, S., Bird, M., Vlaeminck, I., Creemers, E., Wierda, K., Corthout, N., Vermeersch, P., Carpentier, S., Davie, K., Mazzone, M., Gounko, N. V., Aerts, S., Ghesquière, B., Fendt, S.-M., and Vanderhaeghen, P. (2023). Mitochondria metabolism sets the species-specific tempo of neuronal development. *Science*, 379(6632):eabn4705.

Jay Angevine, David Bodian, A. J. C. M. V. E. J. V. H. M. J. K. M. L. M. C. P. R. L. S. S. V. P. A. W. (1970). Embryonic vertebrate central nervous system: revised terminology. the boulder committee. *Anat Rec*, 166(2):257–61.

Jensen, P. and Dymecki, S. M. (2014). Essentials of recombinase-based genetic fate mapping in mice. *Methods Mol Biol*, 1092:437–54.

Jew, B., Alvarez, M., Rahmani, E., Miao, Z., Ko, A., Garske, K. M., Sul, J. H., Pietiläinen, K. H., Pajukanta, P., and Halperin, E. (2020). Accurate estimation of cell composition in bulk expression through robust integration of single-cell information. *Nat Commun*, 11(1):1971.

Kageyama, R., Ohtsuka, T., and Kobayashi, T. (2008). Roles of hes genes in neural development. *Dev Growth Differ*, 50 Suppl 1:S97–103.

Katz, L. C. and Shatz, C. J. (1996). Synaptic activity and the construction of cortical circuits. *Science*, 274(5290):1133–8.

Kelly, S. M., Raudales, R., He, M., Lee, J. H., Kim, Y., Gibb, L. G., Wu, P., Matho, K., Osten, P., Graybiel, A. M., and Huang, Z. J. (2018). Radial glial lineage progression and differential intermediate progenitor amplification underlie striatal compartments and circuit organization. *Neuron*, 99(2):345–361.e4.

Kester, L. and van Oudenaarden, A. (2018). Single-cell transcriptomics meets lineage tracing. *Cell Stem Cell*, 23(2):166–179.

Kim, A. and Pyykko, I. (2011). Size matters: versatile use of piggybac transposons as a genetic manipulation tool. *Mol Cell Biochem*, 354(1-2):301–9.

Kim, D., Paggi, J. M., Park, C., Bennett, C., and Salzberg, S. L. (2019). Graph-based genome alignment and genotyping with hisat2 and hisat-genotype. *Nat Biotechnol*, 37(8):907–915.

Kohwi, M. and Doe, C. Q. (2013). Temporal fate specification and neural progenitor competence during development. *Nat Rev Neurosci*, 14(12):823–38.

Korsunsky, I., Millard, N., Fan, J., Slowikowski, K., Zhang, F., Wei, K., Baglaenko, Y.,

Brenner, M., Loh, P.-R., and Raychaudhuri, S. (2019). Fast, sensitive and accurate integration of single-cell data with harmony. *Nat Methods*, 16(12):1289–1296.

Kouzarides, T. (2007). Chromatin modifications and their function. *Cell*, 128(4):693–705.

Le, T. N., Zhou, Q.-P., Cobos, I., Zhang, S., Zagozewski, J., Japoni, S., Vriend, J., Parkinson, T., Du, G., Rubenstein, J. L., and Eisenstat, D. D. (2017). Gabaergic interneuron differentiation in the basal forebrain is mediated through direct regulation of glutamic acid decarboxylase isoforms by dlx homeobox transcription factors. *J Neurosci*, 37(36):8816–8829.

Le Douarin, N. M. (1993). Embryonic neural chimaeras in the study of brain development. *Trends Neurosci*, 16(2):64–72.

Lee, D. R., Rhodes, C., Mitra, A., Zhang, Y., Maric, D., Dale, R. K., and Petros, T. J. (2022). Transcriptional heterogeneity of ventricular zone cells in the ganglionic eminences of the mouse forebrain. *Elife*, 11.

Lehtinen, M. K., Zappaterra, M. W., Chen, X., Yang, Y. J., Hill, A. D., Lun, M., Maynard, T., Gonzalez, D., Kim, S., Ye, P., D'Ercole, A. J., Wong, E. T., LaMantia, A. S., and Walsh, C. A. (2011). The cerebrospinal fluid provides a proliferative niche for neural progenitor cells. *Neuron*, 69(5):893–905.

Liao, Y., Smyth, G. K., and Shi, W. (2014). featurecounts: an efficient general purpose program for assigning sequence reads to genomic features. *Bioinformatics*, 30(7):923–30.

Lim, L., Pakan, J. M. P., Selten, M. M., Marques-Smith, A., Llorca, A., Bae, S. E., Rochefort, N. L., and Marín, O. (2018). Optimization of interneuron function by direct coupling of cell migration and axonal targeting. *Nat Neurosci*, 21(7):920–931.

Lindtner, S., Catta-Preta, R., Tian, H., Su-Feher, L., Price, J. D., Dickel, D. E., Greiner, V., Silberberg, S. N., McKinsey, G. L., McManus, M. T., Pennacchio, L. A., Visel, A., Nord, A. S., and Rubenstein, J. L. R. (2019). Genomic resolution of dlx-orchestrated transcriptional circuits driving development of forebrain gabaergic neurons. *Cell Rep*, 28(8):2048–2063.e8.

Liodis, P., Denaxa, M., Grigoriou, M., Akufo-Addo, C., Yanagawa, Y., and Pachnis, V. (2007). Lhx6 activity is required for the normal migration and specification of cortical interneuron subtypes. *J Neurosci*, 27(12):3078–89.

Lobo, M. K., Yeh, C., and Yang, X. W. (2008). Pivotal role of early b-cell factor 1 in development of striatonigral medium spiny neurons in the matrix compartment. *J Neurosci Res*, 86(10):2134–46.

Love, M. I., Huber, W., and Anders, S. (2014). Moderated estimation of fold change and dispersion for rna-seq data with deseq2. *Genome Biol*, 15(12):550.

Lui, J. H., Hansen, D. V., and Kriegstein, A. R. (2011). Development and evolution of the human neocortex. *Cell*, 146(1):18–36.

Machon, O., Backman, M., Machonova, O., Kozmik, Z., Vacik, T., Andersen, L., and Krauss, S. (2007). A dynamic gradient of wnt signaling controls initiation of neurogenesis in the mammalian cortex and cellular specification in the hippocampus. *Dev Biol*, 311(1):223–37.

Madisen, L., Zwingman, T. A., Sunkin, S. M., Oh, S. W., Zariwala, H. A., Gu, H., Ng, L. L., Palmiter, R. D., Hawrylycz, M. J., Jones, A. R., Lein, E. S., and Zeng, H. (2010). A robust and high-throughput cre reporting and characterization system for the whole mouse brain. *Nat Neurosci*, 13(1):133–40.

Malatesta, P., Hartfuss, E., and Götz, M. (2000). Isolation of radial glial cells by fluorescent-activated cell sorting reveals a neuronal lineage. *Development*, 127(24):5253–63.

Marchetto, M. C., Hrvoj-Mihic, B., Kerman, B. E., Yu, D. X., Vadodaria, K. C., Linker, S. B., Narvaiza, I., Santos, R., Denli, A. M., Mendes, A. P., Oefner, R., Cook, J., McHenry, L., Grasmick, J. M., Heard, K., Fredlender, C., Randolph-Moore, L., Kshirsagar, R., Xenitopoulos, R., Chou, G., Hah, N., Muotri, A. R., Padmanabhan, K., Semendeferi, K., and Gage, F. H. (2019). Species-specific maturation profiles of human, chimpanzee and bonobo neural cells. *Elife*, 8.

Martínez-Cerdeño, V., Cunningham, C. L., Camacho, J., Antczak, J. L., Prakash, A. N., Cziep, M. E., Walker, A. I., and Noctor, S. C. (2012). Comparative analysis of the subventricular zone in rat, ferret and macaque: evidence for an outer subventricular zone in rodents. *PLoS One*, 7(1):e30178.

Matuzelski, E., Bunt, J., Harkins, D., Lim, J. W. C., Gronostajski, R. M., Richards, L. J., Harris, L., and Piper, M. (2017). Transcriptional regulation of Nfix by NFIB drives astrocytic maturation within the developing spinal cord. *Developmental Biology*, 432(2):286–297.

Mayer, C., Hafemeister, C., Bandler, R. C., Machold, R., Batista Brito, R., Jaglin, X., Allaway, K., Butler, A., Fishell, G., and Satija, R. (2018). Developmental diversification of cortical inhibitory interneurons. *Nature*, 555(7697):457–462.

Mayer, C., Jaglin, X. H., Cobbs, L. V., Bandler, R. C., Streicher, C., Cepko, C. L., Hippenmeyer, S., and Fishell, G. (2015). Clonally related forebrain interneurons disperse broadly across both functional areas and structural boundaries. *Neuron*, 87(5):989–98.

McConnell, S. K. (1985). Migration and differentiation of cerebral cortical neurons after transplantation into the brains of ferrets. *Science*, 229(4719):1268–71.

McConnell, S. K. and Kaznowski, C. E. (1991). Cell cycle dependence of laminar determination in developing neocortex. *Science*, 254(5029):282–5.

McInnes, L., Healy, J., and Melville, J. (2020). UMAP: Uniform Manifold Approximation and Projection for Dimension Reduction. *arXiv:1802.03426 [cs, stat]*. arXiv: 1802.03426.

Meijer, D. H., Kane, M. F., Mehta, S., Liu, H., Harrington, E., Taylor, C. M., Stiles, C. D., and Rowitch, D. H. (2012). Separated at birth? the functional and molecular divergence of olig1 and olig2. *Nat Rev Neurosci*, 13(12):819–31.

Mi, D., Li, Z., Lim, L., Li, M., Moissidis, M., Yang, Y., Gao, T., Hu, T. X., Pratt, T., Price, D. J., Sestan, N., and Marin, O. (2018). Early emergence of cortical interneuron diversity in the mouse embryo. *Science*, 360(6384):81–85.

Miller, M. W. and Nowakowski, R. S. (1988). Use of bromodeoxyuridine-immunohistochemistry to examine the proliferation, migration and time of origin of cells in the central nervous system. *Brain Res*, 457(1):44–52.

Miyata, T., Kawaguchi, A., Okano, H., and Ogawa, M. (2001). Asymmetric inheritance of radial glial fibers by cortical neurons. *Neuron*, 31(5):727–41.

Miyata, T., Kawaguchi, A., Saito, K., Kawano, M., Muto, T., and Ogawa, M. (2004). Asymmetric production of surface-dividing and non-surface-dividing cortical progenitor cells. *Development*, 131(13):3133–45.

Miyoshi, G., Butt, S. J. B., Takebayashi, H., and Fishell, G. (2007). Physiologically distinct temporal cohorts of cortical interneurons arise from telencephalic olig2-expressing precursors. *J Neurosci*, 27(29):7786–98.

Miyoshi, G. and Fishell, G. (2011). Gabaergic interneuron lineages selectively sort into specific cortical layers during early postnatal development. *Cereb Cortex*, 21(4):845–52.

Miyoshi, G., Hjerling-Leffler, J., Karayannis, T., Sousa, V. H., Butt, S. J. B., Battiste, J., Johnson, J. E., Machold, R. P., and Fishell, G. (2010). Genetic fate mapping reveals that the caudal ganglionic eminence produces a large and diverse population of superficial cortical interneurons. *J Neurosci*, 30(5):1582–94.

Molyneaux, B. J., Arlotta, P., Menezes, J. R. L., and Macklis, J. D. (2007). Neuronal subtype specification in the cerebral cortex. *Nat Rev Neurosci*, 8(6):427–37.

Monory, K., Massa, F., Egertová, M., Eder, M., Blaudzun, H., Westenbroek, R., Kelsch, W., Jacob, W., Marsch, R., Ekker, M., Long, J., Rubenstein, J. L., Goebbels, S., Nave, K.-A., During, M., Klugmann, M., Wölfel, B., Dodt, H.-U., Zieglgänsberger, W., Wotjak, C. T., Mackie, K., Elphick, M. R., Marsicano, G., and Lutz, B. (2006). The endocannabinoid system controls key epileptogenic circuits in the hippocampus. *Neuron*, 51(4):455–66.

Moreau, M. X., Saillour, Y., Cwetsch, A. W., Pierani, A., and Causeret, F. (2021). Single-cell transcriptomics of the early developing mouse cerebral cortex disentangle the spatial and temporal components of neuronal fate acquisition. *Development*, 148(14).

Morest, D. K. and Silver, J. (2003). Precursors of neurons, neuroglia, and ependymal cells in the cns: what are they? where are they from? how do they get where they are going? *Glia*, 43(1):6–18.

Morimoto-Suzki, N., Hirabayashi, Y., Tyssowski, K., Shinga, J., Vidal, M., Koseki, H., and Gotoh, Y. (2014). The polycomb component ring1b regulates the timed termination of subcerebral projection neuron production during mouse neocortical development. *Development*, 141(22):4343–53.

Munji, R. N., Choe, Y., Li, G., Siegenthaler, J. A., and Pleasure, S. J. (2011). Wnt signaling regulates neuronal differentiation of cortical intermediate progenitors. *J Neurosci*, 31(5):1676–87.

Nagy, A. (2000). Cre recombinase: the universal reagent for genome tailoring. *Genesis*, 26(2):99–109.

Namihira, M. and Nakashima, K. (2013). Mechanisms of astrocytogenesis in the mammalian brain. *Curr Opin Neurobiol*, 23(6):921–7.

Nelson, B. R., Hodge, R. D., Bedogni, F., and Hevner, R. F. (2013). Dynamic interactions between intermediate neurogenic progenitors and radial glia in embryonic mouse neocortex: potential role in dll1-notch signaling. *J Neurosci*, 33(21):9122–39.

Nery, S., Fishell, G., and Corbin, J. G. (2002). The caudal ganglionic eminence is a source of distinct cortical and subcortical cell populations. *Nat Neurosci*, 5(12):1279–87.

Nishino, J., Kim, I., Chada, K., and Morrison, S. J. (2008). Hmga2 Promotes Neural Stem Cell Self-Renewal in Young but Not Old Mice by Reducing p16Ink4a and p19Arf Expression. *Cell*, 135(2):227–239. Publisher: Elsevier.

Noctor, S. C., Flint, A. C., Weissman, T. A., Dammerman, R. S., and Kriegstein, A. R. (2001). Neurons derived from radial glial cells establish radial units in neocortex. *Nature*, 409(6821):714–20.

Noctor, S. C., Martínez-Cerdeño, V., Ivic, L., and Kriegstein, A. R. (2004). Cortical neurons arise in symmetric and asymmetric division zones and migrate through specific phases. *Nat Neurosci*, 7(2):136–44.

Noctor, S. C., Martínez-Cerdeño, V., and Kriegstein, A. R. (2008). Distinct behaviors

of neural stem and progenitor cells underlie cortical neurogenesis. *J Comp Neurol*, 508(1):28–44.

Oberst, P., Fièvre, S., Baumann, N., Concetti, C., Bartolini, G., and Jabaudon, D. (2019). Temporal plasticity of apical progenitors in the developing mouse neocortex. *Nature*, 573(7774):370–374.

Ohtsuka, T., Sakamoto, M., Guillemot, F., and Kageyama, R. (2001). Roles of the Basic Helix-Loop-Helix Genes Hes1 and Hes5 in Expansion of Neural Stem Cells of the Developing Brain. *Journal of Biological Chemistry*, 276(32):30467–30474.

Olsson, M., Björklund, A., and Campbell, K. (1998). Early specification of striatal projection neurons and interneuronal subtypes in the lateral and medial ganglionic eminence. *Neuroscience*, 84(3):867–76.

Parthasarathy, S., Srivatsa, S., Nityanandam, A., and Tarabykin, V. (2014). Ntf3 acts downstream of sip1 in cortical postmitotic neurons to control progenitor cell fate through feedback signaling. *Development*, 141(17):3324–30.

Pașca, S. P. (2024). Constructing human neural circuits in living systems by transplantation. *Cell*, 187(1):8–13.

Pereira, J. D., Sansom, S. N., Smith, J., Dobenecker, M.-W., Tarakhovsky, A., and Livesey, F. J. (2010). Ezh2, the histone methyltransferase of prc2, regulates the balance between self-renewal and differentiation in the cerebral cortex. *Proc Natl Acad Sci U S A*, 107(36):15957–62.

Petros, T. J., Bultje, R. S., Ross, M. E., Fishell, G., and Anderson, S. A. (2015). Apical versus basal neurogenesis directs cortical interneuron subclass fate. *Cell Rep*, 13(6):1090–1095.

Pilz, G.-A., Shitamukai, A., Reillo, I., Pacary, E., Schwausch, J., Stahl, R., Ninkovic, J., Snippert, H. J., Clevers, H., Godinho, L., Guillemot, F., Borrell, V., Matsuzaki, F., and Götz, M. (2013). Amplification of progenitors in the mammalian telencephalon includes a new radial glial cell type. *Nat Commun*, 4:2125.

Placzek, M. and Briscoe, J. (2005). The floor plate: multiple cells, multiple signals. *Nat Rev Neurosci*, 6(3):230–40.

Pollen, A. A., Nowakowski, T. J., Chen, J., Retallack, H., Sandoval-Espinosa, C., Nicholas, C. R., Shuga, J., Liu, S. J., Oldham, M. C., Diaz, A., Lim, D. A., Leyrat, A. A., West, J. A., and Kriegstein, A. R. (2015). Molecular identity of human outer radial glia during cortical development. *Cell*, 163(1):55–67.

Puelles, L., Kuwana, E., Puelles, E., Bulfone, A., Shimamura, K., Keleher, J., Smiga, S., and Rubenstein, J. L. (2000). Pallial and subpallial derivatives in the embryonic chick and mouse telencephalon, traced by the expression of the genes dlx-2, emx-1, nkx-2.1, pax-6, and tbr-1. *J Comp Neurol*, 424(3):409–38.

Qiu, X., Mao, Q., Tang, Y., Wang, L., Chawla, R., Pliner, H. A., and Trapnell, C. (2017). Reversed graph embedding resolves complex single-cell trajectories. *Nature Methods*, 14(10):979–982.

Rakic, P. (1974). Neurons in rhesus monkey visual cortex: systematic relation between time of origin and eventual disposition. *Science*, 183(4123):425–7.

Rakic, P. (2003). Elusive radial glial cells: historical and evolutionary perspective. *Glia*, 43(1):19–32.

Ramón y Cajal, S. (1911). Histologie du système nerveux de l'homme des vertébrés. *Paris, Maloine*.

Raposo, A. A. S. F., Vasconcelos, F. F., Drechsel, D., Marie, C., Johnston, C., Dolle, D., Bithell, A., Gillotin, S., van den Berg, D. L. C., Ettwiller, L., Flicek, P., Crawford, G. E., Parras, C. M., Berninger, B., Buckley, N. J., Guillemot, F., and Castro, D. S. (2015). Ascl1 Coordinately Regulates Gene Expression and the Chromatin Landscape during Neurogenesis. *Cell Reports*, 10(9):1544–1556.

Rhodes, C. T., Thompson, J. J., Mitra, A., Asokumar, D., Lee, D. R., Lee, D. J., Zhang, Y., Jason, E., Dale, R. K., Rocha, P. P., and Petros, T. J. (2022). An epigenome atlas of neural progenitors within the embryonic mouse forebrain. *Nat Commun*, 13(1):4196.

Ross, S. E., Greenberg, M. E., and Stiles, C. D. (2003). Basic helix-loop-helix factors in cortical development. *Neuron*, 39(1):13–25.

Rubenstein, J. L. and Puelles, L. (1994). Homeobox gene expression during development of the vertebrate brain. *Curr Top Dev Biol*, 29:1–63.

Rubenstein, J. L., Shimamura, K., Martinez, S., and Puelles, L. (1998). Regionalization of the prosencephalic neural plate. *Annu Rev Neurosci*, 21:445–77.

Rulands, S., Iglesias-Gonzalez, A. B., and Boije, H. (2018). Deterministic fate assignment of müller glia cells in the zebrafish retina suggests a clonal backbone during development. *Eur J Neurosci*, 48(12):3597–3605.

Rymar, V. V. and Sadikot, A. F. (2007). Laminar fate of cortical gabaergic interneurons is dependent on both birthdate and phenotype. *J Comp Neurol*, 501(3):369–80.

Saito, T. and Nakatsuji, N. (2001). Efficient gene transfer into the embryonic mouse brain using in vivo electroporation. *Dev Biol*, 240(1):237–46.

Sandberg, M., Flandin, P., Silberberg, S., Su-Feher, L., Price, J. D., Hu, J. S., Kim, C., Visel, A., Nord, A. S., and Rubenstein, J. L. R. (2016). Transcriptional networks con-

trolled by nkx2-1 in the development of forebrain gabaergic neurons. *Neuron*, 91(6):1260–1275.

Satpathy, A. T., Granja, J. M., Yost, K. E., Qi, Y., Meschi, F., McDermott, G. P., Olsen, B. N., Mumbach, M. R., Pierce, S. E., Corces, M. R., Shah, P., Bell, J. C., Jhutty, D., Nemec, C. M., Wang, J., Wang, L., Yin, Y., Giresi, P. G., Chang, A. L. S., Zheng, G. X. Y., Greenleaf, W. J., and Chang, H. Y. (2019). Massively parallel single-cell chromatin landscapes of human immune cell development and intratumoral T cell exhaustion. *Nature Biotechnology*, 37(8):925–936. Number: 8 Publisher: Nature Publishing Group.

Seuntjens, E., Nityanandam, A., Miquelajauregui, A., Debruyn, J., Stryjewska, A., Goebbels, S., Nave, K.-A., Huylebroeck, D., and Tarabykin, V. (2009). Sip1 regulates sequential fate decisions by feedback signaling from postmitotic neurons to progenitors. *Nat Neurosci*, 12(11):1373–80.

Shen, Q., Wang, Y., Dimos, J. T., Fasano, C. A., Phoenix, T. N., Lemischka, I. R., Ivanova, N. B., Stifani, S., Morrisey, E. E., and Temple, S. (2006). The timing of cortical neurogenesis is encoded within lineages of individual progenitor cells. *Nat Neurosci*, 9(6):743–51.

Shimamura, K., Hartigan, D. J., Martinez, S., Puelles, L., and Rubenstein, J. L. (1995). Longitudinal organization of the anterior neural plate and neural tube. *Development*, 121(12):3923–33.

Singh, G. (2017). Chapter 2 - neuroembryology. In Prabhakar, H., editor, *Essentials of Neuroanesthesia*, pages 41–50. Academic Press.

Smart, I. H. M., Dehay, C., Giroud, P., Berland, M., and Kennedy, H. (2002). Unique morphological features of the proliferative zones and postmitotic compartments of the

neural epithelium giving rise to striate and extrastriate cortex in the monkey. *Cereb Cortex*, 12(1):37–53.

Spear, P. C. and Erickson, C. A. (2012). Interkinetic nuclear migration: a mysterious process in search of a function. *Dev Growth Differ*, 54(3):306–16.

Stergachis, A. B., Neph, S., Reynolds, A., Humbert, R., Miller, B., Paige, S. L., Vernot, B., Cheng, J. B., Thurman, R. E., Sandstrom, R., Haugen, E., Heimfeld, S., Murry, C. E., Akey, J. M., and Stamatoyannopoulos, J. A. (2013). Developmental fate and cellular maturity encoded in human regulatory dna landscapes. *Cell*, 154(4):888–903.

Stuart, T., Butler, A., Hoffman, P., Hafemeister, C., Papalexi, E., Mauck, W. M., Hao, Y., Stoeckius, M., Smibert, P., and Satija, R. (2019). Comprehensive Integration of Single-Cell Data. *Cell*, 177(7):1888–1902.e21. Publisher: Elsevier.

Stuhlmann, H., Cone, R., Mulligan, R. C., and Jaenisch, R. (1984). Introduction of a selectable gene into different animal tissue by a retrovirus recombinant vector. *Proc Natl Acad Sci U S A*, 81(22):7151–5.

Su, Z., Wang, Z., Lindtner, S., Yang, L., Shang, Z., Tian, Y., Guo, R., You, Y., Zhou, W., Rubenstein, J. L., Yang, Z., and Zhang, Z. (2022). Dlx1/2-dependent expression of meis2 promotes neuronal fate determination in the mammalian striatum. *Development*, 149(4).

Sugimori, M., Nagao, M., Bertrand, N., Parras, C. M., Guillemot, F., and Nakafuku, M. (2007). Combinatorial actions of patterning and hlh transcription factors in the spatiotemporal control of neurogenesis and gliogenesis in the developing spinal cord. *Development*, 134(8):1617–29.

Sulston, J. E., Schierenberg, E., White, J. G., and Thomson, J. N. (1983). The embryonic cell lineage of the nematode caenorhabditis elegans. *Dev Biol*, 100(1):64–119.

Sunabori, T., Tokunaga, A., Nagai, T., Sawamoto, K., Okabe, M., Miyawaki, A., Matsuzaki, Y., Miyata, T., and Okano, H. (2008). Cell-cycle-specific nestin expression coordinates with morphological changes in embryonic cortical neural progenitors. *J Cell Sci*, 121(Pt 8):1204–12.

Takahashi, T., Nowakowski, R. S., and Caviness, Jr, V. S. (1995). The cell cycle of the pseudostratified ventricular epithelium of the embryonic murine cerebral wall. *J Neurosci*, 15(9):6046–57.

Tang, F., Barbacioru, C., Wang, Y., Nordman, E., Lee, C., Xu, N., Wang, X., Bodeau, J., Tuch, B. B., Siddiqui, A., Lao, K., and Surani, M. A. (2009). mrna-seq whole-transcriptome analysis of a single cell. *Nat Methods*, 6(5):377–82.

Taniguchi, H., Lu, J., and Huang, Z. J. (2013). The spatial and temporal origin of chandelier cells in mouse neocortex. *Science*, 339(6115):70–4.

Tasic, B., Yao, Z., Graybuck, L. T., Smith, K. A., Nguyen, T. N., Bertagnolli, D., Goldy, J., Garren, E., Economo, M. N., Viswanathan, S., Penn, O., Bakken, T., Menon, V., Miller, J., Fong, O., Hirokawa, K. E., Lathia, K., Rimorin, C., Tieu, M., Larsen, R., Casper, T., Barkan, E., Kroll, M., Parry, S., Shapovalova, N. V., Hirschstein, D., Pendergraft, J., Sullivan, H. A., Kim, T. K., Szafer, A., Dee, N., Groblewski, P., Wickersham, I., Cetin, A., Harris, J. A., Levi, B. P., Sunkin, S. M., Madisen, L., Daigle, T. L., Looger, L., Bernard, A., Phillips, J., Lein, E., Hawrylycz, M., Svoboda, K., Jones, A. R., Koch, C., and Zeng, H. (2018). Shared and distinct transcriptomic cell types across neocortical areas. *Nature*, 563(7729):72–78.

Taverna, E., Götz, M., and Huttner, W. B. (2014). The cell biology of neurogenesis: toward an understanding of the development and evolution of the neocortex. *Annu Rev Cell Dev Biol*, 30:465–502.

Telley, L., Agirman, G., Prados, J., Amberg, N., Fièvre, S., Oberst, P., Bartolini, G., Vitali, I., Cadilhac, C., Hippenmeyer, S., Nguyen, L., Dayer, A., and Jabaudon, D. (2019). Temporal patterning of apical progenitors and their daughter neurons in the developing neocortex. *Science*, 364(6440).

Telley, L., Govindan, S., Prados, J., Stevant, I., Nef, S., Dermitzakis, E., Dayer, A., and Jabaudon, D. (2016). Sequential transcriptional waves direct the differentiation of newborn neurons in the mouse neocortex. *Science*, 351(6280):1443–6.

Telley, L. and Jabaudon, D. (2018). A mixed model of neuronal diversity. *Nature*, 555(7697):452–454.

Thakurela, S., Tiwari, N., Schick, S., Garding, A., Ivanek, R., Berninger, B., and Tiwari, V. K. (2016). Mapping gene regulatory circuitry of Pax6 during neurogenesis. *Cell Discovery*, 2(1):1–22. Number: 1 Publisher: Nature Publishing Group.

Tirosh, I., Izar, B., Prakadan, S. M., Wadsworth, M. H., Treacy, D., Trombetta, J. J., Rotem, A., Rodman, C., Lian, C., Murphy, G., Fallahi-Sichani, M., Dutton-Regester, K., Lin, J.-R., Cohen, O., Shah, P., Lu, D., Genshaft, A. S., Hughes, T. K., Ziegler, C. G. K., Kazer, S. W., Gaillard, A., Kolb, K. E., Villani, A.-C., Johannessen, C. M., Andreev, A. Y., Van Allen, E. M., Bertagnolli, M., Sorger, P. K., Sullivan, R. J., Flaherty, K. T., Frederick, D. T., Jané-Valbuena, J., Yoon, C. H., Rozenblatt-Rosen, O., Shalek, A. K., Regev, A., and Garraway, L. A. (2016). Dissecting the multicellular ecosystem of metastatic melanoma by single-cell RNA-seq. *Science*, 352(6282):189–196. Publisher: American Association for the Advancement of Science.

Toma, K., Kumamoto, T., and Hanashima, C. (2014). The timing of upper-layer neurogenesis is conferred by sequential derepression and negative feedback from deep-layer neurons. *J Neurosci*, 34(39):13259–76.

Torigoe, M., Yamauchi, K., Kimura, T., Uemura, Y., and Murakami, F. (2016). Evidence that the laminar fate of lge/cge-derived neocortical interneurons is dependent on their progenitor domains. *J Neurosci*, 36(6):2044–56.

Trapnell, C., Cacchiarelli, D., Grimsby, J., Pokharel, P., Li, S., Morse, M., Lennon, N. J., Livak, K. J., Mikkelsen, T. S., and Rinn, J. L. (2014). The dynamics and regulators of cell fate decisions are revealed by pseudotemporal ordering of single cells. *Nat Biotechnol*, 32(4):381–386.

Turner, D. L. and Cepko, C. L. (1987). A common progenitor for neurons and glia persists in rat retina late in development. *Nature*, 328(6126):131–6.

Turrero García, M. and Harwell, C. C. (2017). Radial glia in the ventral telencephalon. *FEBS Lett*, 591(24):3942–3959.

van Heusden, F., Macey-Dare, A., Gordon, J., Krajeski, R., Sharott, A., and Ellender, T. (2021). Diversity in striatal synaptic circuits arises from distinct embryonic progenitor pools in the ventral telencephalon. *Cell Rep*, 35(4):109041.

van Velthoven, C., Gao, Y., Kunst, M., Lee, C., McMillen, D., Bhaswanth Chakka, A., Casper, T., Clark, M., Rushil Chakrabarty, R., Scott Daniel, S., Tim Dolbeare, T., Ferrer, R., Jessica Gloe, J., Jeff Goldy, J., Junitta Guzman, J., Carliana Halterman, C., Ho, W., Huang, M., James, K., Nguy, B., Pham, T., Ronellenfitch, K., Thomas, E. D., Torkelson, A., Pagan, C. M., Kruse, L., Dee, N., Ng, L., Waters, J., Smith, K. A., Tasic, B., Yao, Z., and Zeng, H. (2024). Evidence that the laminar fate of lge/cge-derived neocortical interneurons is dependent on their progenitor domains. *bioRxiv*.

Vitali, I., Fièvre, S., Telley, L., Oberst, P., Bariselli, S., Frangeul, L., Baumann, N., McMahon, J. J., Klingler, E., Bocchi, R., Kiss, J. Z., Bellone, C., Silver, D. L., and

Jabaudon, D. (2018). Progenitor hyperpolarization regulates the sequential generation of neuronal subtypes in the developing neocortex. *Cell*, 174(5):1264–1276.e15.

Waclaw, R. R., Wang, B., Pei, Z., Ehrman, L. A., and Campbell, K. (2009). Distinct temporal requirements for the homeobox gene gsx2 in specifying striatal and olfactory bulb neuronal fates. *Neuron*, 63(4):451–65.

Waddington, C. (1957). The strategy of the genes: A discussion of some aspects of theoretical biology. *London: Allen & Unwin*.

Wagner, D. E. and Klein, A. M. (2020). Lineage tracing meets single-cell omics: opportunities and challenges. *Nat Rev Genet*, 21(7):410–427.

Wagner, D. E., Weinreb, C., Collins, Z. M., Briggs, J. A., Megason, S. G., and Klein, A. M. (2018). Single-cell mapping of gene expression landscapes and lineage in the zebrafish embryo. *Science*, 360(6392):981–987. Publisher: American Association for the Advancement of Science.

Wamsley, B. and Fishell, G. (2017). Genetic and activity-dependent mechanisms underlying interneuron diversity. *Nat Rev Neurosci*, 18(5):299–309.

Wang, T., Birsoy, K., Hughes, N. W., Krupczak, K. M., Post, Y., Wei, J. J., Lander, E. S., and Sabatini, D. M. (2015). Identification and characterization of essential genes in the human genome. *Science*, 350(6264):1096–101.

Wang, Y., Liu, L., and Lin, M. (2022). Psychiatric risk gene transcription factor 4 preferentially regulates cortical interneuron neurogenesis during early brain development. *J Biomed Res*, 36(4):242–254.

Wichterle, H., Garcia-Verdugo, J. M., Herrera, D. G., and Alvarez-Buylla, A. (1999).

Young neurons from medial ganglionic eminence disperse in adult and embryonic brain. *Nat Neurosci*, 2(5):461–6.

Wichterle, H., Turnbull, D. H., Nery, S., Fishell, G., and Alvarez-Buylla, A. (2001). In utero fate mapping reveals distinct migratory pathways and fates of neurons born in the mammalian basal forebrain. *Development*, 128(19):3759–71.

Wilson, S. W. and Houart, C. (2004). Early steps in the development of the forebrain. *Dev Cell*, 6(2):167–81.

Wonders, C. P. and Anderson, S. A. (2006). The origin and specification of cortical interneurons. *Nat Rev Neurosci*, 7(9):687–96.

Wonders, C. P., Taylor, L., Welagen, J., Mbata, I. C., Xiang, J. Z., and Anderson, S. A. (2008). A spatial bias for the origins of interneuron subgroups within the medial ganglionic eminence. *Dev Biol*, 314(1):127–36.

Woodhead, G. J., Mutch, C. A., Olson, E. C., and Chenn, A. (2006). Cell-autonomous beta-catenin signaling regulates cortical precursor proliferation. *J Neurosci*, 26(48):12620–30.

Wu, Q., Shichino, Y., Abe, T., Suetsugu, T., Omori, A., Kiyonari, H., Iwasaki, S., and Matsuzaki, F. (2022). Selective translation of epigenetic modifiers affects the temporal pattern and differentiation of neural stem cells. *Nat Commun*, 13(1):470.

Xu, Q., Cobos, I., De La Cruz, E., Rubenstein, J. L., and Anderson, S. A. (2004). Origins of cortical interneuron subtypes. *J Neurosci*, 24(11):2612–22.

Xu, Q., Guo, L., Moore, H., Waclaw, R. R., Campbell, K., and Anderson, S. A. (2010). Sonic hedgehog signaling confers ventral telencephalic progenitors with distinct cortical interneuron fates. *Neuron*, 65(3):328–40.

Yamashita, M. and Emerman, M. (2006). Retroviral infection of non-dividing cells: old and new perspectives. *Virology*, 344(1):88–93.

Yuzwa, S. A., Borrett, M. J., Innes, B. T., Voronova, A., Ketela, T., Kaplan, D. R., Bader, G. D., and Miller, F. D. (2017). Developmental emergence of adult neural stem cells as revealed by single-cell transcriptional profiling. *Cell Rep*, 21(13):3970–3986.

Zechner, C., Nerli, E., and Norden, C. (2020). Stochasticity and determinism in cell fate decisions. *Development*, 147(14).

Zeng, C., Pan, F., Jones, L. A., Lim, M. M., Griffin, E. A., Sheline, Y. I., Mintun, M. A., Holtzman, D. M., and Mach, R. H. (2010). Evaluation of 5-ethynyl-2'-deoxyuridine staining as a sensitive and reliable method for studying cell proliferation in the adult nervous system. *Brain Res*, 1319:21–32.

Zenker, M., Bunt, J., Schanze, I., Schanze, D., Piper, M., Priolo, M., Gerkes, E. H., Gronostajski, R. M., Richards, L. J., Vogt, J., Wessels, M. W., and Hennekam, R. C. (2019). Variants in nuclear factor i genes influence growth and development. *Am J Med Genet C Semin Med Genet*, 181(4):611–626.

Zhang, Y., Liu, T., Meyer, C. A., Eeckhoute, J., Johnson, D. S., Bernstein, B. E., Nusbaum, C., Myers, R. M., Brown, M., Li, W., and Liu, X. S. (2008). Model-based Analysis of ChIP-Seq (MACS). *Genome Biology*, 9(9):R137.

Zheng, G. X. Y., Terry, J. M., Belgrader, P., Ryvkin, P., Bent, Z. W., Wilson, R., Ziraldo, S. B., Wheeler, T. D., McDermott, G. P., Zhu, J., Gregory, M. T., Shuga, J., Montesclaros, L., Underwood, J. G., Masquelier, D. A., Nishimura, S. Y., Schnall-Levin, M., Wyatt, P. W., Hindson, C. M., Bharadwaj, R., Wong, A., Ness, K. D., Beppu, L. W., Deeg, H. J., McFarland, C., Loeb, K. R., Valente, W. J., Ericson, N. G., Stevens, E. A.,

Radich, J. P., Mikkelsen, T. S., Hindson, B. J., and Bielas, J. H. (2017). Massively parallel digital transcriptional profiling of single cells. *Nature Communications*, 8(1):14049. Number: 1 Publisher: Nature Publishing Group.

Aknowledgements

I am deeply grateful to my PhD supervisor, Christian Mayer, for all his support, guidance, and patience throughout my PhD journey.

A huge thank you to the wonderful members of the Mayer Lab for their help and the scientific discussions. I am especially grateful to Ann and Florian, with whom I worked on the paper manuscript. Your support, collaboration, and friendship played a big role in shaping this thesis.

I would like to sincerely thank my thesis committee—Wolfgang Enard, Magdalena Götz, and Silvia Cappello—for their time, insightful feedback, and valuable advice throughout the course of my PhD.

My gratitude also goes to the International Max Planck Research School (IMPRS) for giving me the opportunity to pursue my PhD and for all the support along the way.

Erklärung
Declaration

Hiermit erkläre ich, *
Hereby I declare

☒ dass die Dissertation nicht ganz oder in wesentlichen Teilen einer anderen Prüfungskommission vorgelegt worden ist.
that this work, complete or in parts, has not yet been submitted to another examination institution

☒ dass ich mich anderweitig einer Doktorprüfung ohne Erfolg **nicht** unterzogen habe.
*that I did **not** undergo another doctoral examination without success*

☐ dass ich mich mit Erfolg der Doktorprüfung im Hauptfach
that I successfully completed a doctoral examination in the main subject

und in den Nebenfächern
and in the minor subjects

bei der Fakultät für
at the faculty of _____

der
at _____
(Hochschule/*University*)
unterzogen habe.

☐ dass ich ohne Erfolg versucht habe, eine Dissertation einzureichen oder mich der Doktorprüfung zu unterziehen.
that I submitted a thesis or did undergo a doctoral examination without success

Munich, 10.10.2025 _____ Yana Kotlyarenko _____
Ort, Datum/*place, date* Unterschrift/*signature*

*) Nichtzutreffendes streichen/
delete where not applicable

Eigenständigkeitserklärung

Hiermit versichere ich an Eides statt, dass die vorliegende schriftliche Dissertation / Masterarbeit / Bachelorarbeit / Zulassungsarbeit mit dem Titel

Competence of Inhibitory Neuron Progenitors in the Telencephalon

von mir selbstständig verfasst wurde und dass keine anderen als die angegebenen Quellen und Hilfsmittel benutzt wurden. Die Stellen der Arbeit, die anderen Werken dem Wortlaut oder dem Sinne nach entnommen sind, wurden in jedem Fall unter Angabe der Quellen (einschließlich des World Wide Web und anderer elektronischer Text- und Datensammlungen) kenntlich gemacht. Weiterhin wurden alle Teile der Arbeit, die mit Hilfe von Werkzeugen der künstlichen Intelligenz de novo generiert wurden, durch Fußnote/Anmerkung an den entsprechenden Stellen kenntlich gemacht und die verwendeten Werkzeuge der künstlichen Intelligenz gelistet. Die genutzten Prompts befinden sich im Anhang. Diese Erklärung gilt für alle in der Arbeit enthaltenen Texte, Graphiken, Zeichnungen, Kartenskizzen und bildliche Darstellungen.

Munich, 14.04.2025

(Ort / Datum)

Yana Kotlyarenko

(Vor und Nachname in Druckbuchstaben)

Yana Kotlyarenko

(Unterschrift)

Affidavit

Herewith I certify under oath that I wrote the accompanying Dissertation / MSc thesis / BSc thesis / Admission thesis myself.

Title: Competence of Inhibitory Neuron Progenitors in the Telencephalon

In the thesis no other sources and aids have been used than those indicated. The passages of the thesis that are taken in wording or meaning from other sources have been marked with an indication of the sources (including the World Wide Web and other electronic text and data collections). Furthermore, all parts of the thesis that were de novo generated with the help of artificial intelligence tools were identified by footnotes/annotations at the appropriate places and the artificial intelligence tools used were listed. The prompts used were listed in the appendix. This statement applies to all text, graphics, drawings, sketch maps, and pictorial representations contained in the Work.

Munich, 14.04.2025

(Location/date)

Yana Kotlyarenko

(First and last name in block letters)

Yana Kotlyarenko

(Signature)

Stand: 26.08.2024

Regeln für den Einsatz von Werkzeugen der Künstlichen Intelligenz (KI) für prüfungsrelevante Tätigkeiten

1. Der Einsatz von KI-Werkzeugen für prüfungsrelevante Leistungen ist möglich.

2. Der Einsatz von KI-Werkzeugen zur Optimierung, Übersetzung, Korrektur von Rechtschreibung und Grammatik von selbstgenerierten Texten und zur Optimierung von Designaspekten selbstgenerierter Abbildungen ist ohne Kennzeichnung zulässig.

3. Von KI-Werkzeugen de novo generierte und in der Arbeit verwendete Textabschnitte und Abbildungen sind durch Fußnoten/Anmerkungen an den entsprechenden Stellen deutlich zu kennzeichnen und das KI-Tool ist analog zu Literaturquellen anzugeben. Die verwendeten Prompts sind im Anhang zu listen.

4. Textabschnitte, die durch den iterativen Einsatz von KI-Tools erzeugt wurden, sind zu kennzeichnen.

5. Die Autorin / der Autor ist für die Korrektheit und korrekte Darstellung in schriftlichen Leistungen und Präsentationen verantwortlich.

6. Quellen / Referenzen müssen nach den Regeln der guten wissenschaftlichen Praxis zitiert werden.

Rules for the use of artificial intelligence (AI) tools for examination-relevant activities

1. The use of AI tools for examination-relevant performances is possible.

2. The use of AI tools to optimize, translate and correct the spelling and grammar of self-generated texts and to optimize self-generated illustrations is permitted without indication.

3. Text sections and illustrations de novo generated by AI tools and used in the thesis must be clearly marked by footnotes/annotations at the appropriate places and the AI tool must be indicated analogously to literature sources. The prompts used have to be listed in the appendix.

4. Sections of the text generated through iterative use of AI tools should be marked.

5. The author is responsible for the correctness and proper presentation in written performances and presentations.

6. Sources / references must be cited in accordance with the rules of good scientific practice.

Stand: 26.08.2024